Surface Modification and Micro/Nano Structure Control of Cellulose Nanofibrils Film and Wet-Spinning Fibers

A Dissertation
Presented to
The Academic Faculty

By

Wei Liu

In Partial Fulfillment
Of the Requirements for the Degree
Doctor of Philosophy in the
School of Chemical and Biomolecular Engineering

Georgia Institute of Technology

May 2020

Surface Modification and Micro/Nano Structure Control of Cellulose

Nanofibrils Film and Wet-Spinning Fibers

Approved by:

Professor Yulin Deng, Advisor
School of Chemical & Biomolecular
Engineering
Georgia Institute of Technology

Professor Carson J. Meredith
School of Chemical & Biomolecular
Engineering
Georgia Institute of Technology

Professor Meisha L. Shofner
School of Material Science
Engineering
Georgia Institute of Technology

Professor Christopher O. Luettgen
School of Chemical & Biomolecular
Engineering
Georgia Institute of Technology

Professor Robert J. Moon
School of Material Science
Engineering
Georgia Institute of Technology

Date Approved: March 20, 2020

ACKNOWLEDGEMENTS

I would like to express my sincerest gratitude to my thesis advisor, Dr. Yulin Deng, for his great support and wise guidance. Dr. Deng's support should date back to the year 2012 when I was a visiting student in his group. There is no doubt that my study in Dr. Deng's group is the most precious time in my life. I learned a lot from Dr. Deng's remarkable attitude of diligence, strictness and immense knowledge. He brought me into the world of scientific research and inspired me to develop a critical way of thinking about problems, which will benefit me for a lifetime. Here, I also would like to show great appreciation to my thesis committee members, Professor Carson Meredith, Professor Christopher Luettgen, Professor Meisha Shofner, and Professor Robert Moon. I really appreciate your invaluable suggestions, encouragements and generous support to my research and career development.

Besides, I would like to show my deepest appreciation to my loving family. My wife, Lingfeng Li, gives me selfless love and support. My son, Elijah, brings me happiness and laughter. My parents, give me all. Because of your company, my Ph.D. journey becomes much more enriching, colorful, and fulfilling.

I am grateful to my co-workers, lab members, faculties and friends at Georgia Tech. Especially, I want to thank Dr. Jian Gong, Dr. Guanglei Zhao, Dr. Weibing Wu, Dr. Wei Mu, Dr. Xiaodan Zhang, Dr. Hu Fan, Xu Du, Zhe Zhang, Yutao Gong, Wenqin You, Mingyue Zhang, Junhe Chen and all previous and current researchers in Dr. Deng's group. I also want to thank Dr. Jeffery Wang, who supported me for one-year research before entering the Ph.D. program. I thank your help and support in both research and life during the past years.

TABLE OF CONTENTS

LIST OF TABLES

LIST OF FIGURES

LIST OF ABBREVIATIONS

3D	Three-Dimensional
AKD	Alkyl ketene dimers
BC	Bacterial cellulose
C.I.	Crystallinity index of cellulose
$C_{16}OH$	Hexadecanol
CAH	Contact angle hysteresis
CAN	Ammonium nitrate
CMC	Sodium carboxymethyl cellulose
CNC	Nanocrystals
CNF	Cellulose nanofibril
CTAB	Cetyltrimethylammonium bromide
D	Apparent crystallite size
$d_{110/200}$	Interplanar distances
DCM	Dichloromethane
DMA	Dynamic mechanical analysis
DMAP	4-dimethyl aminopyridine
DP	Degree of polymerization
DTG	Derivative Thermogrametric
FE-SEM	Field emission scanning electron microscope
f_H	Herman's orientation factors
FT-IR	Fourier transform infrared
GA	Glutaraldehyde
GMA	Glycidyl methacrylate
Gt	Gigatonne
HDI	Hexamethylene diisocyanate
LDPE	Low density polyethylene
MMA	Methyl methacrylate
M_w	Molecular weight

PE	Polyethylene
PEO	Poly ethylene oxide
PLA	Polylactic acid
PMMA	Poly methyl methacrylate
Poly-(DADMAC)	Poly(diallyldimethylammonium chloride)
PP	Polypropylene
PS	Polystyrene
PVA	Polyvinyl alcohol
PVC	Polyvinyl chloride
TDI	Toluene diisocyanate
TEMPO	2,2,6,6-Tetramethyl-1-Piperidinyloxy
TGA	Thermogravimetric analysis
THF	Tetrahydrofuran
TOCNF	Tempo-oxidized cellulose nanofibrils
WAXD	Wide-angle X-ray diffraction
WCA	Static water contact angle
WRV	Water retention value
wt %	Weight Percent
XRD	X-ray diffraction
χ_c	Crystallinity of PLA

SUMMARY

With the depletion of fossil resources and growing environmental issues, developing sustainable and "green" materials that simultaneously possess advanced properties has become more and more important. Nano-cellulose, including cellulose nanofibrils (CNFs), nanocrystals (CNC) and tempo-oxidized cellulose nanofibrils (TOCNs), have been of great research interest due to their advantages of abundance, biodegradability, non-toxicity, excellent biocompatibility and recyclability. The aim of this thesis is the surface modification of cellulose nanofibrils, controlling nano/micro structures of the composite films and wet-spinning fiber developments.

This dissertation includes four components:

1. Fabrication of non-fluorinated superhydrophobic nanocellulose membranes

In the first part, patterned nanocellulose membrane surfaces were fabricated by a simple pressing process. After chemical modification with non-fluorinated and low-cost industrial chemicals, such as alkyl ketene dimers (AKD), wax, and isocyanate, some nanocellulose membranes showed water contact angles >150°. The combination of micro-sized pattern and nanosized cellulose fibers created a hierarchical structure that contributed to the superhydrophobic properties. SEM and optical microscopy were used to characterize the fiber network and hierarchical structures. Wetting experiments showed that water droplets roll off the cellulose membrane with fabricated pillar size lower than 100 μm after chemical modification with AKD, wax, or isocyanate. The process used in this superhydrophobic cellulose membrane fabrication is simple, cost-effective, and amenable to scale up so it has the potential to be used as a liquid packaging material.

2. In situ modification of nanocellulose with AKD emulsion for PLA composite reinforcement

In this project, PLA composite films were prepared with the reinforcement of hydrophobically modified nanocellulose. The hydrophobic modification of nanocellulose was conducted in situ in water suspension using an AKD emulsion, which alternates the CNF surface from hydrophilic to hydrophobic directly in water. After the modification and thermal treatment using AKD molecules, the CNF can be uniformly re-dispersed in organic solvent and a hydrophobic PLA polymeric matrix. SEM, FT-IR and XRD were used in the characterizations of AKD modified CNFs and their composites with PLA. Different AKD additions and CNF contents were investigated in the composite fabrication. The mechanical strength measurement verified the reinforcement of CNF in the composites. The highest tensile strength of 45 MPa with Young's modulus 2.52 GPa was achieved in this study.

3. Nano-structure control of nanocellulose frameworks for PLA composite reinforcement

In this study, 3D porous and simultaneously high-strong nanocellulose frameworks were prepared and used as reinforcement for the PLA composite fabrication. Three different drying processes, i.e. room-temperature drying, heat-drying and freeze-drying, were combined in the nanocellulose framework preparation. The room-temperature drying and heat-drying improved the irreversible hydrogen bonding between nano fibrils and provided the high-strength property of the frameworks. The re-wetting and freeze-drying resulted in a porous structure and large specific area that improves the interaction with the PLA polymeric matrix. Furthermore, with the chemical modification of isocyanates, e.g., TDI and HDI, PLA molecules were crosslinked and covalently

bonded to the nanocellulose frameworks. As a result, the CNF-PLA composite films with high mechanical performances were obtained. The highest tensile strength and modulus achieved 205 MPa and 5.8 GPa respectively.

4. Wet-spinning of nanocellulose filaments fabrication by chemical and mechanical approaches

In the last part, nanocellulose filaments were prepared by wet-spinning. To improve the mechanical strength, chemical modification and fibril orientation were researched in this work, including three aspects. Firstly, optimization of operation conditions of wet-spinning, i.e., the solid contents of nanocellulose paste, the nozzle diameters and the spinning speeds, were investigated. Secondly, the chemical additives were screened for increasing the fibril interactions, such as chemical bonding agents (citric acid, boric acid, glutaraldehyde and glyoxal etc.), polymers and inorganic nanoparticles. Thirdly, the post-treatments including wet-stretching and wet-twisting were investigated for filament mechanical improvement. The obtained nanocellulose filaments were characterized by FT-IR, SEM and wide-angle X-ray diffraction. With optimized operations, the nanocellulose filament with the highest tensile strength of 211 MPa and modulus of 18.2 GPa in this study was obtained.

CHAPTER I: INTRODUCTION

Petroleum-based synthetic polymers, or plastics, have been widely used in many manufacturing processes and products. For example, packaging is the largest plastics market due to its light-weight property, high durability, and plenty of availability of plastics[1]. Up to the year 2015, total plastic production exceeded 8.3 gigatonnes (Gt) worldwide[1]. More than 416 billion plastic bags were consumed per month globally based on the reported data[1, 2]. However, petroleum-based materials are unsustainable, non-biodegradable and non-renewable. Because of the highly stable chemical bonding of plastic molecules, the disposal process of plastic wasters are very difficult and have caused worldwide "white pollution"[3]. It is reported that 6.3 Gt of plastic waste was produced in 2015, and by 2050, global plastic waste will increase to 12 Gt[1, 4]. These plastic wasters can even take up to 1,000 years to be decomposed in landfills or oceans[5, 6]. Therefore, it is urgent to develop sustainable technologies and alternative materials that are not only durable but also easily biodegradable.

The natural sourced cellulosic material is a good candidate as the alternative to plastics. Cellulose is a basic substance in the cell wall of plants. It is the most abundant and most popular natural polymer on earth[7]. The global production of cellulose reaches $\sim 1.5 \times 10^{12}$ tons per year through photosynthesis by the plant[8, 9]. The abundance of cellulose provides adequate supply for the material market. Compared to traditional synthetic polymers from fossil sources, cellulose materials have the advantages of bio-degradability, non-toxicity, excellent biocompatibility and recyclability[10-13]. With the depletion of fossil resources and growing environmental problems, using cellulose as the renewable and biodegradable raw material in various applications is a

proposed solution as it successfully meets the environmental and recycling requirements.

Nanocellulose is nano-sized cellulose fiber, which usually has several to tens of nanometers in diameter and several micrometers in length. Nanocellulose material includes cellulose nanofibrils (CNFs), nanocrystals (CNC) and TEMPO-oxidized cellulose nanofibrils (TOCNs) depending on the different manufacture methods, such as mechanism treatment, acid hydrolysis or TEMPO oxidation, etc[12]. Nanocellulose materials have received growing research interests due to their outstanding physical and chemical performance such as low weight, high aspect ratio, and excellent mechanical strength properties. Nanocellulose has proven to be a versatile material with a vast array of potential commercial applications including composites and foams for automotive, aerospace, and building construction[14, 15]. In addition to material performance properties like gelation, shear-thinning, exceptionally high strength, and lightweight, nanocellulose has a strong sustainability profile.

The advantages of nanocellulose, however, are often limited by their high hydrophilic properties used in the application of polymer reinforce filers and packing. For example, nanocellulose material has poor compatibility with hydrophobic engineered polymer matrices; nanocellulose fabricated packaging membranes absorb water or moisture leading to erosion in humid environments[16, 17]. The hydrophilicity of nanocellulose is due to the abundant hydroxyl groups on the fiber surface, as the cellulose fibrils are prepared in water solution[18, 19]. Surface modification is the most common method to solve the compatibility problem in polymer nanocomposites.

On the other hand, structural defects exist in the prepared nanocellulose material that largely limits their wide application. For example, although the single crystallized nanocellulose fiber has

a high mechanical tensile strength of 6-7 GPa, the practical prepared macro nanocellulose filaments usually have the moderate tensile strength of 100-400 MPa in most reports because of the misalignment of the nanofibers and boundary or void defects among the nanofibers[12, 20-22]. Therefore, the micro/nano structure control during the nanocellulose material fabrication is a critical strategy to improve the final performances.

This dissertation focuses on the surface chemical modification and micro/nano structure control of cellulose nanofibrils for the preparation of composite film and strong wet-spinning fibers. The whole dissertation contains 8 chapters. The first chapter is the introduction. Chapter II is a brief review of nanocellulose materials. This chapter aims to introduce the background of nanocellulose and the state-of-the-art of modification by chemicals as well as its applications. Chapter III is "Problem Analysis and Objectives", which states the challenges and objectives of the 4 research projects we have conducted and the corresponding solutions are proposed. In chapter IV, we have performed the study of surface structure patterning for fabricating non-fluorinated super-hydrophobic nanocellulose membranes. Chapter V is about the in situ modification of nanocellulose with AKD emulsion for PLA composite reinforcement. Chapter VI focuses on nano-structure control of nanocellulose frameworks for PLA composite reinforcement. Chapter VII is nanocellulose filament fabrication by chemical and mechanical improvements. Chapter VIII is the overall conclusion and future directions.

CHAPTER II: LITERATURE REVIEW

2.1 Background of Cellulose nanofibrils (CNFs), Tempo-oxidized cellulose nano-fibrils (TOCN) and cellulose nanocrystals (CNC)

Nanocellulose material includes cellulose nanofibrils (CNFs), nanocrystals (CNC), TEMPO-oxidized cellulose nanofibrils (TOCNs) and bacterial cellulose (BC), etc. Cellulose nanofibrils are high aspect ratio cellulose nano-strings with the diameter less than 100 nm and the length up to several micrometers, depending on the source of cellulose fiber and preparation method (as shown in Fig. 2.1)[23-28]. Generally, CNFs have a high aspect ratio of ~100, low density of 1.6g cm^{-3} and crystalline region tensile strength and modulus in the range of 7.5-7.7 GPa and 78-220 GPa respectively[12, 26, 27]. These excellent mechanical performances even exceed the behavior of aramid polymers and glass fibers[29, 30].

CNFs can be prepared by several methods from wood pulp, including chemical hydrolysis, high shear force, mild enzyme hydrolysis, or combination of these to control the diameters in nanoscale range[23, 25, 31]. The fibers are moderately degraded and opened into their substructural fibrils and micro-fibrils[8, 32]. In addition to the abundant availability of CNFs, the excellent properties of CNFs have attracted the potential use of CNFs in various applications.

CNFs can be chemically modified with different reagents, such as N-octadecyl isocyanate and synthetic polymer precursors because the fiber surface possesses abundant active hydroxyl groups that are produced by the nano-fibrillated process[33-35]. Charged groups or other functional groups can be introduced on the surface of CNFs via treatment with chemicals such as maleic anhydride,

glycidyl methacrylate, and succinic anhydride[33, 36, 37]. Hydrophobic modifications via silanization, carboxymethylation, fluorinated coating as well as plasma treatment are used to modify CNFs for different applications[35, 38-41]. These modifications enable nanocellulose to have good compatibility and combination with other engineered polymers for composite fabrication[17, 42, 43].
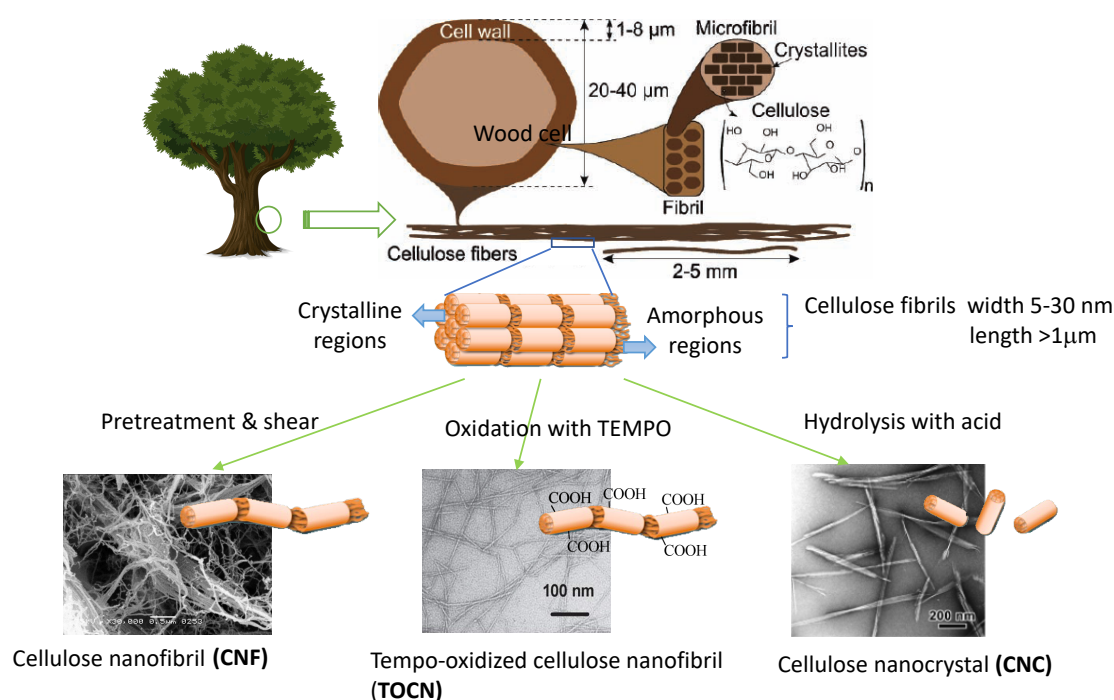
Figure 2. 1 The structure of nanocellulose in various length scales[44] and illustrations of CNF, TOCN and CNC.

Tempo-oxidized cellulose nanofibrils (**TOCNF**) are a new type of nanocellulose prepared from oxidation of cellulose fibers by TEMPO. TEMPO, with the name of 2,2,6,6-tetramethylpiperidine-1-oxyl radical, can position-selectively and catalytically oxidize C_6 primary hydroxyls of cellulose to carboxylate groups[45, 46]. Native wood celluloses can be converted to individual nanofibers with 3–4 nm in width and at least several microns in length after the oxidation. The ζ-potentials of TOCNFs are approximately -75 mV in water due to the cellulose fibers becoming anionically charged. Because of

the electrostatic repulsion, the TOCNF fibers could be individually dispersed in water by mechanical disintegration treatment. Self-standing TOCNF films are transparent and flexible, with high tensile strengths of 200–300 MPa and elastic modulus of 6–7 GPa[47, 48]. This kind of new cellulose-based nanofiber has potential as an environmental-friendly and novel bio-based nanomaterials in high-tech fields.

Cellulose nanocrystals (**CNCs**) are rigid rod-like cellulose particles after intense hydrolysis and treatment with ultrasound. The preparation of CNCs is also possible through high energy mechanical disintegration, as well as enzymatic and acidic hydrolysis of a cellulose suspension to cleave the amorphous parts of cellulose[49, 50]. Enzymatic hydrolysis is conducted in a milder condition than the aggressive acid hydrolysis and yields nanocrystals that possess much greater strength. CNC has a typical width of a few nanometers and length of hundreds of nanometers but such dimensions depend on the amorphous cellulose content, cellulose source and conditions used during hydrolysis[11, 51, 52]. CNCs display a large elastic modulus (~150 GPa), high strength (~7 GPa) and a very low thermal expansion coefficient (~10^{-7} K^{-1})[52, 53]. The stability of cellulose nanocrystals is strongly dependent on the size polydispersity, the dimensions of the CNC particles, and their surface charge. Generally, negative charges are introduced on the surface of CNCs during the acidic hydrolysis process. Because of the electrostatic repulsion, the CNC suspension shows a good dispersion and forms a hydrogel network[52, 54]. Due to their regular and precise rigid-rod shape, CNCs can highly improve the mechanical characteristics in composited materials. The nanocomposites display significantly enhanced mechanical behavior even when the CNC content is low.

2.2 Structure features of nanocellulose

Cellulose is a linear chain homopolymer of ringed glucose molecules (i.e. D-glucopyranose units). The repeat D-glucopyranose units linked together through enantioselectivity β-1,4 glycosidic bond, which is oxygen covalent linkage of C_1 in one glucose ring and C_4 of the adjoining ring ($1 \rightarrow 4$ linkage, shown in Fig. 2.2)[12]. The number of anhydroglucose rings (also known as the degree of polymerization, DP) in the cellulose chain is generally between 10,000 to 15,000, but it is dependant on the source of cellulose materials[12]. Cellulose has a flat ribbon-like configuration because of the intrachain hydrogen bonding between OH groups and oxygens of both the adjoining ring molecules and the glycosidic bonds. The intermolecular hydrogen bonding, with the van der Waals interactions, stabilize the parallel stacking of adjoining cellulose chains to form the elementary fibrils, and then generate larger microfibrils by further aggregation. The formed cellulose fibrils consist of crystalline structure regions where the cellulose chains are arranged by highly ordered hydrogen bond systems and amorphous domains in a disordered state. We can obtain cellulose nanofibrils by breaking the inter-chain hydrogen bonding of microfibrils into nano-sizes, and obtain cellulose nanocrystals if the amorphous domains are removed.

2.2.1 Crystalline structures

Crystalline cellulose has several polymorphs: cellulose I, II, III and IV[12]. Cellulose I is the common phase in naturally produced cellulose. Cellulose I also has two different crystalline structures: cellulose Iα with the triclinic structure (space group P$_1$) and Iβ with the monoclinic structure (space group P2$_1$)[12]. Most algae and bacteria produce Iα structure cellulose but for higher plant cell walls, cellulose Iβ is the dominant polymorph. However, cellulose Iα and Iβ usually coexist in the cellulose source with various ratios. In the chain axis direction, the relative

displacement of cellulose sheets (i.e., the parallel stacking of cellulose chains) along the ''hydrogen bonded'' planes (lattice planes $(110)_t$ and $(200)_m$) is different between cellulose Iα and Iβ[55]. The different relative displacements lead to minor differences in properties, such as elastic, mechanical and thermal behavior, for cellulose Iα and Iβ. The Iα phase of cellulose is metastable and it can be converted to Iβ through hydrothermal treatments (e.g., 260 °C) in alkaline solution, or high-temperature treatments in organic solvents[56, 57]. Some researchers report the conversion from Iα to Iβ by using Iα rich algal and bacterial cellulose. The percentages Iα to Iβ conversion can be controlled under different treatment conditions, however, it still cannot obtain 100% converted Iβ polymorph.
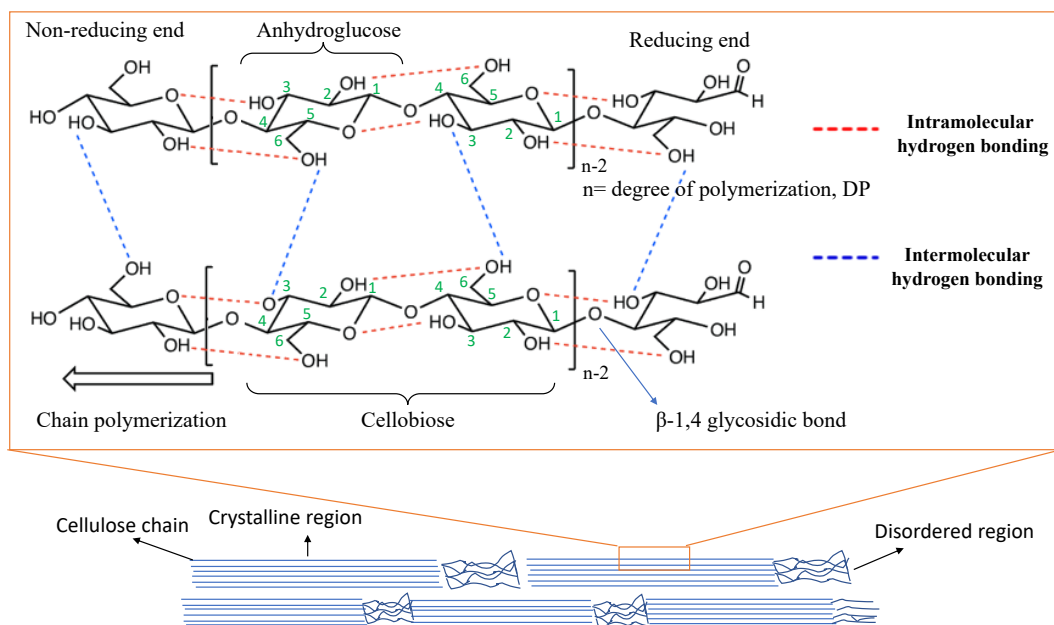
Figure 2. 2 (A) Chemical structure and hydrogen bonding of nanocellulose; (B) Schematic showing of the crystalline and amorphous regions of nanocellulose.[58]

Cellulose II has a monoclinic structure and it is the most stable structure in four different polymorphs. Cellulose II is produced in the recrystallization process from the cellulose solution

and mercerization process treated by aqueous sodium hydroxide. Therefore, cellulose II generally exists in synthetic textile fibers such as cellophane, Rayon and Tencel. Cellulose III is converted from the treatment of cellulose I or II with liquid ammonia, and cellulose IV is generally formed in the thermal treatments of Cellulose III. These structures are detailed in the published literature.

2.2.2 Hydrogen bonding

Hydrogen bonding is essential for the structural stability and properties of cellulose. Hydrogen bonding is widely distributed in the cellulose structure, which includes intra- and intermolecular hydrogen bonding. The intramolecular hydrogen bonds mostly occur between O3-H and O5 of neighboring glucopyranose units with a distance of 2.75 Å, and between O2-H and O6' with a distance of 2.87 Å[59], as shown in Fig. 2.2 A. These intramolecular hydrogen bonds can be detected by the characterizations of X-ray diffraction, neutron diffraction, NMR and IR spectroscopy, and they are closely related to the single chain conformation and stiffness. Neutron Crystallographic studies show that there are two coexisting bonding types in the hydrogen bonding networks (noted as network A and B) of native crystalline cellulose[59], as shown in Fig. 2.3 A. The research indicates that cellulose Iβ has a better hydrogen bonding geometry than Iα, and therefore, the hydrogen bonding network A is estimated to account for a higher percentage (70–80%) in the hydrogen bonding configuration of cellulose Iβ. In cellulose II crystalline, the hydrogen bonding is proposed similar to that of cellulose I. Molecular dynamic simulations show that a flip transition from network A to network B of O2-H and O6 hydrogen bonding after annealing of cellulose II.

Besides the intra- and intermolecular hydrogen bonding, there is existing the hydrogen bond interaction between the water inside cellulose fibrils and the hydroxyl group in the cellulose chains.

The native cellulose has a high affinity to other hydroxyl compounds, such as water. The interaction of cellulose with water causes significant changes in mechanical properties, structural stability and hydration state of cellulose. It is well known that there are at least two different statuses of water present in cellulose: one is the "free" water which is the capillary water inside crystalline structure, and the other is "bound" water associated with the cellulose molecules. Recent Small-angle neutron scattering and molecular dynamics simulations research has further resolved two types of bound water in cellulose: "non-freezing bound" water that gradually becomes mobile with increasing temperature and "freezing bound" water which is confined water that accumulates in the narrow spaces between the microfibrils and can abruptly become mobile at ~260 K[60, 61].
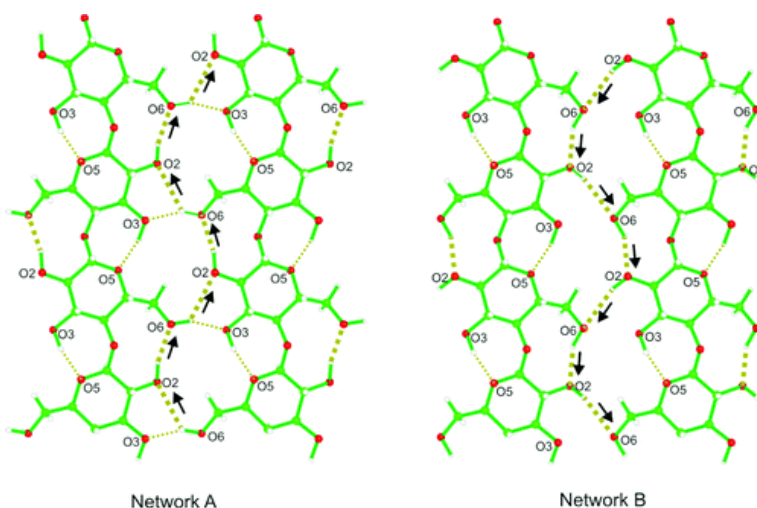
Figure 2. 3 Two different hydrogen networks (A and B) in the nanocellulose chain[59].

2.2.3 Hornification and re-wetting

Hornification occurs during the drying process of cellulose, which is associated with the forming of irreversible hydrogen bonding[62]. Elevating temperature will accelerate this process. In the structure of wood pulp manufactured paper, irreversible hydrogen bonding causes pore closure[63]. Figure. 2.4 A illustrates the drying process of cellulose fibers. Larger pores usually

undergo inelastic deformation during the drying and the irreversible adhesion of pore walls to each other could also occur in hornification[64, 65]. In the nanocellulose based membrane, the pore closure is more complete than that of wood pulp based paper. As a result, the nanofibrils form a dense network with smaller and more uniform dimensions during the hornification. The CNF formed dense network shows very good oxygen barrier properties[66].

Re-wetting is a process of breaking hydrogen bonding and opening of the lattice by water. The cell-wall model suggested by Scallan in 1977 shows how water interacts with the cellulose microstructure during the re-wetting process after hornification[62, 67]. In Fig. 2.4 B, (i) illustrates the dry structure of cellulose which is a tightly bound array of microfibrils by hydrogen bonds. Figure (ii) shows the initiation of swelling by water. When water is introduced, the "hydrogen bond" planes are forced apart, resulting in internal fibrillation. Figure (iii) shows an intermediate state of swelling by further breaking of hydrogen bonds by water, and (iv) shows complete delamination (swelling) of the lamella. During the swelling, the structure causes some of the lenticular pores with their ends closed, which is called "zipping up"[62]. Re-wetting of dried nanocellulose fibrils will obtain only partial unzipping structure because hornification increases non-reversible bonding interaction between neighboring microfibrils, leading to restricting expansion on wetting.

TEMPO nanocellulose fibrils have an abundance of carboxyl acid groups. Research shows that the introduction of carboxyl groups on nanocellulose fibers can increase the water retention value, which is the amount of water uptake by dried nanocellulose material[68]. The room-temperature dried TEMPO nanocellulose can reversibly disperse to its initial status in water[64]. There are two effects of carboxyl group that are considered in the study to contribute to the drying/re-wetting process[48, 62]. Firstly, carboxyl groups form the strong hydrogen bonding with

hydroxyl groups of the cellulose chain; secondly, ester groups can be formed between the carboxyl groups and hydroxyl groups of adjacent microfibrils. The formation of ester groups cause covalent crosslinking of cellulose chains. However, both of the two suggested mechanisms are difficult to quantify.
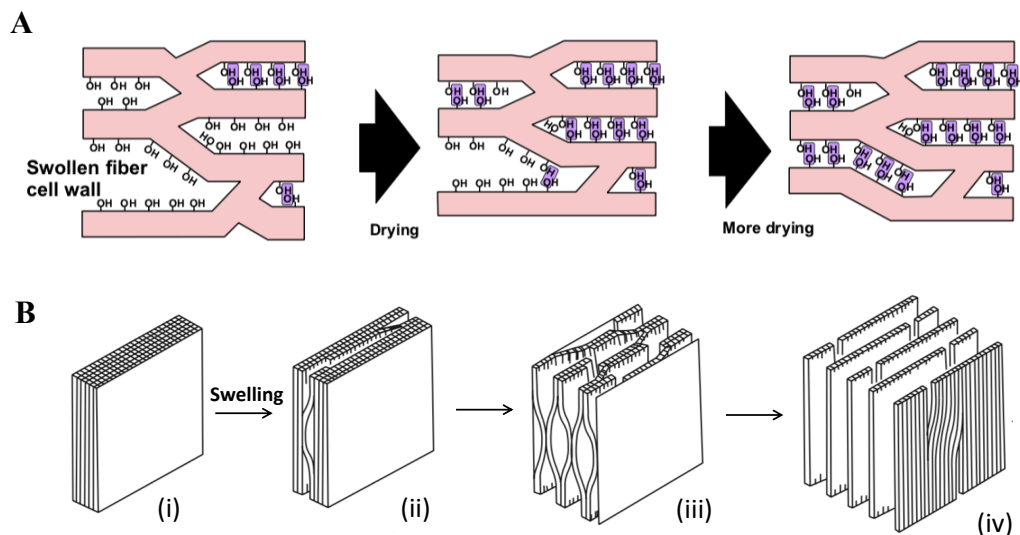
Figure 2. 4 The multi-lamina model for cellulose drying process (A) and swelling process (B) [62, 63].

2.3 Chemical modification

The chemical modification of nanocellulose is focused on the reactions with hydroxyl groups on the nanocellulose fibrils. Some of the chemical modifications can be conducted in aqueous solution; and some types of chemical reactions with nanocellulose hydroxyl groups are water sensitive that should be performed in organic solvent. This section summarized the approaches reported in the literature for nanocellulose chemical modification in aqueous, non-aqueous or emulsion solutions.

2.3.1 Chemical modification in aqueous solution

Nanocellulose material is highly hydrophilic and it can be dispersed well in water solution. The chemical modification in aqueous solution includes two strategies: non-covalent and covalent surface modifications. Chemicals such as surfactants or polyelectrolytes that can be adsorbed on the surface of nanocellulose are typically used in the non-covalent surface modifications. Therefore, the interactions between nanocellulose substrate and modifier are mainly contributed by hydrophilic affinity, hydrogen bonds, electrostatic attractions or van der Walls forces.

The anionic surfactants consisting of mono- and di-esters of phosphoric acid with alkylphenol tails were applied in the modification of CNCs by Heux et al[69, 70]. The obtained surfactant modified CNCs can be dispersed very well in non-polar solvents because of the surfactant molecules coating on the surface of the CNCs to form a thin layer with a thickness of about 15 Å[71]. After the modification with phosphate ester anionic surfactant, the surfactant coated CNCs were applied as filler in the reinforcement of polymers, such as isotactic polypropylene (isoPP) and polylactic acid (PLA)[69-71]. Due to the good dispersion of CNCs in a polymer matrix, the tensile strength and elongation at break were improved compared to the unreinforced samples.

Nonionic polymers (such as polyvinyl alcohol (PVA)[72, 73] and polyethylene oxide (PEO)[74, 75]) and nonionic surfactants (such as sorbitan monostearate[76] and Tween 20[77]) are widely used in the nanocellulose modification. The chosen surfactants commonly consist of hydrophobic moieties and hydrophilic blocks which can interact with nanocellulose fibrils through hydrogen bonding or hydrophilic affinity. The hydrophobic moiety in surfactant molecules can change the surface property of nanocellulose from hydrophilicity to hydrophobicity. Another example is by mimicking the natural lignin-carbohydrate structures, artificially synthesized xyloglucan

oligosaccharide-poly(ethylene glycol)-polystyrene triblock copolymer was used in the surface adsorption on CNCs[78]. The excellent dispersion ability of modified CNCs in nonpolar solvents was obtained.
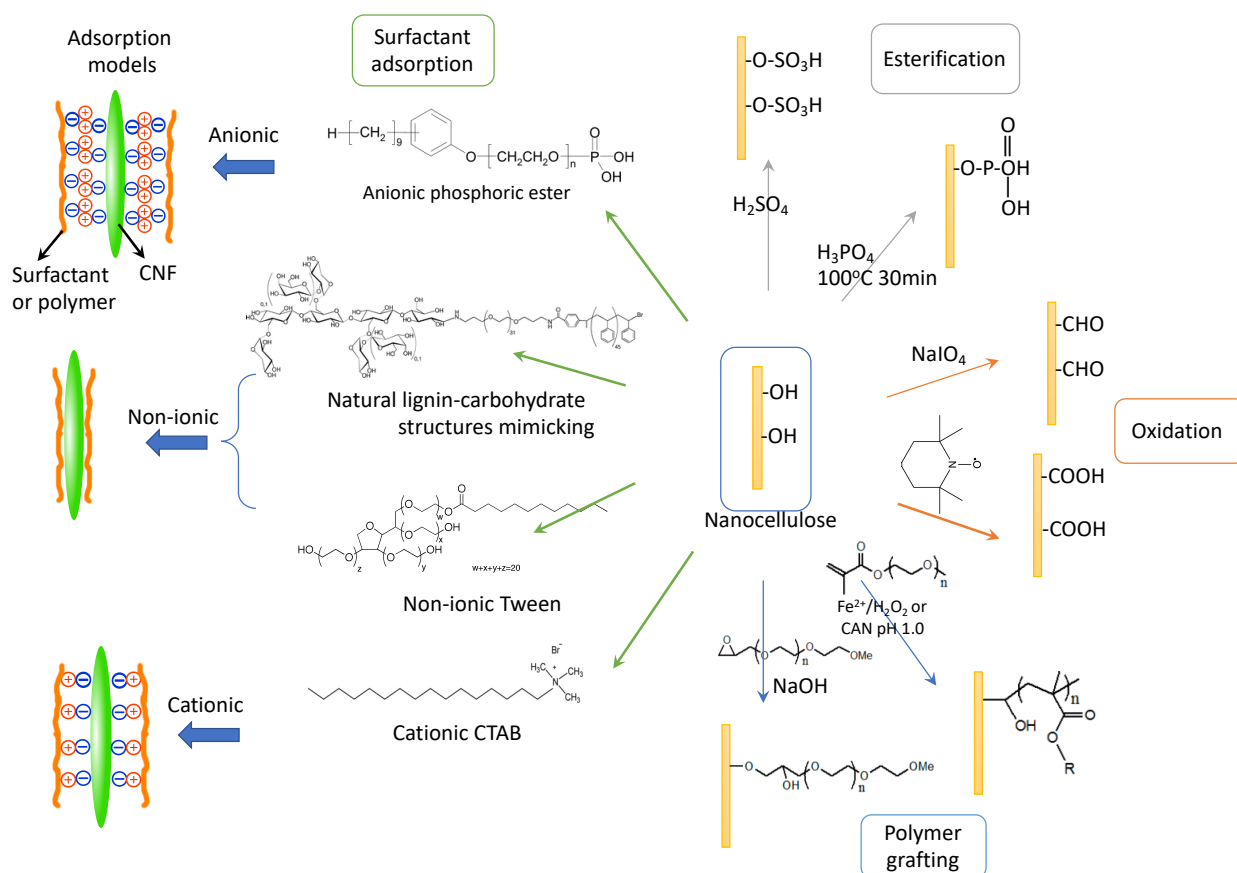
Figure 2. 5 Common chemical modifications of nanocellulose in water.

Cationic surfactants can be easily applied in the nanocellulose adsorption modification because the nanocellulose fibrils are naturally negative-charged or they can be facially converted to negative charge. The commonly used surfactants are quaternary ammonium salts such as cetyltrimethylammonium bromide (CTAB) or cationic polymers such as poly(diallyldimethylammonium chloride) (poly-(DADMAC)), poly(allylamine hydrochloride)

(poly(AAH)), and polyethyleneimine (poly-(EI)) etc[79-82]. The adsorption models for anionic, non-ionic and cationic surfactant adsorption on the nanocellulose surface were illustrated in Fig. 2.5.

Covalent surface modifications in aqueous solution were reported by using sulfuric acid or phosphoric acid for the esterification of the hydroxyl groups[83-85]. The acid-catalyzed hydrolysis of nanocellulose occurs simultaneously with the esterification. Therefore, the amounts of reacted sulfate ester groups or phosphate groups depend on the conditions such as hydrolysis time, temperature, acid concentration, etc. This makes it very difficult to precisely control the esterification reactions. The oxidation of nanocellulose is another method used in aqueous modification. The oxidation can introduce negative charges on the surface of nanocellulose fibrils. Therefore, the dispersibility can be largely improved by the oxidation. TEMPO is a widely chosen catalyst because it can high-selectively oxidize the hydroxyl groups of nanocellulose into carboxyl acid groups under mild conditions[48, 86]. In another way, $NaIO_4$ can break the glucose ring to produce two aldehyde groups. In the following reaction, negatively charged $-SO_3^-$ can be introduced onto the nanocellulose through sulfonation reaction by using Na_2SO_3[87]. Different oxidative reagents, such as Fenton's reagent (Fe^{2+}/H_2O_2) or ceric ammonium nitrate (CAN), were successfully used to create free radicals on the CNC surface to initiate polymerization reaction in water, such as the free radical polymerization of methyl methacrylate (MMA) and glycidyl methacrylate (GMA)[88-90].

2.3.2 Non-aqueous solution modification

Many different types of chemical reactions can be used for the hydrophobic modification of nanocellulose. However, the modifying agents are generally sensitive to water so that the chemical modification can only be done by using dried CNC/CNF, and in most cases, organic solvent must

be used. Fig. 2.6 summarized some of the techniques that react with the hydroxyl groups of nanocellulose, e.g. isocyanates, epoxides, acid halides, and acid anhydrides are the most common for direct modifications[12, 91].

- **Esterification**. Esterification is widely studied in the modification, e.g., acetylation of nanocellulose. Acid anhydride is usually used as the esterification agent. It was reported that the nanocellulose acetylation can be performed without the use of any catalyst at 120 °C for 21 hours by using acetic anhydride[92]. The condition could be more mild, i.e., at 30 °C for 4 hours, with the use of sulfuric acid or perchloric acid as catalyst[93]. There is no structural and morphological changes of the nanocellulose fibers in the acetylation under both reaction conditions. But slightly morphological and crystalline structure changes were observed by use of pyridine as a solvent, acetic anhydride as acetylation agent and sulfuric acid as catalyst under the condition at 80 °C for 5 h. Organic fatty acid chlorides have been reported in the esterification of CNCs. The fatty acid chlorides could have aliphatic chains with different lengths from C_{12} to C_{18}. The reaction was conducted in toluene medium under reflux for 4 h and hydrochloric acid could be in situ formed during the reaction[94]. Therefore, triethylamine (TEA) was used as the catalyst and neutralizing agent. The obtained esterified CNC has a highly hydrophobic property, and thus they were easily dispersible in non-polar solvents for nanocomposite fabrication. Researches show that after loading the hydrophobic nature of acetylated BNC into either acrylic resins or PLA matrix, the mechanical properties, transparency features (decrease of refractive index) and low hygroscopicity of obtained nanocomposites were considerably improved[94-96].

- **Silylation**. The hydroxyl groups of nanocellulose can be partially silylated using different alkyldimethylchlorosilanes[97]. The alkyl groups in the silylating reagents could have various carbon backbones ranging from short carbon lengths of isopropyl and n-butyl to long lengths of n-

octyl and n-dodecyl. The silylation of nanocellulose reaction was reported to be carried out in toluene at room temperature and imidazole was added into the reaction system for the neutralization of released hydrochloric acid during the reaction[98]. The resulting silylated CNCs were successfully incorporated into the PLA matrix by melt-extrusion and the integrity of CNC structures were preserved after the extrusion[98]. Silylation reaction was also applied to fabricate superhydrophobic nanocellulosic surface towards non-polar liquids. Perfluorodecyltrichlorosilane and octyltrichlorosilane were grafted onto nanocellulose fibrils by the chemical vapor deposition method at elevated temperature. The silylated superhydrophobic material shows high water repelling property and high tensile strength at high relative humidity conditions. Other research shows that amino-, ene- or thiol-functionalized silanes were also covalently grafted on nanocellulose.

- **Urethanization.** The agents, isocyanates, react with hydroxyl groups to form a urethane linkage at the surface of nanocelluloses. This process is also called carbanylation. It has been reported that an excess of isocyanate was used in the reaction with CNCs and/or CNFs in toluene at the temperature between 100 and 110 °C[34, 99]. The results showed sufficient efficiency of the reaction to enhance the hydrophobicity of prepared material. The use of n-butyltindilaurate as catalyst further improved the reaction and decreased the required amount of isocyanate[34]. Because the isocyanates are highly sensitive to water, the urethanization can only be done in organic solvent medium. However, to enhance further the grafting efficiency, this process requires the transfer of nanocellulose from aqueous medium to toluene without drying to avoid the strong aggregation of nanocellulose fibrils.

- **Polymer grafting.** There are two basic strategies for grafting of polymers on the surface of nanocellulose: "grafting onto" or "grafting from"[91, 100]. The "grafting onto" approach applies

pre-synthesized polymer chains with reactive end groups in the modification of hydroxyl groups of the cellulose surface. The advantage of "grafting onto" method is that it offers the possibility of controlling the properties of the resulting material because the pre-synthesized polymer can be fully characterized before grafting. However, the steric hindrance of long polymer chains can prevent the diffusion to reach available reactive sites at the nanocellulose surface through already attached polymer layers. Therefore, the surface grafting density is generally low by using the "grafting onto" method.

Li et al. reported an epoxy-terminated copolymer of polylactide and glycidyl methacrylate (PLA-co-PGMA) prepared by free radical polymerization and its application in the surface modification of bacterial cellulose[101]. The pre-synthesized PLA-co-PGMA copolymer was characterized by Fourier transform infrared (FT-IR) and gel permeation chromatography. The grafting of PLA-co-PGMA efficiently improved the compatibility of nanocellulose in the PLA/cellulose composites. Similar efforts were reported by using epoxy-terminated PEO, amine-terminated polymers and isocyanate-terminated copolymer as grafting agents in the modification of nanocellulose[102-105]. One excellent example is that prepared polyurethane-CNC nanocomposites showed ultrahigh tensile strength and strain-to-failure with strongly improved modulus[105].

The "grafting from" approach uses polymer monomer which can be polymerized and in situ grafted on the nanocellulose fibrils using the surface hydroxyl groups as initiating sites. The typic reaction is ring-opening polymerization (ROP), in which the monomer is cyclic molecules (mainly lactones). For example, polycaprolactone (PCL) could graft on the CNC surface using stannous octoate ($Sn(Oct)_2$) as the catalyst and the reaction temperature of 95 °C in toluene[106, 107]. The grafted PCL was able to crystallize at the surface of CNCs and the resulting CNC composite could

18

be melt-blended with the virgin PCL matrix to form PCL-g-CNC masterbatches. The CNCs grafted with PCL-*b*-PLA copolymer were successfully prepared in the following research[108]. The obtained products showed distinct crystallization behavior and dispersion ability blended with a mixture of PCL and PLA. Other radical polymerization techniques, such as atom transfer radical polymerization (ATRP), were also widely used in the polymer grafting modification for advanced nanocellulose material fabrications[109].
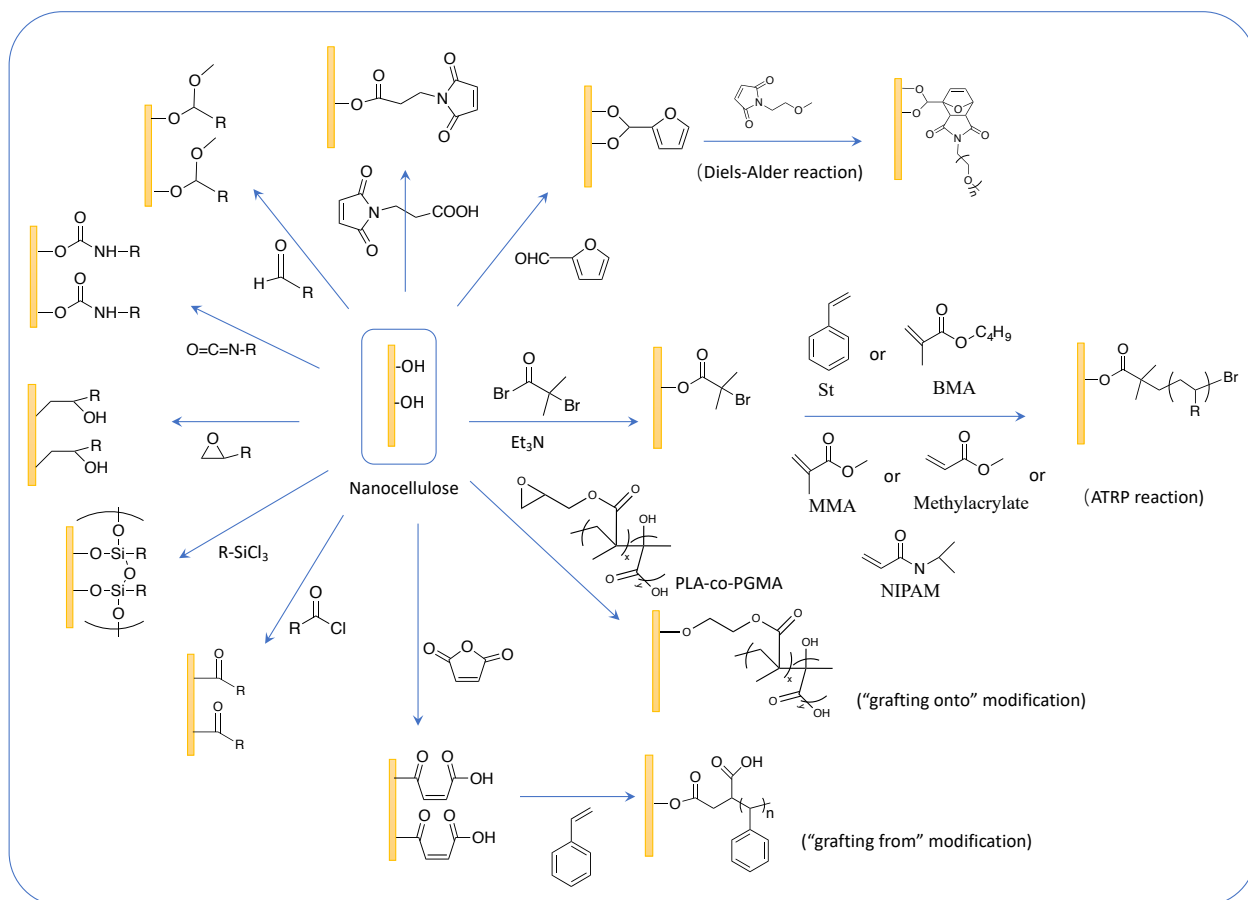
Figure 2. 6 Typical chemical modifications of nanocellulose in organic medium. St: styrene; BMA: butyl methacrylate methyl methacrylate; NIPAM: N-isopropylacrylamide; PLA-co-PGMA: polylactide and glycidyl methacrylate[103, 110, 111].

2.4 State-of-the-art engineering applications

2.4.1 Nanocellulose membranes and barriers

Membrane or film is the most common form of nanocellulose materials. Paper may be the earliest membrane application of cellulose material but it is manufactured by common cellulose fibers not nano-sized fibrils. Nanocellulose materials have many unique advantages over the common cellulose fibers. For example, nanocellulose fibrils have large specific surface areas and also the ability to form strong hydrogen bonding networks. Therefore, a strong and dense membrane material can be created via hydrogen bonding. This makes them very hard for various molecules (even for the oxygen gas molecules) to pass through. This property is excellent for barrier applications, and this is what the packaging industry is looking for.

Packaging materials require sufficient barrier performance against oxygen, water vapor, grease oil, and microorganisms. The materials based on the fossil derived synthetic plastics are not renewable and cannot be bio-degradable. Nanocellulose membranes recently have received increasing interest in sustainable packaging and barrier applications[66]. As shown in Fig. 2.7, J. Y. Zhu in the US Forest Products Lab demonstrated a facile production of films made from nano-fibrillated cellulose with optical transparency as low as 12% and strong and stiff mechanical properties. The tensile strengths and moduli of the nanocellulose films were approximately 10 and 6 times higher than the films made from common fibers[112]. Xia et al. prepared a free-standing, highly transparent nanocellulose film with excellent oxygen barrier properties[113]. The resulting CNF films showed high transparency (85–90% at 600 nm) and an extremely low oxygen permeability value of 0.007 ml μm kPa^{-1} m^{-2} day^{-1} at 23 °C and 50% relative humidity (RH). Even at 80% RH, the oxygen permeability is only 0.584 ml μm kPa^{-1} m^{-2} day^{-1}, which is 100 times lower

than most plastic films such as poly(ethylene terephthalate) and poly(vinyl chloride). Thermal treatment under elevated temperature was confirmed important in the fabrication because of the loss of porous structure after thermal treatment, resulting in higher gas barriers and lower water retention values[113, 114].
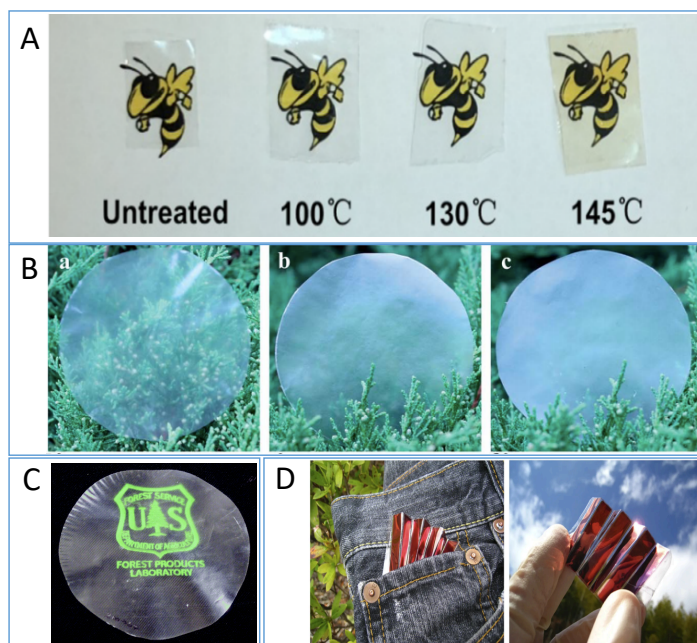
Figure 2. 7 (A) Images of transparent TOCN membranes with post thermal treatments. (B) Nanocellulose membrane with tunable haze for electronic applications. (C) Transparent Nanocellulose membranes produced in U.S. Forest Products Lab. (D) Portable solar cells based on nanocellulose membrane substrate. [92, 112, 113, 115]

Nanocellulose also has an optically transparent property and this is important for the fabrication of the sustainable substrate-based electronic devices. Research studies showed the preparation of highly transparent paper with a tunable transmission haze by rationally managing the ratio of nanoscale cellulose fibers to macroscopic cellulose fibers[115, 116]. The obtained novel transparent nanocellulose substrate achieved an ultrahigh transmittance (~96%) and ultra-high

optical haze (~60%). In another study, a nanocellulose membrane was used in portable solar cells and a high power conversion efficiency of 3.2% was demonstrated[117].

- **Technologies for nanocellulose membrane fabrication.** Different processes are theoretically applicable for the nanocellulose membrane fabrication, but in this chapter, we will briefly introduce layer-by-layer (LbL) assembly and casting evaporation and filtration (Fig. 2.8).

  - ➤ **Layer by layer (LbL)** assembly is a widely used technique for multilayer film fabrication on solid supports. By solution-dipping, spin-coating or spray-coating, two (or more) components are alternately deposited to form a very thin film[118]. The growth of the multiple layers of structures relies on electrostatic interactions or hydrogen bonds between layers. The advantages of this approach are feasible thickness control at the nano-scale and the preservation of important properties for resulting film, such as gas barrier or wet-strength. By this way, researchers have prepared layer-by-layer films of nanocellulose alternating with chitosan[119, 120] or various cationic polymers such as poly(ethyleneimine), poly(allylamine hydrochloride), and poly(diallyldimethyl ammonium chloride)[121, 122].

  - ➤ **Casting from solution and evaporation.** This technique is based on the evaporation of solvent (usually water) under moderate temperature to obtain the membrane. The evaporation rate can be controlled to void the wrinkle or shrinkage during the drying process. Organic solvents can also be used in this method. However, the main issue in this technique is the good dispersibility of fibrils needs to be achieved and for this reason, water or hydrophilic solvents are ideal systems. This procedure is not commonly applied in industrial manufacturing because of the time-consuming process of evaporation;

22

however, it is convenient for laboratory-scale research. Svagan et al. successfully cast nanocellulose membranes combined with a 50/50 amylopectin-glycerol blend[123]. The nanocellulose fibrils were well dispersed and predominantly oriented randomly in the membrane, resulting in the high tensile strength and high modulus. Xia et al also prepared high performance oxygen gas barrier by casting of TEMPO nanocellulose[113].

➢ **Filtration.** Vacuum filtration was demonstrated using nanocellulose paper-like membrane preparation. Compared with the water drainage in paper-making, the dewatering of nanocellulose is slow due to the high surface area of nanocellulose, which has more capacity to hold water than conventional cellulose fibers. However, this procedure is more efficient than casting evaporation[124]. Research showed that the nanocellulose membrane which has a heterogeneous distribution of fiber dimensions could be easily formed by vacuum filtration with all filter openings[125, 126]. Nanofibrillated cellulose was added into the ordinary wood-pulp suspension in order to achieve relatively high strength, high resistance to oxygen, and high transparency.
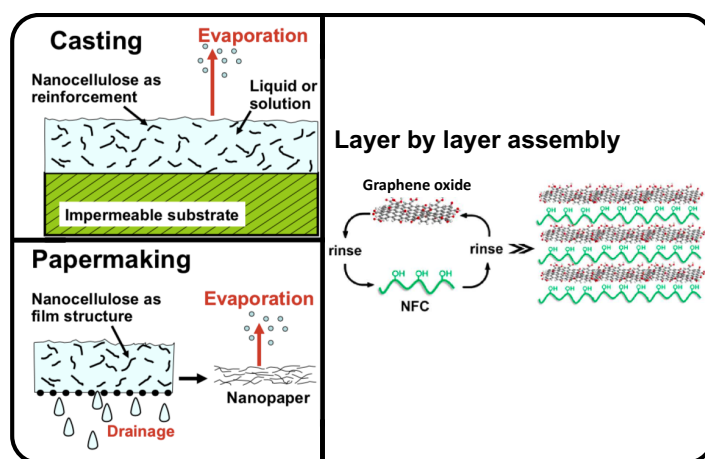
Figure 2. 8 Schematic illustration of casting, water drainage and layer by layer assembly for nanocellulose membrane fabrication.[127, 128]

- **Challenges.** There are several challenges that still exist in the nanocellulose membrane or barrier fabrication[128, 129]. (1) Nanocellulose membranes fail to block wetting or the membrane/barrier performance is compromised by high humidity or moisture. This is because nanocellulose is a highly hydrophilic material. The strategies to solve this problem could be the chemical modification of the cellulose fibrils, using waxes and other coatings on the membrane and curable cross-linking treatments. (2) Membranes break or crack due to stress above their strength at the weakest point. Strategies related to coupling agents for fibril bonding and avoiding agglomeration with low reinforcement would help to remedy the strength issue. (3) Membrane manufacturing rate is slow relative to the competition with traditional plastic films. New technologies such as spray-coating or efficient dewatering approach would be applied in the nanocellulose membrane manufacturing. (4) Oxygen barrier is inadequate to meet the stretch goals of package designers. Enhancement of hydrogen bonding and chemical crosslinking could be performed in future researches.

2.4.2 Nanocellulose-polymer composites

Nanocellulose-polymer composites are multiphasic heterogeneous materials. The polymer matrix is a continuous phase while nanocellulose is a discontinuous reinforcement phase[130]. Nanocellulose-polymer composite has improved properties compared with the pure polymer matrix phase. However, individual components in the resultant composites retain their physical identities, although the components are bonded together in the mixed phases via physical or chemical ways. Nanocellulose materials have large specific surface areas, high aspect ratios (the ratios of length by diameter), exhibiting a better mechanical strength than micro-sized fibers. In recent years, nanocellulose-polymer composites have received increasing interests among the scientific and industrial fields because the obtained materials can achieve significant

improvements in mechanical properties, dimensional stability, and solvent or gas barrier properties, with a low loading concentration of CNF fillers.
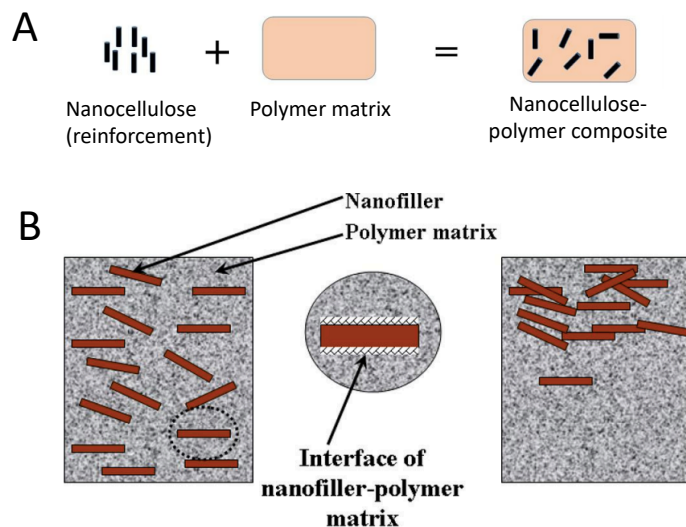
Figure 2. 9 (A) Schematic illustration of nanocellulose-polymer composites. (B) Schematic showing good dispersion and aggregation of nanocellulose in the polymer matrix[130].

Properties of nanocellulose-polymer composites depend on three major factors: properties of polymer matrix, properties of nanocellulose and the interfacial interaction between nanocellulose filler and matrix polymer. Furthermore, good dispersion and distribution of nanocellulose in the continuous polymer matrix have a significant effect on their interfacial interaction and the final properties. The forming of hydrogen bonding between the adjacent nanocellulose fibrils causes poor dispersion of nanocellulose fillers in nonpolar polymeric matrices. The aggregation of nanocellulose also increases in the polymer matrix with the reducing of nanocellulose sizes because the nano-sized fibrils have large specific surface area and tend to bond together. To solve these issues, surface modification with hydrophobic molecules could reduce the aggregation of nanocellulose in the polymer domain structure. The chemical modifications reactions, such as

esterification, silylation, carboxylation, polymer grafting with nonpolar molecules etc., are detailed in Chapter 2.3. The attached phenolic groups or long hydrophobic alkyl chains on the nanocellulose surfaces after modification could improve the hydrophobicity and the dispersion in the nonpolar polymer matrix. Therefore, in case of good dispersion, the mechanical properties of nanocellulose-polymer composites should lie between the properties of nanocellulose and polymer matrix.

- **Processing of nanocellulose-polymer composites.** There are two basic types of preparation methods for the nanocellulose-polymer composites: physical methods (including solution processing and melt mixing) and chemical method (in situ polymerization)[130].

  ➢ **Solution processing.** Solution processing is a simple method to prepare nanocellulose-polymer composites. Nanocellulose fillers can be dispersed in the polymer matrix solution by physical agitation such as mechanical stirring, ultrasonic methods or homogenizing, etc. After obtaining the homogeneous mixture, the composites can be prepared by casting or solvent evaporation to obtain the membranes or films. Water could be an ideal choice for the processing medium in the preparation of nanocellulose composites with water-soluble polymer latex such as PVA. This is because nanocellulose has good dispersion ability in water due to plenty of surface hydroxyl groups. However, most of engineering polymers, such as polyethylene (PE), polypropylene (PP), polyurethane and polylactic acid (PLA), are hydrophobic and can only be dissolved in organic solvents[130]. Therefore, the compatibility and distribution of hydrophilic nanocellulose fibrils in organic solvent is a big challenge.

➢ **Melt mixing**. By melt mixing, nanocellulose can be dispersed into a melted polymer matrix, and extrusion method is generally used for the nanocomposites fabrication[131]. Homogenous distribution of nanocellulose in the polymer matrix is critical in this method to improve the mechanical properties of prepared nanocomposites because the dispersion is difficult in the high viscous melted polymer. Janak Sapkota et al reported a nanocellulose-low-density polyethylene (LDPE) composite with significantly improved mechanical characteristics and homogeneous appearance using an organic-solvent-free two-step process[132]. This is achieved by first mixing an aqueous slurry of an LDPE powder (average particle size of <600 μm) and aqueous suspensions of CNCs. Then, removing most of the water and extrusion under elevated temperature at 170 ºC were conducted to obtain the composite.

➢ **In situ polymerization.** In this method, nanocellulose could be impregnated in monomer solution, then, in situ polymerization was conducted in the processing of nanocellulose polymer nanocomposite. For example, an efficient approach for the one-pot synthesis of a ready-for-use stable nanocomposite was reported by a mini-emulsion polymerization of styrene (Sty) and 2-ethyl hexylacrylate (EHA) in the presence of cellulose nanocrystals (CNCs) with methacryloxypropyl trimethoxysilane (MPMS) as a coupling agent (as shown in Fig. 2.10)[133] . Nanocellulose could be adsorbed on the surface of the polymer particles due to the hydrogen bonding with silanol groups. During the film formation, condensation reaction between the surface silanol groups of the MPMS and the hydroxyl groups of nanocellulose would take place to form uniformly distributed nanocomposite[134].
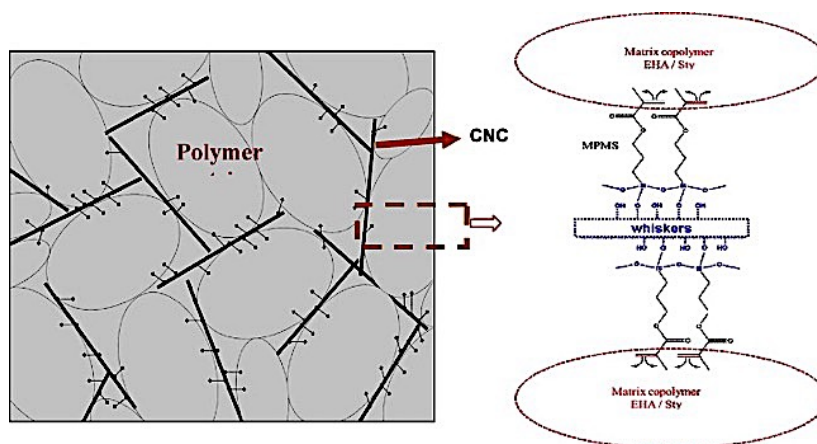
Figure 2. 10 Schematic structure of CNC-polymer composite in situ polymerized with methacryloxypropyl trimethoxysilane (MPMS) [134].

- **Nanocellulose-polylactic acid (PLA) composites.** PLA is a biodegradable polymer and receives increasing commercial interest in diverse applications. The nanocellulose-PLA composites exhibit high mechanical strength, thermoplastic characteristics and biocompatibility[135]. The challenge for high-performance PLA nanocomposites production is to improve the compatibility between nanocellulose and PLA polymer matrices in order to increase the dispersion of nanocellulose particles in PLA matrix. There are many research reports on biodegradable nanocellulose-PLA composites films and membranes for engineering applications. Erin et al. reported the fabrication of nanocomposite film by blending different amounts of CNC in polylactic acid using melt compounding, melt fiber spinning and compression molding[136]. The results show that 1 wt% CNC addition in the PLA increased elastic modulus of the nanocomposite, but the elastic modulus was decreased with further addition of 2 wt% and 3 wt% CNC in the PLA. In order to improve the compatibility of nanocellulose with PLA, nanocellulose (prepared from cassava residue by mechanochemical method) was hydrophobically modified with stearic acid reported by Huang et al[137]. When 1% modified nanocellulose modified nanocellulose was added, the tensile strength of the nanocomposite films is enhanced by 40.03%, the elastic modulus is

enhanced by 55.65% compared to the neat PLA, but the flexibility of the film decreases. Arjmandi et al. reported a nanocellulose/PLA/montmorillonite hybrid nanocomposite with largely enhanced mechanical properties, but the tensile strength and elongation at break were decreased when the amount of nanocellulose was increased to 3 wt%[138]. In another study by Goffin et al., poly(ε-caprolactone) (PCL) grafted nanocellulose was used to improve the storage modulus of nanocomposite[139]. Moreover, many researchers summarized that the nanocellulose amount to PLA is critical to homogenous dispersion in polymer matrices for improving intermolecular interaction between nanocellulose fibrils and PLA matrix[138].

2.4.3 Nanocellulose aerogel

Nanocellulose aerogel is an ultralight and flexible foam-like material made by nanocellulose. This kind of material has a high porosity and specific surface area which is similar to silica-based aerogels but much softer and more flexible. Nanocellulose-based aerogel has been defined by previous reports as "a highly porous solid of ultra-low density and with nanometric pore sizes formed by replacement of liquid in a gel with gas"[140]. In some cases, CNF-derived aerogel is strong with the moduli reaching as high as 6 GPa and densities as low as 0.0046 g/cm^3 (99.7% porous)[141]. These properties expand their potential uses in applications requiring porosity and mechanical flexibility and strength.

Nanocellulose-based porous aerogel can be fabricated by using two methods: supercritical drying and ice sublimation (freeze-drying). Freeze-drying is commonly performed using a vacuum oven at low temperature (-55 °C) and low pressure (≤ 0.02 mbar). The freeze-drying process is often combined with ice templating (IT)[142]. The main challenge in the nanocellulose aerogel fabrication is how to maintain the porous structure during solvent (water) removal. The pores could

be deformed, resulting in warping and collapse or cracking of the porous material, by capillary pressure-induced stresses during the evaporation of water.
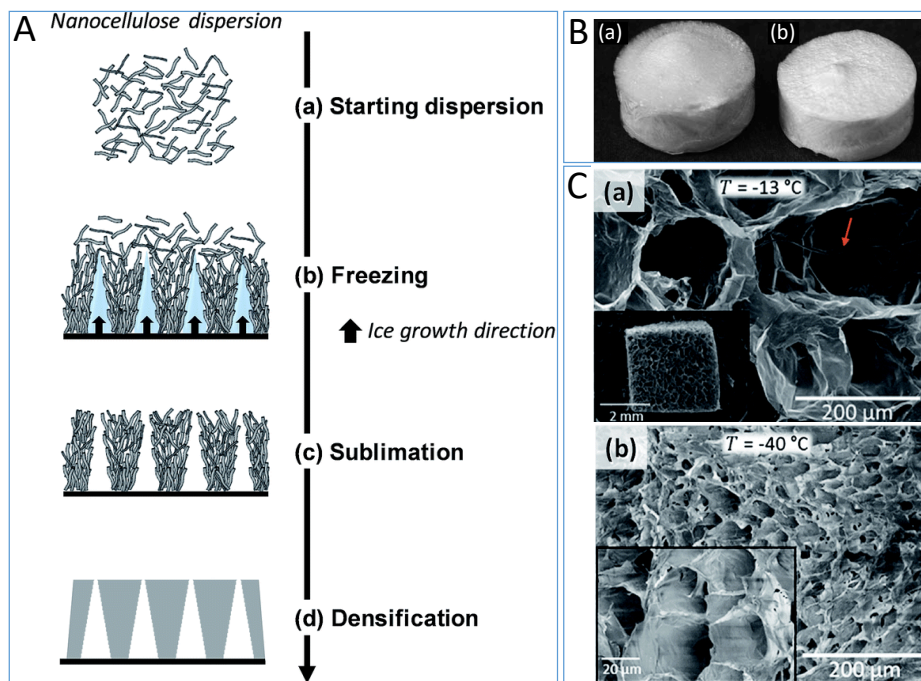
Figure 2. 11 (A) Schematic illustration of the directional ice-templating effect in the freezing of nanocellulose suspension[143]. (B) Images of nanocellulose aerogel obtained by freeze-drying[144]. (C) Illustration of pore structures obtained by homogeneous freezing under different temperatures[145].

- **Homogeneous freezing.** In the freeze-drying, the liquid medium (usually water) in the nanocellulose gel is mainly eliminated by sublimation. The fibrils maintain frozen state during the whole process. This is the key factor to prevent pore structural collapse[141, 142]. Therefore, liquid freezing under the low temperature plays an important role in the pore structure formation (including pore morphology and pore distribution) of nanocellulose aerogels. The freezing step usually conducted by either dipping the nanocellulose suspension in a liquid nitrogen bath or placing it in a freezer. The liquid

crystallization depends on the cooling rate and temperature[146]. Rapid freezing leads to a homogeneous pore structure and increased aerogel porosity because of inhibition of the agglomeration of cellulose fibrils and the growth of ice crystals. However, slower freezing can result in larger pores after ice sublimation. Zhang et al. investigated three different cooling methods by liquid nitrogen (-196 °C for 30 min), an ultralow temperature freezer (-80 °C for 12 h), and a conventional refrigerator (-20 °C for 24 h)[147]. It was found that effective inhibition of the self-agglomeration of nanocellulose fibrils could be achieved by liquid nitrogen freezing due to the rapid formation of ice crystals and this produced a uniform and smooth surface structure of obtained nanocellulose aerogel.

Due to the high surface tension of water, the chain entanglement and self-agglomeration of nanocellulose reduces the specific surface area of obtained aerogel. Low interfacial tension alcohol, such as tert-butyl alcohol was used in the nanocellulose aerogel preparation to avoid the agglomeration problem[148, 149]. The hydroxyl group can form a hydrogen bond with nanocellulose fibrils and the steric hindrance of butyl groups can prevent the agglomeration of nanocellulose. Research showed that tert-butyl alcohol can effectively protect the porous structure of nanocellulose through solvent exchange and freeze-drying[148, 150].

- **Directional ice templating.** Directional ice templating will be produced under a directional thermal gradient (Fig. 5). Homogeneous freezing produces isotropic foams with cellular 3D cell structure. However, unidirectional ice templating results in formation of a honeycomb structure, which is 2D pores aligned parallel to the freezing direction[151]. This is caused by the directional crystallization of ice in the freezing.

During the directional ice templating, the redistribution and orientation of nanocellulose

fibrils could be occurring, which would produce particular mechanical properties.

Modification can be conducted to improve the properties of nanocellulose aerogels for various

applications. Cross-linking and polymer grafting are commonly used in the improvement of

aerogel stability and hydrophobic modification. For example, Zhai et al. created superhydrophobic

cross-linked CNF and PVA aerogel microspheres by the combination of emulsification and

followed thermal chemical vapor deposition of methyltrichlorosilane[152]. The obtained material

can be used as an effective oil/organic solvent absorbent. Zhang et al. report a TEMPO-oxidized

nanofibril aerogel that can be used for fast and high efficient molecules or ions extraction, e.g., the

removal of phenol and Cu^{2+} from water[153]. Inorganic metal nanoparticles and metal oxides were

also introduced in the nanocellulose aerogel preparation either by typical precipitation or chemical

vapor deposition on the surface of aerogels. Nanocellulose aerogel material has broad applications,

however, the drawbacks of the preparation method, i.e., freeze-drying method, requires long

processing times and high energy consumption[141].
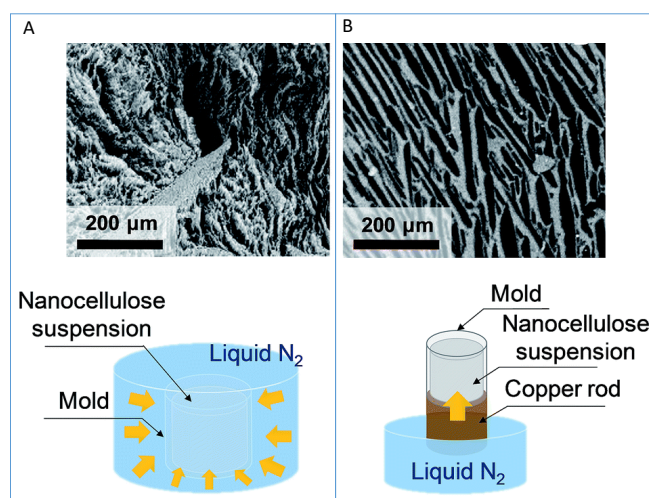
Figure 2. 12 (A) Illustration of homogeneous freezing and obtained CNF aerogel pore structure (B)

Illustration of unidirectional ice templating and obtained pore structure [154].

2.4.4 Nanocellulose filaments

Highly crystallized individual cellulose fiber shows extraordinary mechanic properties. The theoretical modulus reaches as high as 173 GPa due to the ordered intramolecular hydrogen bonding[155]. However, The continuous macro-fibers made from nanocellulose are difficult to maintain the extraordinary performance of individual nano-fibers. Most commonly prepared nanocellulose filaments are reported with the tensile strength of 100-400 MPa and Young's modulus of 10-20 GPa[20, 156-158]. The significant performance loss could be possibly caused by several reasons: **(a)** intrinsic defects existed in nano-cellulose materials; **(b)** length limitation of highly crystallized individual cellulose fibers; **(c)** boundaries, voids and week bonding among the nano cellulose fibers and **(d)** misalignment of the nanofibers[159]. In fact, the loss in mechanical properties during the transition from nano individual fiber to practical macroscale fiber frequently happens in the engineering processing. It can be demonstrated by the cases of carbon nanotubes and graphene. Carbon nanotubes can only be fabricated into moderate mechanical fibers (~200-300 MPa tensile strength) but the tensile strength of individual carbon nanotube reaches a high level of 63 GPa[12, 22].

Various strategies have been pursued to align cellulose nanofibers to remedy the imperfections within cellulose fibers. Alignment of cellulose nanofibers in filaments has several effects that can improve their strength: **(1)** Alignment reduces voids or pores among cellulose nanofibers; **(2)** Alignment increases the contact area among fibers, which will lead to increase of bonding force between fibers; **(3)** The generated long period stacking structure can improve the stress performance of filament. Magnetic and electric fields are early applied in the fiber alignment control[160, 161]. However, considering the sophisticated operation of magnetic and electric field,

shear orientation is a simple method and it has a greater potential practically to improve fibril alignment.

Hydrodynamic alignment is one of the shear orientations that can be easily achieved. As the flow accelerate or decelerate, fibrils in the flow will tend to orient themselves perpendicular (deceleration) or parallel (acceleration) to the flow direction[162]. This could occur in spinnerets as well as in spinning using a syringe. Håkansson reported a process combining hydrodynamic alignment and dispersion-gel transition to produce nanocellulose filaments from a low-concentration of nanofibrils in water[163]. The preferential fibril orientation along the filament direction can be controlled by the process parameters, such as flow rate, liquid pressure and fibril concentration. Furthermore, Mittal et al. designed a double flow-focusing channel used for CNF assembly[164]. The Young's modulus reached up to 86 GPa and the tensile strength reached 1.57 GPa. Wet-drawing and wet-twisting are other strategies to improve the orientation of nanocellulose in fabricated filaments. As shown in Fig. 2.13, Wang et al. prepared a super-strong, super-stiff macrofibers with bacterial cellulose nanofibers trough the wet-drawing and wet-twisting[165]. The obtained nanocellulose macrofibers reached a high tensile strength (up to 826 MPa) and an extraordinary specific Young's modulus of 36.4 GPa.
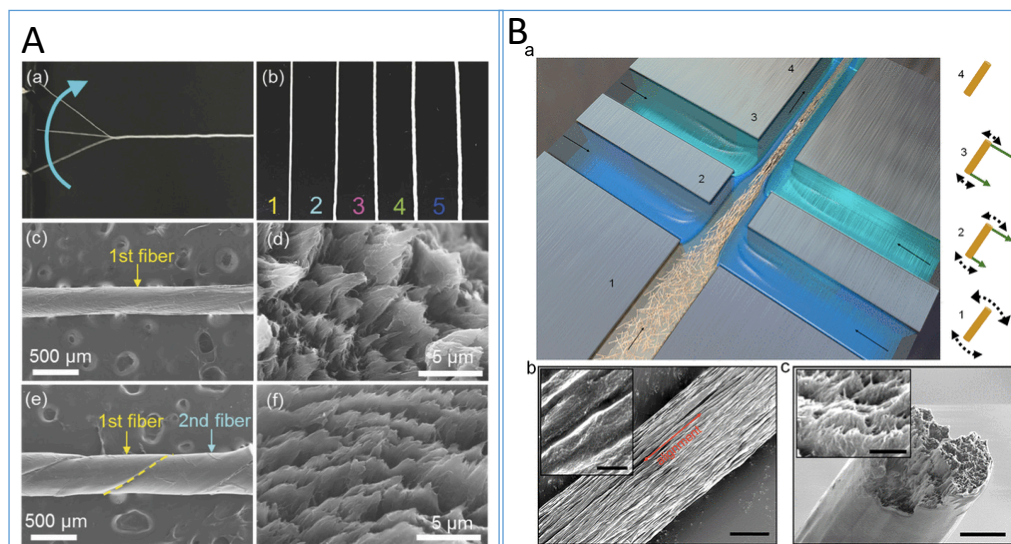
Figure 2. 13 (A) Prepared bacterial cellulose nanofibers trough the wet-drawing and wet-twisting method. (B) Schematic showing of the double flow-focusing channel for CNF filament fabrication and the SEM images of obtained nanocellulose filaments[164, 165].

Besides the orientation, the structure and inter-fiber bonding may be the other factors affecting the mechanical properties[166, 167]. Therefore, covalent or ionic crosslinking of cellulose fibers are used to enhance inter-fibril bonding and reduce voids among fibers. Especially in high-moisture condition, the mechanical properties would decrease substantially since the hydrogen bonds are weakened. Yao et al. studied a Fe^{3+} and Cu^{2+} crosslinked nanocellulose filament, which exhibited Young's modulus of 16.4 GPa and tensile strength of 248.6 MPa[20]. Owing to the high strength, stiffness and biodegradability, CNF based filaments could be used in a broad variety of applications, such as functionalized to produce conductive or magnetic material, composites, nonwovens, textiles, bioactive or flame-retardant structures[168].

CHAPTER III PROBLEM ANALYSIS AND OBJECTIVES

Objective 1 Fabrication of super-hydrophobic nanocellulose membranes.

Problem analysis: Cellulose nanofibrils (CNFs), as reviewed in Chapter 2, have received great interest in advanced materials development, such as packaging materials, soft substrates for electronic devices and reinforcing fillers for polymer composites. As a packaging or substrate material, the advantages of CNF, however, are often limited by their intrinsic highly hydrophilic property that would easily be eroded by water and moisture. It is a promising way to fabricate cellulosic superhydrophobic surfaces which completely cannot be wetted by water. Surface roughness and low surface energy are two critical factors to increase water repellence. Coating of nanoparticles, such as nano SiO_2 or TiO_2 particles, on the surface of nanocellulose fibrils is one of the methods to increase surface roughness, but the nanoparticle aggregation and coating stability are serious issues. Plasma etching is another method to create nano-scaled roughness; however, plasma treatment is a tedious and costly process that can only be applied on a small scale. Surface chemical modification is important to reduce surface energy. In order to reach superhydrophobicity, fluorine-containing compounds are commonly used in the modification, but fluorine-containing compounds are not safe and high cost. To overcome these challenges, it is required to develop a novel method that is economical and facile to operate, and does not use fluorinated chemicals.

Objective-1: The objective mainly focuses on superhydrophobic nanocellulose fabrication. The key strategy for this objective is to develop a low-cost and facile method to make the surface roughness on the nanocellulose membrane and simultaneously conduct the chemical modification using non-fluorinated chemicals. The two factors, the roughness and chemical modification, are essential to the water repellent performance. In this objective, we will use template-pressing

36

method to make the patterned surface roughness which is a high-efficient method that could be completed in several seconds. For chemical modification, we will choose the chemicals containing long C-C chains to reduce the surface energy of nanocellulose fibers. The safe and cheap industrial products such as mineral wax and alkyl ketene dimer (AKD, one of paper sizing agents) are potential chemicals in the modification.

Objective 2 Reinforcement of PLA composite film by using in situ modified nanocellulose fibrils.

<u>**Problem analysis:**</u> Nanocellulose can be used as the reinforcing filler for polymer composite fabrication. The main challenge for nanocellulose is poor compatibility with hydrophobic polymer matrix because cellulose is typically a hydrophilic material and nanocellulose is prepared in water solution. Surface chemical modification is the most common method to solve the compatibility problem. Unfortunately, all the currently reported methods for hydrophobic nanocellulose surface modification can only be conducted either by using dried CNF or in organic solvent. Nanocellulose drying causes hornification and agglomeration thus losing their unique properties in the modification. Organic solvent exchange for CNF is a time-consuming and tedious process and could cause environmental pollutions. As a result, we expect that the chemical modification of CNF could be conducted in situ in water suspension to avoid the CNF drying or solvent exchange for the modification.

<u>**Objective-2:**</u> This objective is to incorporate CNF fibrils as fillers into PLA polymer matrices to improve their mechanical strength. PLA is considered as "green" material that is sustainable and biodegradable. The challenge in this objective is that the PLA polymer matrix is hydrophobic which is not compatible with the hydrophilic CNFs. Our strategy is to convert CNF fibers from

hydrophilic to hydrophobic firstly by using chemical modification. In this objective, we will in situ modify the CNF fibers in water suspension with AKD emulsion. The emulsion used in the modification can avoid the de-activation of AKD with water and thus enable the successful modification of CNF in water suspension.

Objective 3 Reinforcement of PLA composite film using 3D CNF frameworks with controlled porous structures.

Problem analysis: How to uniformly distribute CNF fibrils in the polymer matrix is another challenge for CNF and polymer composite fabrication. The discontinuity of interfacial interaction between nanocellulose fillers and polymer matrix will weaken the mechanical properties of resultant nanocomposites. The possible reasons for the non-homogeneous dispersion of nanocellulose fibrils in their polymer composite could be attributed to, firstly, the hydrophilic nature of nanocellulose, which is not compatible with most of engineering polymer matrices due to their hydrophobic property, such as PLA; secondly, the hornification and agglomeration during the pretreatment of CNF fibrils.

Objective-3: This objective is to prepare a high strength composite film by combining a PLA polymer matrix with 3D porous CNF frameworks as reinforcement. In traditional nanocellulose composite fabrication, the uniform distribution of nanocellulose fibrils in the polymer matrix is a challenge. To solve the nonuniform distribution issue, we will use nanocellulose 3D porous frameworks as reinforcement in the composite fabrication. The high porosity and large specific surface area will result in strong interaction with PLA polymer matrix and significant improvement of mechanical performance.

Objective 4 Preparation of CNF filament using different chemical and mechanical approaches

Problem analysis: Highly crystallized individual cellulose fiber shows an extraordinary mechanic property as reviewed in Chapter 2. However, transferring the extraordinary performance of individual nanofibers to a practical nanocellulose filaments remains a challenge. This could be attributed to defects, voids or week bonding existing in the practical nanocellulose filaments, and mis-alignment of the nanofibers. To increase the fiber orientation and reduce the defects and voids, hydrodynamic alignment is the common approach in reported literature. Special experimental setups have been designed for hydrodynamic alignment of nano-fibrils; however, hydrodynamic fiber orientation is sensitive to the operation parameters and is difficult to be repeated. To overcome these challenges, we will combine the hydrodynamic alignment and chemical bonding of fibrils to improve the interaction between nanofibers. In addition, wet-stretching and wet-twisting could be applied because the wet-stretching process is believed that it helps to hydrodynamic align nanocellulose fibers and improves the ordered orientation along the fiber axis and wet-twisting can increase the bonding force between interacting fibers.

Objective-4: This objective is to prepare CNF filaments by using wet-spinning. To improve the mechanical strength of the filament, chemical bonding and hydromechanical fiber alignment would be the two possible ways to increase the interaction between fibrils. In the chemical bonding, we will use binding agents so that the fibers can be covalently bonded together. For hydromechanical fiber alignment, we will optimize operational conditions for wet-spinning, such as spinning speed and nozzle diameter. By this way, fiber orientation and thus the mechanical strength will be improved. In addition, to further increase the fiber interaction, wet-stretching and wet-twisting of filament will also be conducted.

CHAPTER IV Surface Structure Patterning for Fabricating Non-fluorinated

Superhydrophobic Cellulosic Membranes[1]

4.1 Introduction

Natural cellulose materials (e.g., cotton and wood fiber) have been used in broad applications, such as paper manufacturing, textiles, packing and building materials, and so on. Compared to the synthetic petroleum-derived fibers, cellulose materials have the advantages of biodegradability, renewability, and nontoxicity[13, 17]. Cellulose nanofibrils (CNF) and cellulose nanocrystals (CNC) are nanosized cellulose materials, and the abundant surface hydroxyl groups enable facile functionalization to create novel materials[169], such as stimuli-responsive nanomaterials[170, 171], smart electronic devices, and wearable electronic device packaging[172, 173]. However, cellulose fibers are intrinsically hydrophilic and can absorb water or moisture, leading to erosion in humid environments. Fabricating hydrophobic or superhydrophobic surfaces is a promising way to enhance the moisture resistance of cellulose materials and minimize the water erosion issues, especially for the materials used in humid environments, such as packaging or building materials.

Superhydrophobic surfaces have attracted great scientific and industrial interest for decades. Many superhydrophobic surfaces have been created on silicon, glass, metal plate, metal mesh and plastic substrates[174, 175]. For silicon surfaces, well patterned and micrometer-sized cylindrical pillar arrays and mushroom-like arrays were fabricated[176-178]. The water contact angle can reach very high because of the re-entrant structure in the side wall of pillars. Nano-particles and needle-like or lotus-leaf-like nanostructures were introduced on the metal surface to generate the hierarchical roughness for improving the hydrophobicity[179-183]. These results provide different

rational strategies for water-repellent or superhydrophobic fabrication. The key factors between them are surface roughness and low surface energy that can repel and support water droplets to avoid spreading[178].

For cellulose based material, there are various strategies that can reach superhydrophobicity. The first strategy is to increase surface roughness using nano-particles, such as nano SiO_2 or TiO_2 particles, through in-situ wet deposition, dip coating or spray coating on the material surface[184-186], but the nano-particle aggregation and coating stability are obvious issues. Another method is to create nano-scaled roughness on the surface of fibers directly by etching, for example, plasma pretreatment[187-190]. However, plasma treatment is a tedious and costly process that only applied in a small scale. To achieve low surface energy, fluorine-containing compounds commonly used in cellulose fiber modification[191-193]. Because fluorine-containing compounds are not safe and high cost, developing an economical and facial method that does not use fluorine chemicals and easy to scale up is of great interest.

Herein, we present a facile fabrication of pattern featured superhydrophobic cellulose membrane with a quick templated pressing method and non-fluorinated chemical modification. The stainless-steel mesh, which possesses regularly arranged mesh holes, functions as template or mold in the pressing method. By pressing the nano-cellulose slurry on the mesh, the cellulose slurry fills into the mesh holes and the shape is maintained after removal from the mesh mold. After drying, the pillar featured pattern can be well-established on the surface of cellulose membrane (shown in Fig.4.1). Different from the pillar array fabricated on the silicon wafer surface, cellulose fibers inherently have sub-micron or nanometer structures. The micro-sized pattern and nano-sized cellulose fiber network creates a hierarchical structure that can improve the superhydrophobic properties. After simple chemical modification with non-fluorine chemicals,

41

such as AKD, wax or isocyanate, the fabricated cellulose membranes show a good superhydrophobic property. This method has significant advantages: (1) The pattern fabrication by templated pressing can be quickly completed even in several seconds and is easy to scale up. (2) The featured sizes of patterns are tunable by using different mesh sizes of metal or plastic meshes, which is readily accessible in the industry. (3) Low cost and non-fluorine compounds are used in chemical modification through simply heating.
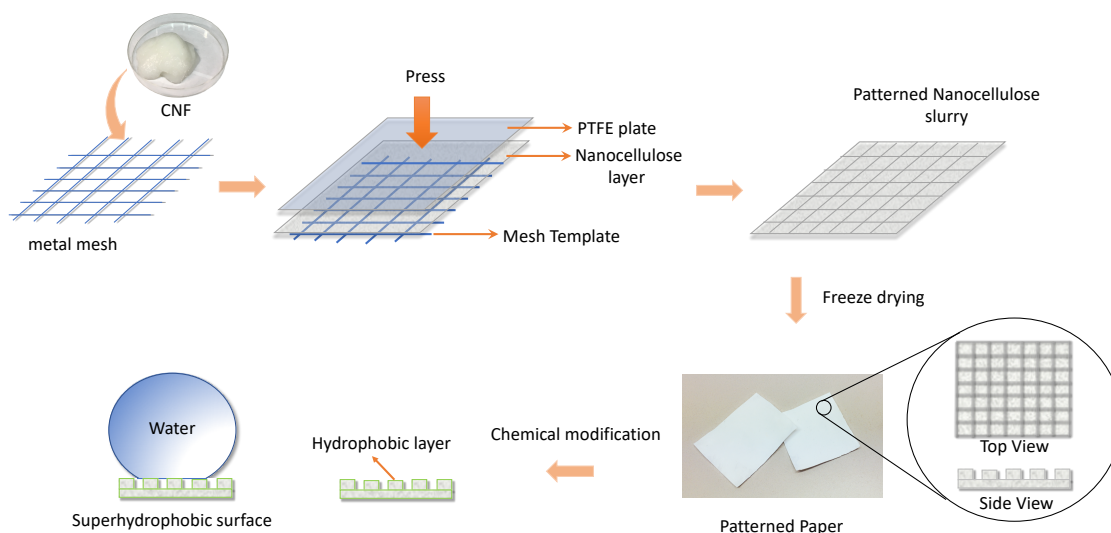
Figure 4. 1 Schematic diagram of pressing process for preparation of patterned surface nano-cellulose membrane.

4.2 Experimental Section

4.2.1 Materials

Cellulose nanofibril slurry (CNFs, fiber content 3.4%) prepared from mechanically refined bleached softwood Kraft pulp was purchased from the University of Maine Process Development Center. Toluene diisocyanate (TDI) was purchased from TCI America. Hexadecanol ($C_{16}OH$) and

solvents toluene, benzene and tetrahydrofuran (THF) were purchased from Alfa Aesar. Polymers, including poly methyl methacrylate (PMMA, $M_w\sim200,000$), polystyrene (PS, $M_w\sim250,000$), low density polyethylene (LDPE), polypropylene (PP, $M_w\sim230,000$) and polyvinyl chloride (PVC, $M_w\sim250,000$), solid wax and solid alkyl ketene dimers (AKD) are industrial grade products.

4.2.2 Preparation of surface textured nanocellulose membrane and chemical modification

Cellulose nanofibril slurry was coated on stainless steel mesh to form a thin layer of cellulose nano-fibrils with a thickness about 2-3 mm. The cellulose layer along with the mesh was pressed with a hydraulic machine under the pressure of 1 MPa and maintained for 10 seconds. About 70% of water in the nanocellulose slurry was removed after pressing. A half-dried cellulose membrane with pressed pattern was obtained and was frozen in liquid nitrogen for 15 min. The cellulose membrane was freeze-dried under the vacuum of 20 mTorr (VirTis Freezemobile 25EL sentry 2.0) for 1 day.

Before chemical modification, the modifier was dissolved in organic solvent to form a homogenous solution. Eight different modifiers were chosen for the chemical modification: PMMA, PS, PE, wax and AKD were dissolved in toluene respectively; PVC was dissolved in THF; PP was dissolved in benzene; TDI and hexadecanol ($C_{16}OH$) at the molar ratio 4:1 were used as co-modifiers and dissolved in toluene. All the modifier concentrations dissolved in solvents are 5 wt.%. The prepared cellulose membrane was immersed in the modifier solution and heated to boiling for 5 min. After immersion, the cellulose membrane was removed from the modifier solution. Excess fluid on the membrane was then absorbed with tissue paper (KimWipe, Kimberly-Clark Co.). The obtained membrane was then placed in an oven at 100 °C for 10 min to evaporate solvent and strengthen the polymer coating layer.

To make useful comparisons, different textured paper substrates (copy paper (Staples, 92 bright), paper towel (Uline EZ Pull Sr.) and filter paper (Whatman, qualitative grade 1)) were used in the chemical modifications with AKD, wax and TDI+C_{16}OH. The procedures were the same as the treatment of prepared membranes.

4.2.3 Template modification for tuning of asperity size and patterned coating on substrate

To obtain metal meshes with different pore sizes that are not able to be purchased from the supplier, an electro-deposition of Cu on the metal meshes was conducted. Experimentally, the metal mesh was used as the working electrode which connects to the negative electrode of external direct current power source. A copper plate was used as the counter electrode connected to the positive electrode of power source. The metal mesh and copper plate were immersed in 0.1 mol l^{-1} $CuSO_4$ solution. The deposition current was controlled at 20 mA. During the electrolysis, the copper was deposited on the metal wire of mesh. Therefore, the diameter of metal wire was increased and the mesh hole was decreased. The electro-deposition treated metal mesh was directly used as template for tuning of asperity size in the patterned cellulose membrane fabrication

The pattern coating was conducted on the substrate of copy paper (Staples, 92 bright). A thin layer of nanocellulose slurry (3.4 wt%) with a thickness about 2-3 mm using a doctor blade with controlled thickness was coated on copy paper substrate by glass rod doctor blade, then covered with a mesh template. The following pressing and freeze-drying procedures were the same as the patterned cellulose membrane fabrication described in 4.2.2. The pattern coated on copy paper was obtained after freeze-drying and was chemically treated with wax, AKD or TDI + C_{16}OH respectively.

4.2.4 Wetting ability measurement

Static water contact angle measurement of patterned nanocellulose membrane was performed using ramé-hart contact angle goniometers 100-25-A model (ramé-hart instrument co.) at ambient environment. A droplet of 8 μL deionized water was placed on the prepared membrane surface for the measurement. Dynamic advancing and receding contact angles were measured by increasing and decreasing the droplet volume, with an initial volume of 8 μL and a step change of 0.3 μL. The contact angle measurements were repeated five times for each fluid. Different fluids including coffee, sweet tea, Sprite®, red wine, Fanta® and Coca, which were obtained from Walmart supermarket, were used in the static contact angle measurement with 8 μL of applied fluid.

Long-term contact angle measurement and knife scratching test were completed. In the long-term contact angle measurement, 8 μL of deionized water was used and the contact angle was continuously measured in 20 min. The scratch test was performed using a knife to longitudinally and transversely scratch the patterned surface, and then the water contact angle was measured.

4.2.5 Other characterization

The surface morphology of aerogels was examined via LEO 1530 thermally assisted field emission scanning electron microscope (**FE-SEM**) with an acceleration voltage of 10 kV. Samples were gold-sputtered prior to SEM images.

Optical Microscopic images were obtained using Leica DMLM light microscope connected to a color video camera. The 3D structure simulation is calculated from the brightness value of each image pixel using a Matlab program, based on the condition that light linearly decays with the passed thickness cellulose membrane.

Fourier transform infrared (**FT-IR**) spectra of both original and modified samples were measured by KBr pellets on a Bruker Vertex 80V spectrometer in the scan range of 4000-400 cm^{-1} of 32 scans with resolution 4 cm^{-1}.

Thermogravimetric Analysis (**TGA**) and Derivative Thermogrametric (**DTG**) were performed using Perkin Elmer STA600 simultaneous thermal analyzer to evaluate thermal degradation of original and sulfonated sample in the range of 40-600°C at a rate of 10°C/min under a nitrogen flow rate of 20 ml min^{-1}.

4.3 Result and discussion

4.3.1 Morphology of surface roughness

Figure 4.2 shows the patterned surface of the cellulose membranes with 4 different characteristic pattern sizes (noted as membrane-1 to -4 in A to D respectively). The left column and the second left column show the top view and side view of SEM images. From the top view images, the cellulose membrane surfaces exhibit a lattice-like pattern that is molded by the stainless mesh. The islands highlighted by red lines are molded pillar locations. The 3D structures are clearly illustrated from the side view, which shows regularly arranged square pillars distributed on the surface of nano-cellulose membrane. Four different meshes with various mesh sizes were used for the pillar patterns fabrication. For the membranes from 1 to 4, the pillars show different widths of 349.5±3.5, 110.0±4.7, 60.1±2.9 and 36.3±3.7 μm respectively (summarized in Table 4.1). The pillar heights of the 4 different membranes are 70.7±3.2, 39.3±4.1, 19.5±3.1 and 19.8±2.9 μm according to the side view of SEM images.

The optical microscopy images of the 4 different membranes are shown in the third left column in Fig. 4.2. The images illustrate bright and dark patterns based on light transmission. The thicker the location is, the darker it will show in the image because of the light absorbance and light scattering. We obtained 4 different optical microscopy patterns that are similar to the SEM top view images. According to Beer–Lambert law, the transmittance, which reflects brightness in the image, depends on the light transmitted path length through the membrane. Assuming that the light transmittance has a linear relationship with the light path length, the thickness profile of the membranes can be calculated based on the brightness data of optical microscopy images. The simulation results are shown in the right column in Fig. 4.2. The red color shows high thickness locations and the blue color shows the places with low thickness. The simulation results reveal the 3D profiles of pillar-like patterns on the nanocellulose membranes.

Table 4. 1 Parameters of different patterned membranes

#	Pillar width (μm)	Gap between pillars (μm)	Solid area fraction (%)
1	349.5 ±3.5	263.3±4.3	0.33±0.005
2	110.0±4.7	117.0±4.5	0.24±0.014
3	60.1±2.9	68.3±3.4	0.22±0.016
4	36.3±3.7	88.6±3.8	0.08±0.013
5	89.0±4.2	149.7±4.8	0.14±0.010
6	49.5±4.5	191.3±4.9	0.04±0.006

Different from the pillar array built on the Si wafer[176, 194], the mesh molded nanocellulose pillars do not have a smooth surface because nanocellulose fibers are inherently in Nano-size. As a result, nano and sub-micron scaled roughness are presented on the molded pillars surface. Figure 4.4 shows the magnified SEM images of the cellulose pillars. We can see that the pillar surface is not perfectly smooth but plenty of nano-cellulose fibers randomly distributed on it. The magnified 3D surface profile simulation clearly shows the sub-micron roughness on top of the patterned pillar

(shown in Fig. 4.3). The nano-cellulose fibers were shown in magnified SEM images (E) and (F) in Fig. 4.4. The diameter is several nanometers. Due to the surface -OH groups of cellulose nanofibers, agglomerated bundles are formed by H-bonding between neighboring nanofibers. Therefore, the cellulose pillar maintains molded shape after removing the mesh template. Cellulose pillars constitute the ordered pillar array and disordered nanofibers contribute to the nano-scaled roughness on each pillar. Herein, multiple scaled roughness and patterned structure are fabricated on the cellulose membrane.
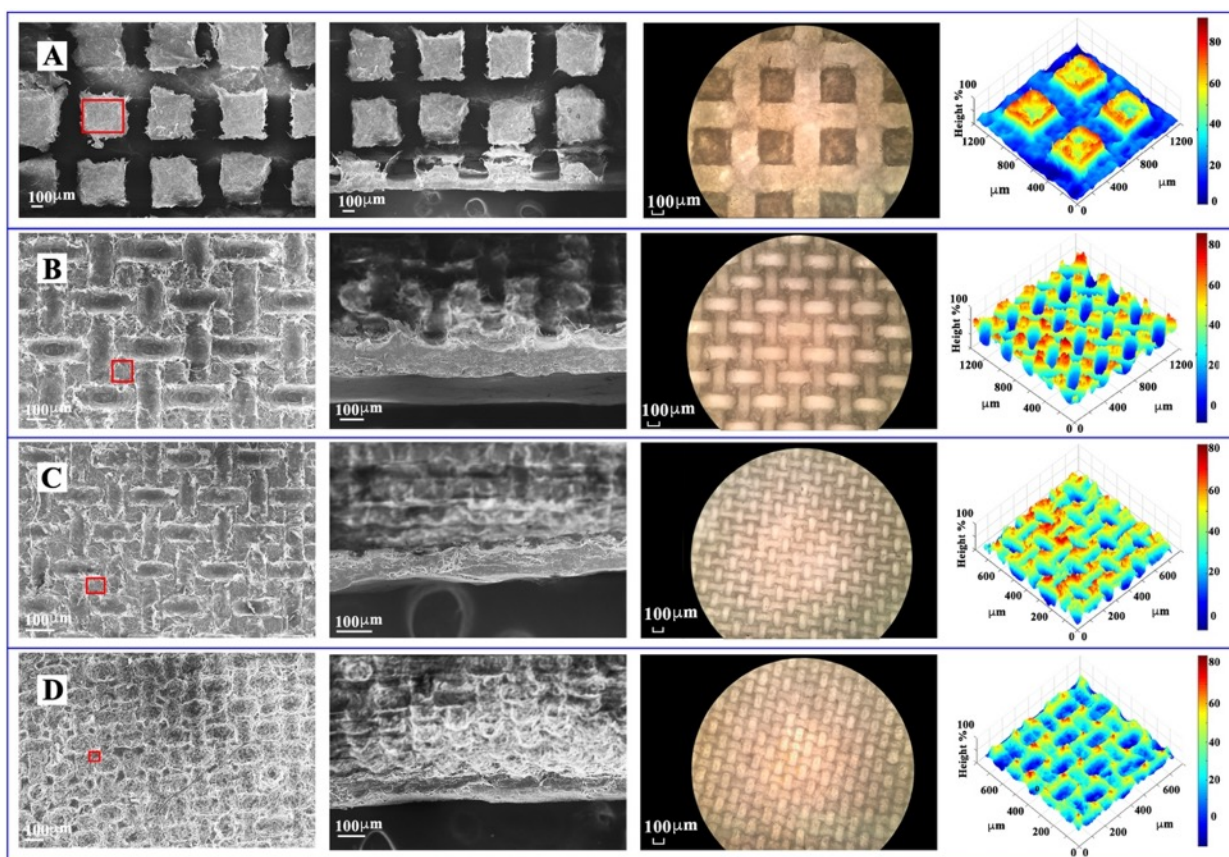
Figure 4. 2 Top view, side view of SEM images, optical microscopy images and 3D profile simulation (from the left to the right column) of the 4 different pattern sizes featured nano-cellulose membranes (noted as membrane-1 to -4 in A to D respectively).

4.3.2 Wettability of patterned cellulose membrane after chemical modification

To obtain superhydrophobic performance, chemical modification was conducted on the patterned membrane surface since modification changes the surface energy. Different polymers and chemicals, including PMMA, PS, PP, PE, PVC, wax, AKD and isocyanate agent, were applied. To compare with the patterned surface, the polymers and chemicals were coated on glass slides to make smooth coated surfaces. The static water contact angles were measured on different coated smooth surfaces and patterned membrane-2 respectively, as shown in Fig. 4.5 (A). It can be concluded that, firstly, the patterned roughness can increase the hydrophobicity. For example, the water contact angle on PS-coated smooth surface is 83° but on the prepared patterned membrane, the water contact angle increases to 130°. Secondly, the more hydrophobic the applied chemicals are, the higher the contact angle can be obtained. After modifications with AKD, wax or isocyanate, the resulting contact angles of patterned membrane-2 are higher than 150°, indicating the superhydrophobic property.
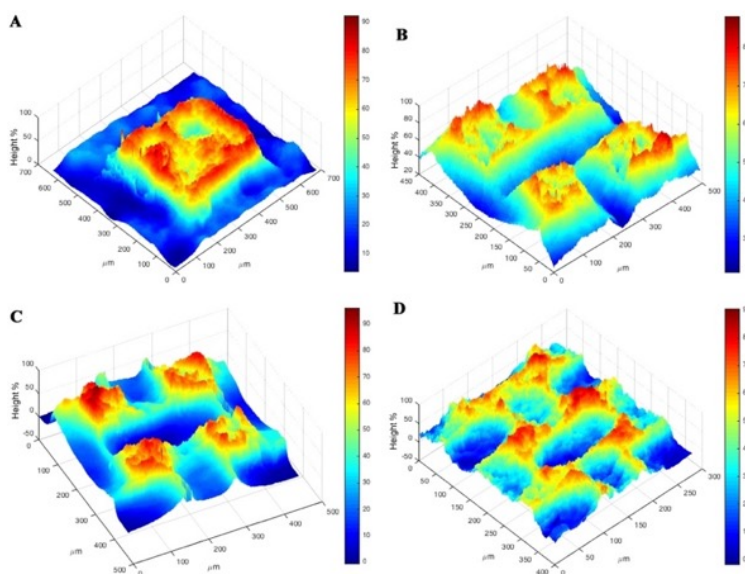
Figure 4. 3 (A-D) Magnified 3D profile simulation of patterned nanocellulose membranes-1 to -4 respectively.
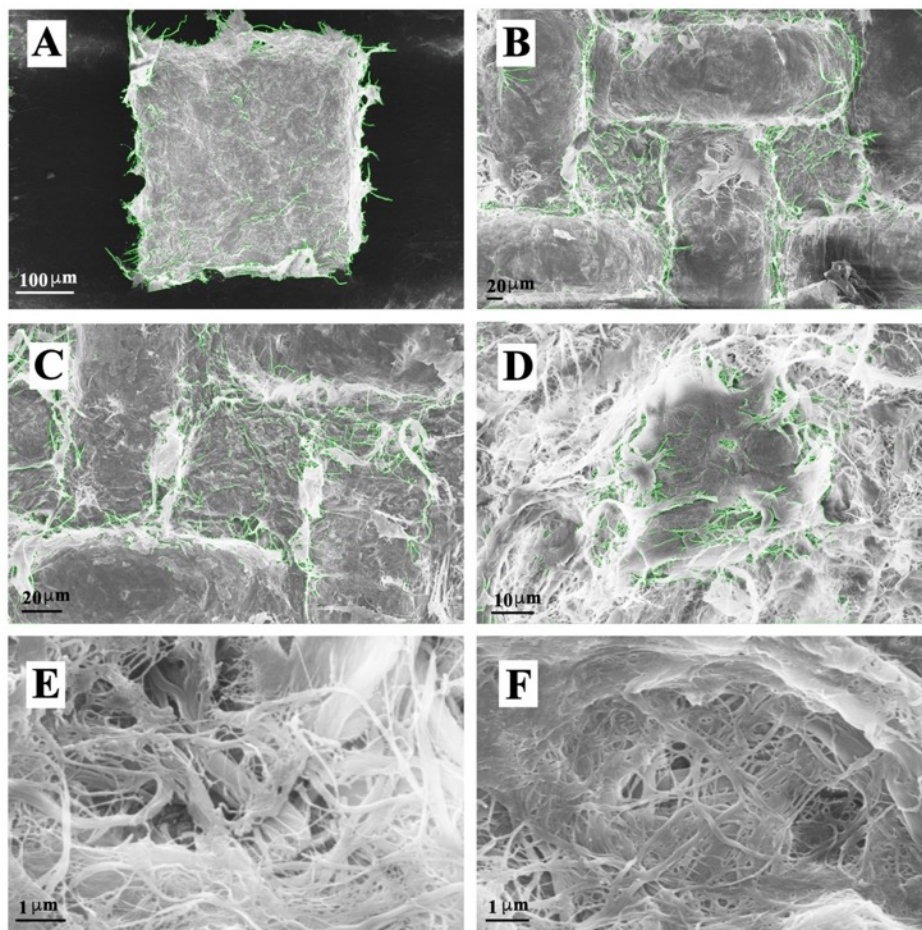
Figure 4. 4 Magnified SEM images of the Nano cellulose pillars. (A-D) Pillar on the nanocellulose membrane-1 to -4 respectively; (E and F) typical SEM images of nanocellulose fibers (came from membrane-2 and -3). The nano-cellulose fiber edge was highlighted with green color which was generated by a Matlab program.

Comparing with copy paper, filter paper and paper towel, the patterned nano-cellulose membrane shows an outstanding hydrophobic performance since the contact angles for the 3 kinds of representative papers are only around 120-130° even after AKD, wax or isocyanate modifications, as shown in Fig. 4.5 (B). The microscopy images of the chosen papers were inserted to Fig. 4.5 (B). As can be seen that the copy paper has a relatively smooth surface and plenty of particle fillers attached to the fibers. The images show that filter paper is comprised of long fibers

and paper towel has some broken fibers. The superhydrophobic behavior of prepared membrane-2 is ascribed to the patterned roughness which is shown in the inserted image in Fig. 4.5 (B). Without the patterned roughness, the CNF membranes which have the same drying and chemical treatment processes cannot reach superhydrophobicity, showing the water contact angle 99-113° (Fig. 4.6).
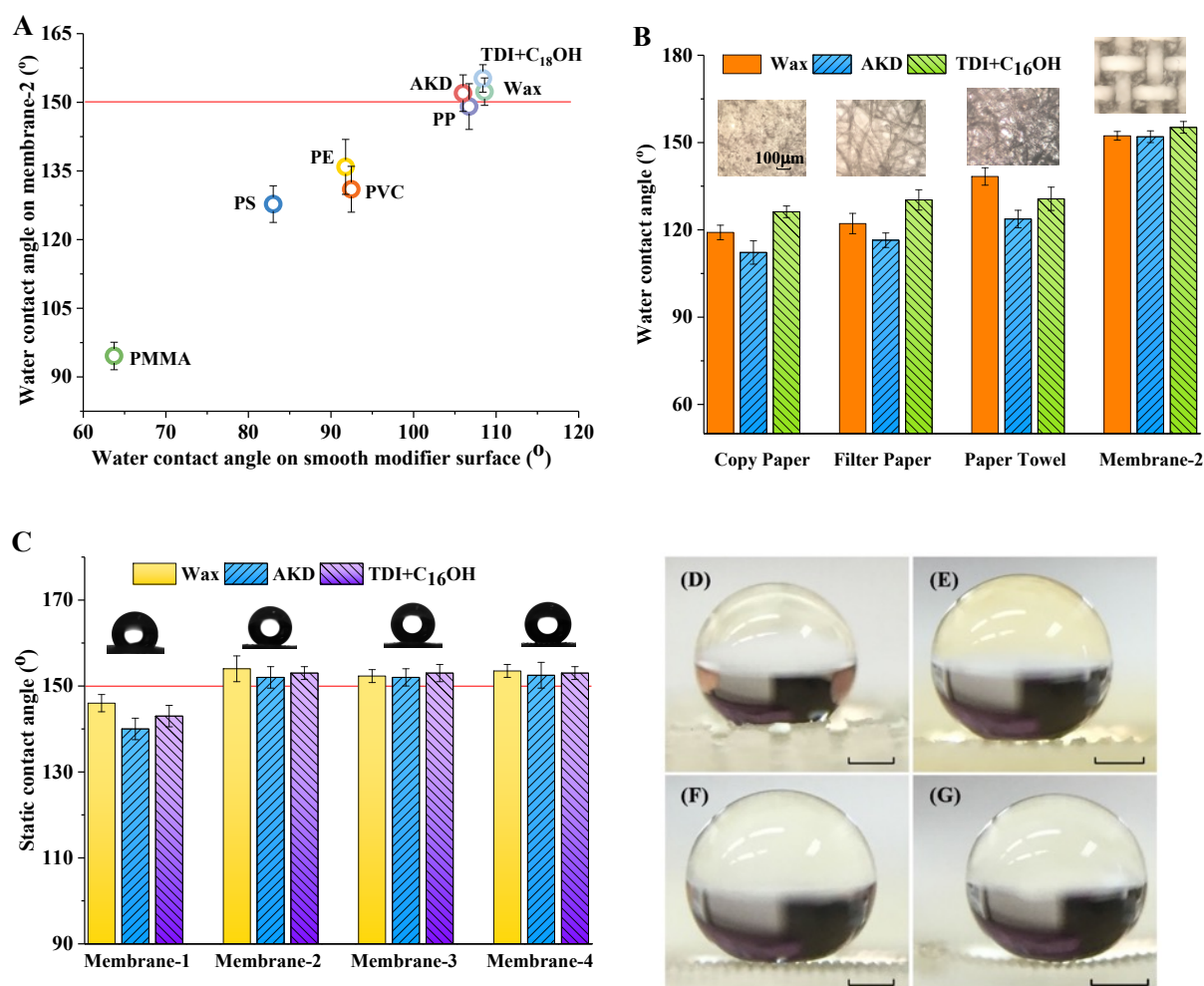
Figure 4. 5 (A) Plot of static water contact angles on modified smooth surface and patterned cellulose membrane; (B) Water contact angle comparisons of patterned membrane with different papers. Inserts: microscopy images of copy paper, filter paper, paper towel and patterned membrane-2; (C) Water contact angles of 4 different patterned nanocellulose membranes. Inserts:

photographs of the water droplets sitting on wax modified membranes; (D-G) magnified photograph of the solid-water-air interface of patterned membrane-1 to -4 respectively (scale bar 400 μm).

Modifier:	Wax	TDI+C$_{16}$OH	AKD
Water contact angle:	109.3^o	112.8^o	99.6^o
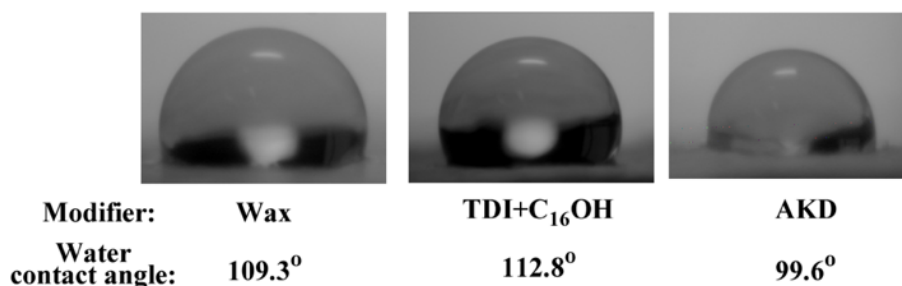
Figure 4. 6 Water contact angles of chemical modified CNF membranes which have no surface pattern but the same drying and chemical treatments with wax, TDI+C$_{16}$OH and AKD.

Figure 4.5 (D to G) shows magnified solid-air-water interfaces when the water droplets sat on the surfaces of 4 different prepared membranes. It can be clearly seen that the water droplet on the top of the asperities and the air packages are trapped below the droplet, suggesting the Cassie−Baxter state on the membrane surface.

The water wettability of 4 different nano-cellulose membranes templated by 4 different sized meshes was measured. As exhibited in Fig. 4.5 (C), after modifications with three different chemicals, including AKD, wax and isocyanate, the prepared membranes have a high water-contact angle except for membrane-1. This is because the membrane-1 has a big pillar size that cannot support the water repellent to superhydrophobic. Decreasing the pillar size, as the membranes-2 to -4 show, the water contact angles increased to higher than 150°. The obtained membrane-2 can reach 150° water contact angle and has a large surface pattern size (~110 μm) that is easy to fabricate, therefore, membrane-2 was chosen as a representative membrane used in the following studies.

4.3.3 FT-IR and TGA characterizations

With AKD modification, the long alkane chain of AKD can react with the hydroxyl group of nanocellulose fibers through ester bonding and then graft on the fiber surfaces, as shown in Fig 4.7 and discussed later. In TDI+C$_{16}$OH modification, the TDI molecule acts as a bridge that connects with the C$_{16}$OH and nanocellulose fibers. However, wax modification is a physical absorption process without chemical reaction.
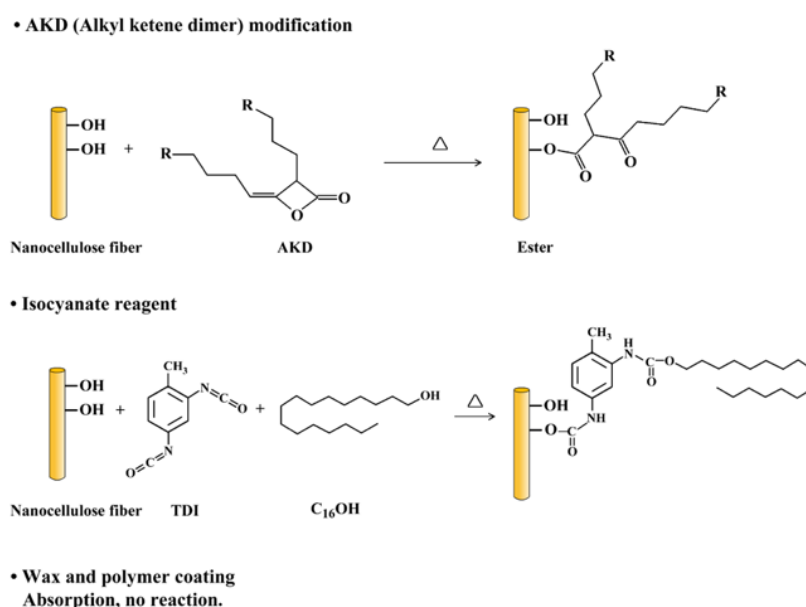
Figure 4. 7 Chemical reactions between cellulose fiber and the modifiers (AKD and TDI + C$_{16}$OH)

The chemical structure changes of modified membranes can be verified by FT-IR spectroscopy (Fig. 4.8 (A)). The spectrum of native cellulose membrane shows the O–H stretching vibration at 3440 cm^{-1} and the C–O stretching vibration at 1060 cm^{-1}. Moreover, the spectrum shows a characteristic peak of β-glycosidic bond absorption at 895 cm^{-1} and cellulose characteristic peaks at 2920 cm^{-1} and 1634 cm^{-1} [195].
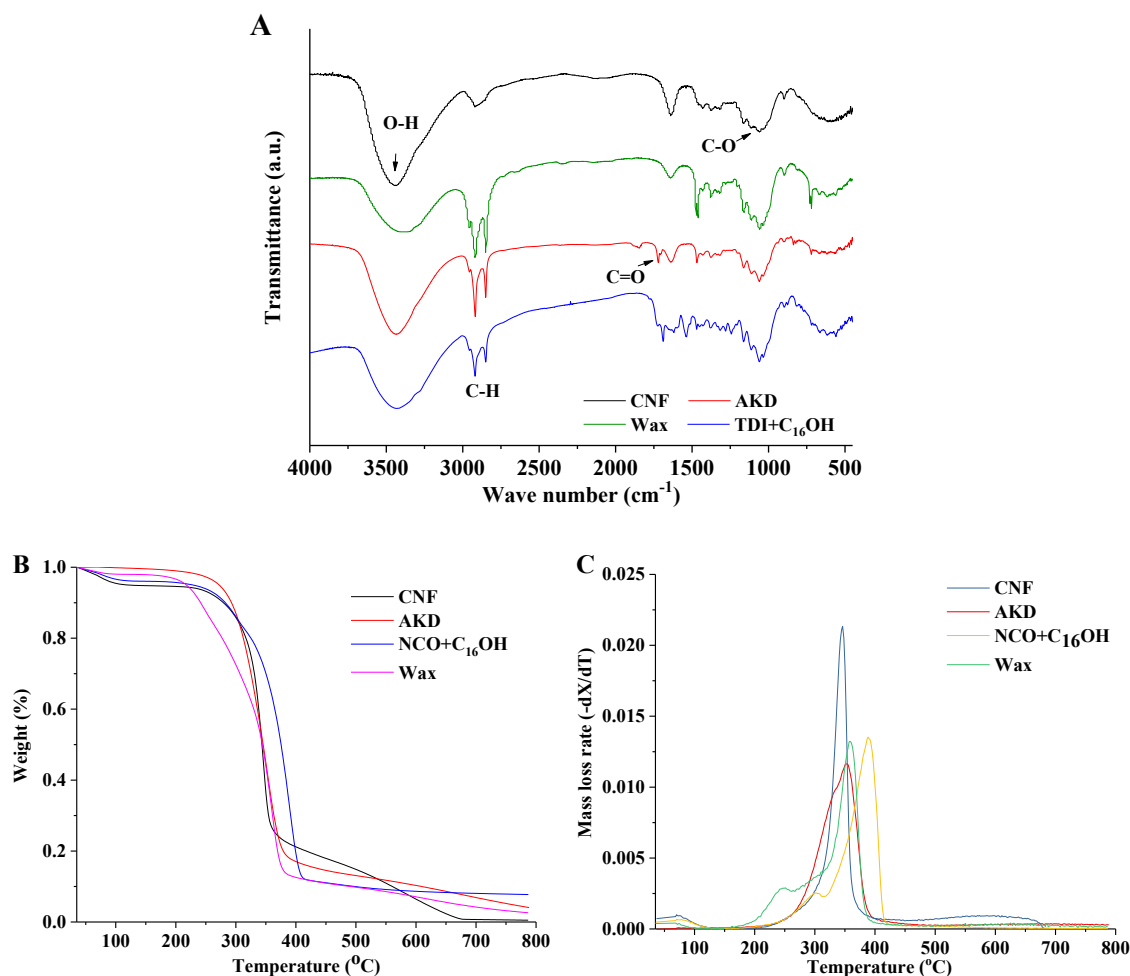
Figure 4. 8 (A) Fourier transform infrared (FT-IR) spectra, (B) Thermogravimetric curves and (C) derivative thermo-gravimetric curves of initial and chemical modified membrane-2.

Different absorption peaks were observed from the FT-IR spectra of modified nano-cellulose membranes. For the spectrum of wax modified membrane, the band at 2921cm^{-1}, 2848 cm^{-1}, 1469 cm^{-1}, and 724 cm^{-1} shows the presence of C–H stretching vibration of CH$_2$ in a long-chain alkyl group. The AKD modified membrane showed the same C–H stretching peaks as wax because of the long-chain alkyl groups in AKD molecule that gives the AKD good hydrophobicity. In addition, the characteristic peak at 1722 cm^{-1} can be ascribed to the absorption of β-ketone ester, indicating that AKD has reacted with hydroxyl groups on the surface of cellulose[196, 197]. In the

modification by isocyanate, the formed product should be carbamates with the hydroxyl groups of hexadecanol and cellulose. Therefore, in the spectra of TDI+C$_{16}$OH membrane, the occurrence of peaks at 1691 cm^{-1} can be ascribed to the stretching vibration of C=O in carbamates but the absorption of the aromatic ring and the groups attached to the amide nitrogen atoms are not easy to detect in this case.

Thermogravimetric (TG) curves of chemically modified membranes are shown in Fig. 4.8 (B). As can be seen from the TG curve of initial nano-cellulose membrane, the weight loss was nearly 100% after the temperature reaches 700°C. The derivative thermo-gravimetric curve indicated that the temperature at the maximum decomposition rate for initial nano-cellulose membrane was 350°C. For chemical modified membranes, the temperature value at the maximum decomposition rate was slightly increased, as shown in Fig. 4.8 (C). In addition, the loss of a small amount of volatile components can be seen in the decomposition temperature of 200-300°C for chemical modified membranes.

4.3.4. Tuning of asperity size and patterned coating on substrate

Metal meshes with different mesh sizes were used as templates to fabricate the patterned membranes-1 to -4. The templates can be modified as well by copper electro-deposition, for the purpose of membrane asperity size tuning, as shown in Fig. 4.9. The diameter of mesh wires was increased after the electro-deposition and the hole opening of metal mesh was decreased. By this way, the asperity size, i.e. the width of patterned pillar and the gap between neighboring pillars, can be controlled. The obtained mesh templates after copper electro-deposition and prepared nanocellulose membrane-5 and -6 by using modified templates were shown in Fig. 4.10. The gap between two molded pillars was increased from 127 μm of membrane-2 to 150 μm of membrane-

5 and further to 191 μm of membrane-6 (summarized in Table 4.1). In addition, the corresponding

pillar width was decreased from 108 μm to 89 μm and further to 49.5 μm respectively, leading to

a decrease of solid area fraction on surface. Solid area fraction refers to the geometric top area of

pillars to the total geometric area of membrane, which is a key parameter to affect the

hydrophobicity.

The measured static contact angles of membrane-1 to -6 versus surface solid area fraction

were plotted in Fig. 4.11 (A). The surface solid area fraction decreases from 0.33 to 0.04 in the

order of membrane-1, -2, -3, -5, -4 and -6. With the decrease of solid area fraction, the static water

contact angle increases. The membranes with wax modification have slightly higher contact angles

than that of membranes with the modification of TDI+C_{16}OH and AKD at the same characteristic

sizes of pillars. But the contact angles with 3 different chemical modifications are all higher than

150º, which means the superhydrophobicity, when the solid area fraction is lower than 0.25.
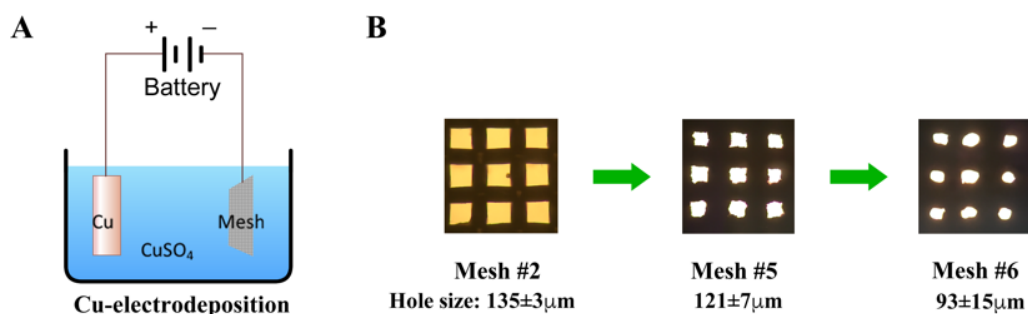
Figure 4. 9 (A) Copper electrodeposition device for template modification. (B) optical

microscopic images of initial mesh #2 and mesh #5, #6 after electrodeposition.
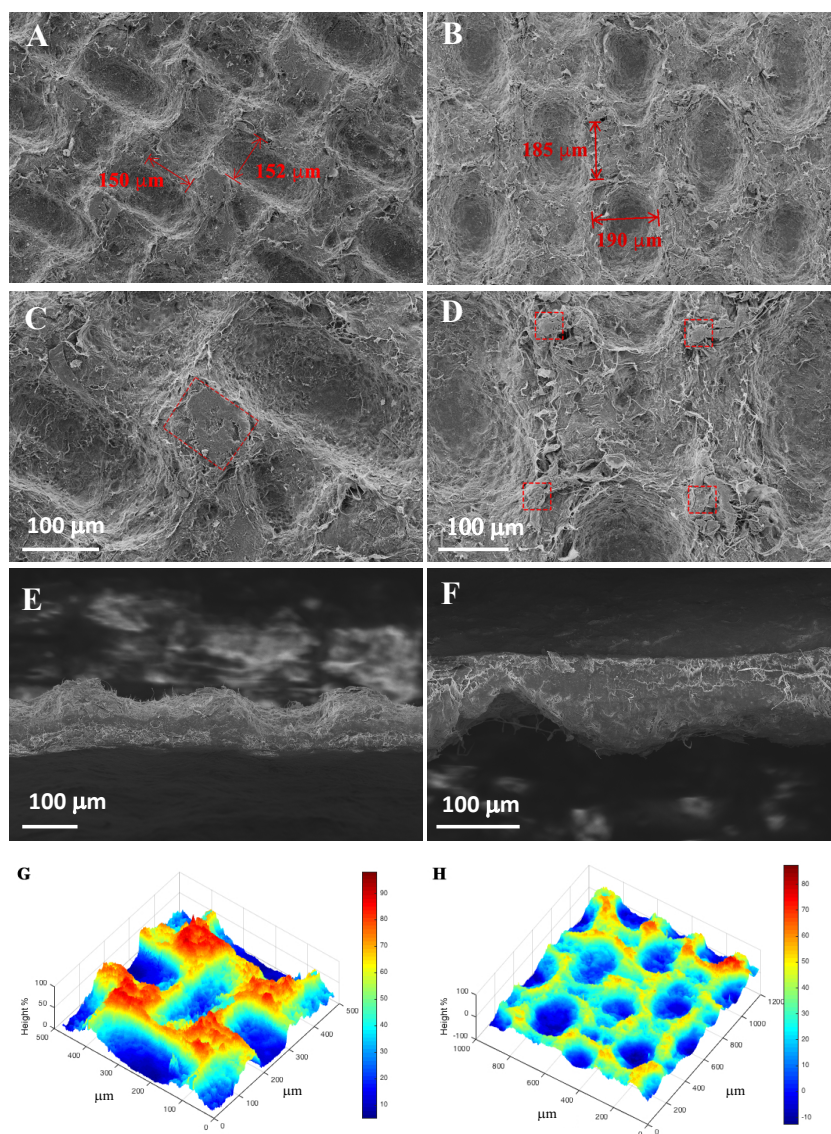
Figure 4. 10 (A, C, E and G) SEM image of patterned surface, magnified SEM image of molded pillar, SEM image of cross-section and 3D profile simulation of membrane 5 respectively; (B, D, F and H) SEM image of patterned surface, magnified SEM image of molded pillar, SEM image of cross-section and 3D profile simulation of membrane 6 respectively.

The contact angle hysteresis (CAH), defined as the difference between the advancing and receding contact angle in a dynamic process, is an important parameter to characterize superhydrophobic surfaces. Low CAH indicates the low friction for water droplet rolls off the

surface. The CAH in this study was summarized in Fig. 4.11 (B), showing that the CAH drops with the decrease of solid area fraction. Although the membrane-2 has a high static contact angle over 150°, the CHA value is still high (>10°). When the solid area fraction is lower than 0.21 (membrane-3, -4, -5 and -6), the CAH value drops to lower than 10°, which means a very low moving fraction for water droplets and possibly forms a self-clean surface. The optical microscopic images of membrane-5 and -6, and the interface images of water droplets sat on the surface were inserted in Fig. 4.11 (B).
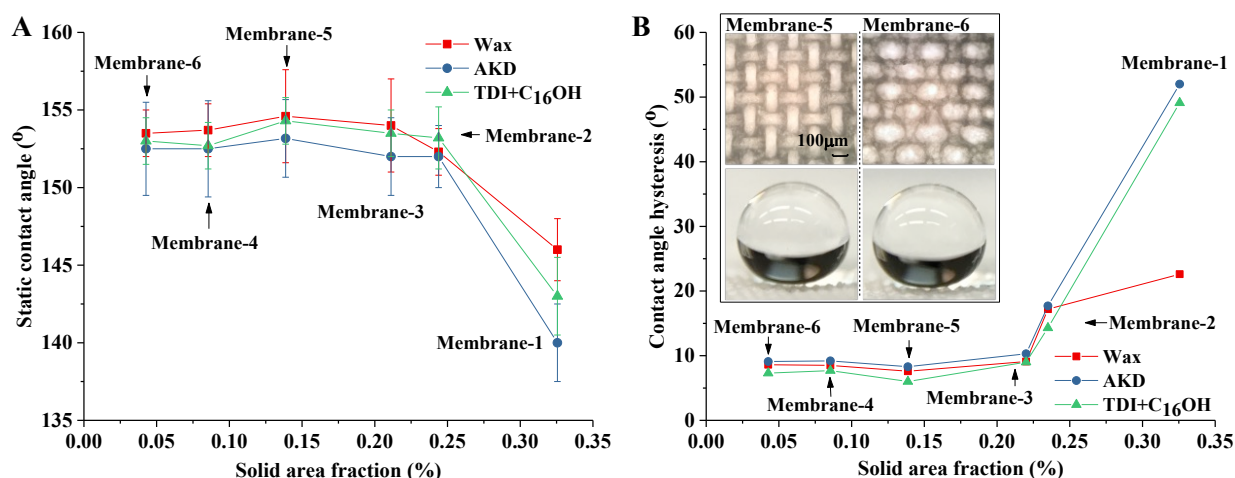
Figure 4. 11 (A) Static contact angles of chemical modified membranes-1 to -6 with different surface solid area fractions; (B) Contact angle hysteresis of prepared membranes-1 to -6. Inserts: optical microscopic images of membrane-5 and -6 (top), and the interface images of water droplets sitting on the surface (bottom).

The patterned surface can also be coated on substrates to form a composite membrane. By simply putting nanocellulose slurry on the surface of substrates and then templated pressing, the pattern layer can be formed on the substrate surface. In this study, a patterned composite membrane was fabricated by combining a microfiber copy paper layer and a patterned nano-cellulose layer (as shown in Fig. 4.12). After modification with wax, the measured static water contact angle

reached over 150°, verifying a superhydrophobicity which is the same as prepared nanocellulose membranes.
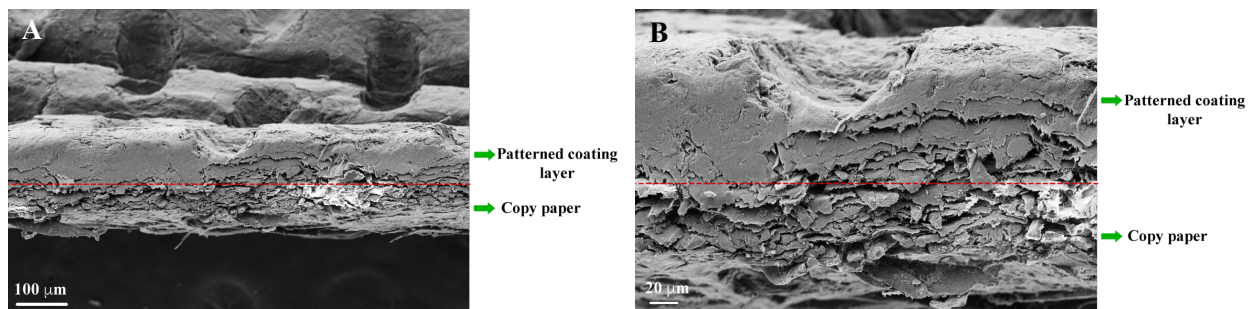
Figure 4. 12 (A) Side-view SEM image of patterned layer coated on copy paper substrate; (B) Magnified image.

4.3.5. Wettability for other solutions and stability

Besides water, several liquids that are common sources of stains in daily life were applied to investigate the wettability of the prepared membrane. Figure 4.13 (A) includes the contact angles of solutions of coffee, tea, Sprite®, Coca, Fanta® and red wine. It is important to note that the surface tension of these solutions are varied because some salts and organics are dissolved in the solutions, such as sugar in Sprite®, Coca and Fanta®, alcohol in red wine and caffeine in coffee and tea. The surface tension of the solutions may be decreased or increased compared with that of water. Therefore, the measured contact angles fluctuate around 140-150°, as shown in Fig. 4.13 (A). In general, most of the chosen solutions have high contact angles on prepared membrane-2. More importantly, the solution drops can easily roll off the prepared membranes without significant adhesion. Figure 4.13 (B) shows dynamic rolling-off processes of different solutions from isocyanate reagent modified membrane-2, suggesting that prepared membrane cannot be contaminated by these soft drinks so it should be used as soft drink containers.

59
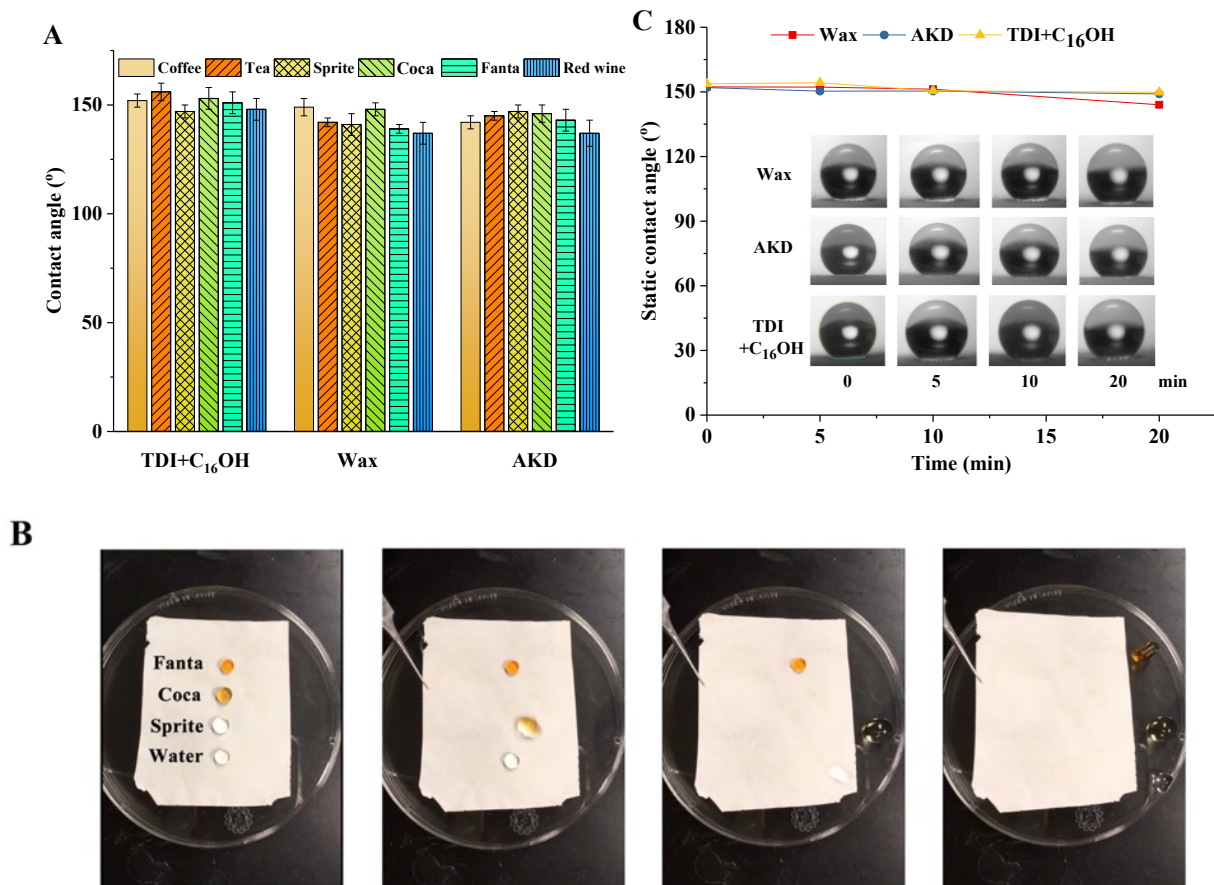
Figure 4. 13 (A) Static contact angles of different solutions on chemical modified membrane-2. (B) Dynamic process of different liquids rolling off isocyanate modified membrane-2. (C) Plots of water contact angle versus contact time on the modified membrane-2. Insets: photographs of the water drops sat on the membrane-2.

The contact time effect was also investigated on the chemical modified membrane-2. As we can see from Fig. 7 (C), the water contact angles for AKD and isocyanate modified membrane-2 maintain stability as the water contact time increases from 0 to 20 min. The wax modified membrane shows a little decrease but the contact angles are still around 150° after 20 min contact time. The physical coating of wax modification but not chemical bonding can explain the slight decrease of water contact angle. Different from wax, the AKD and isocyanate reagent can chemically bond with the surface –OH group of cellulose to form a chemically stable structure that

can maintain high water contact angles during long contact time. The knife scratching test was also performed according to the literature method[185, 198, 199]. After scratching by a knife, the membrane surface was cut and broken (figures were shown in Fig. 4.14), but the patterned pillars were not completely removed. The measured water contact angle was slightly decreased to 145~149°, and the water droplets can smoothly roll off the tilted surface in the testing (Fig. 4.14).
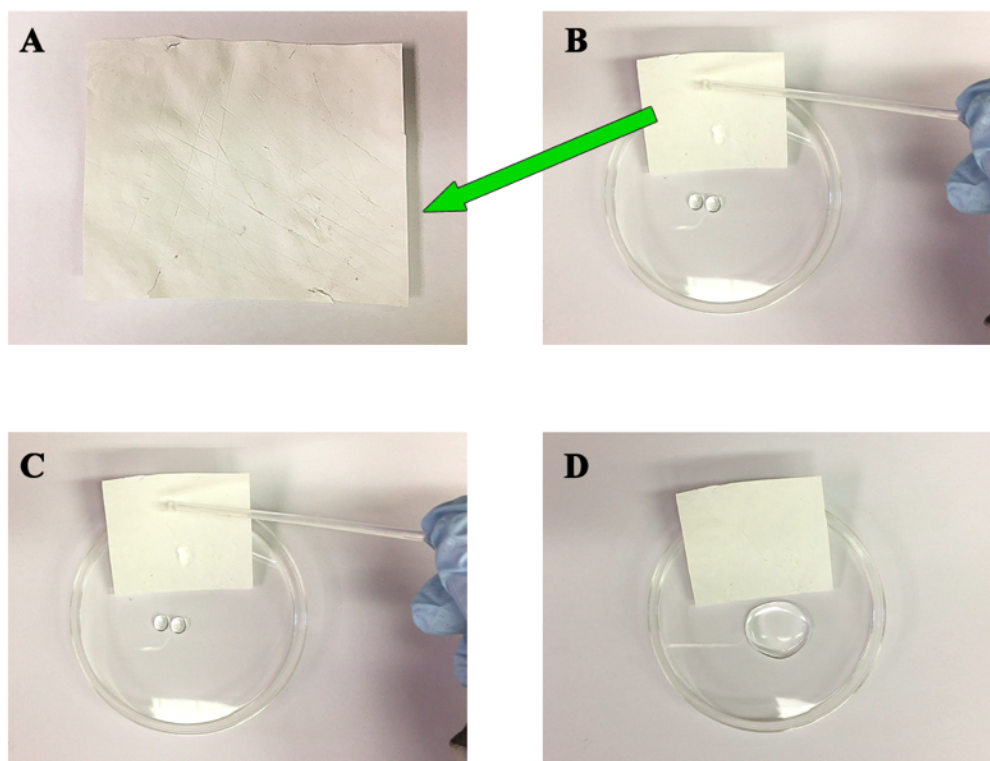
Figure 4. 14 (A) Scratched membrane 2 (wax modified) with a knife. (C-D) Images of water droplets rolling off the broken surface in a tilt angle.

4.4 Conclusion

In summary, patterned nanocellulose membranes were fabricated by a fast template pressing method. The superhydrophobicity of prepared membranes was supported by (1) the micro-sized pattern and nano-sized fibers formed hierarchal roughness structures; and (2) the low surface energy after chemical modification with long alkane chains. The prepared membrane showed a

good repellent ability to water and common stain fluids, and good hydrophobic behavior in the long-term measurement and knife scratch testing. The asperity size of patterns was tuned by modification of the templates by electro-deposition, and the patterned surface was extended to be used as a coating layer on substrates. By this way, the patterned surface can be potentially employed in the packaging industry due to the economic, fast and environmentally friendly process.

CHAPTER V In situ modification of nanocellulose with AKD emulsion for PLA composite reinforcement

5.1 Introduction

Nanocellulose has proven to be a versatile material with a vast array of potential industrial applications including composites and foams for automotive, aerospace, and building construction; viscosity modifiers for cosmetics and oil drilling fluids; and high performance fillers for paper, packaging, paints, plastics, and cement[18, 200-202]. In addition to material performance properties like gelation, shear thinning, exceptionally high strength, and light weight, nanocellulose has a strong sustainability profile[203, 204]. The relatively low cost of cellulose nanomaterials creates an opportunity to use them as reinforcing fibers in composite materials. Reinforcing polymers to create promising, environmentally safe, lightweight construction materials for the car industry have attracted great research and industrial interests.

Since cellulose is intrinsically hydrophilic, nanocellulose cannot disperse well in a hydrophobic polymer matrix such as polyethylene (PE), polypropylene (PP) or polylactic acid (PLA). Chemical modification of the reactive surface -OH groups of nanocellulose to make the surface hydrophobic and compatible with hydrophobic media has received growing interest in both scientific and industrial researches[205, 206]. Hydrophobic surface modification is able to improve the dispersion and distribution of nanocellulose in polymers, plastics, or resin matrices during composite processing. Furthermore, interfacial compatibility between the nanocellulose particles and polymer matrices could be also improved to create strong polymer composites[207, 208].

Hydrophobic surface modification of nanocellulose has been successfully performed using various chemical treatments. However the current methods cannot be accepted by the polymer industry because CNC and CNF are water suspensions, and hydrophobic modification agents are water insoluble or water sensitive so the modification must be conducted either at dry condition or in organic solvents. It is well known that drying cellulose nanofibrils (CNFs) or cellulose nanocrystals (CNC) is an energy intensive process. Furthermore, significant hornification of cellulose nanomaterials occurs after drying, due to the irreversible formation of hydrogen bonds. These irreversible hydrogen bonds cannot be broken after rewetting, resulting in a significant change in the physical properties of CNC/CNF. To effectively graft hydrophobic polymer or monomer on CNC/CNF surface, the dried nanocellulose materials have to be re-dispersed in an organic solvent. Poor re-dispersibility limits the real industrial application using CNC/CNF as reinforcement filler for plastics, rubbers and many other engineering polymer materials. Also, environmental pollution and high cost of using organic solvent for CNC/CNF are also a big concern of the industry.

In this study, in situ hydrophobic modified CNF was used as mechanically reinforced filler in the poly lactic acid (PLA) composite fabrication directly in water. To improve the dispersion and compatibility with hydrophobic PLA, in situ chemical modifications of CNF were conducted (as shown in Fig. 5.1). To avoid CNF drying or solvent exchange process, industrial alkyl ketene dimer (AKD) emulsion was used for CNF hydrophobic modification in the water suspension. The emulsion used in the modification can protect the activity of AKD in water and enable the successful modification of CNF. Therefore, drying or organic solvent exchange is not required in the modification. With the in situ modifications, CNF was successfully incorporated into the PLA matrix and it showed the reinforcing effect in prepared PLA composite films.

A

B
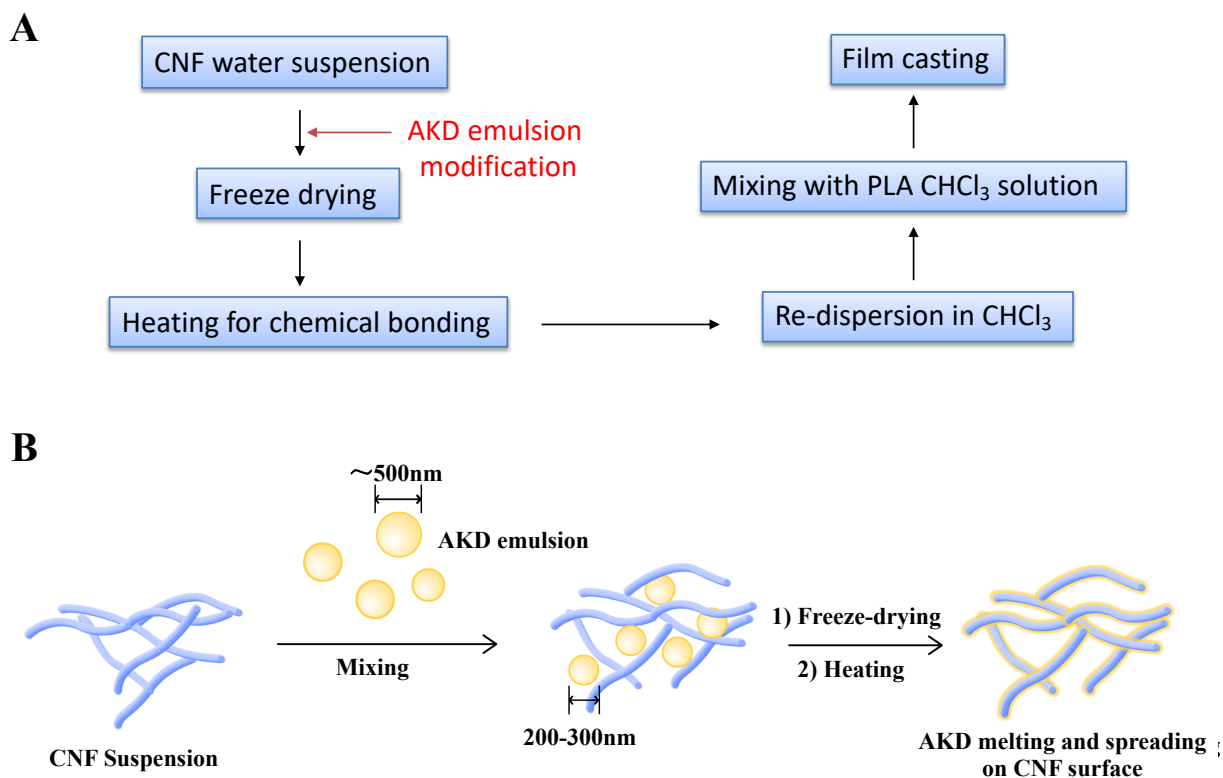
Figure 5. 1 (A) Schematic diagram of in situ chemical modifications for nanocellulose and PLA composite fabrication. (B) Illustration of in situ modification of CNF in water suspension using AKD emulsion.

5.2 Experimental Section

5.2.1 Materials

Cellulose nanofibril slurry (CNFs, fiber content 3.4%) prepared from mechanically refined bleached softwood Kraft pulp was purchased from the University of Maine Process Development Center. Toluene diisocyanate (TDI) was purchased from TCI America. Hexamethylene diisocyanate (HDI), 4-dimethyl aminopyridine (DMAP) and solvent dichloromethane (DCM) were purchased from Alfa Aesar. Poly lactic acid (PLA, M_w~250,000), solid alkyl ketene dimers (AKD) and AKD water emulsion are industrial grade products.

5.2.2 In situ modification of CNF with AKD emulsion in water suspension.

CNF slurry was diluted into the solid concentration at 1 wt% by adding deionized (DI) water with vigorous stirring with a high speed homogenizer. AKD emulsion was added into the CNF water suspension and homogened at a high speed at 2,100 rmp for 20 min to form a homogeneously mixed suspension. Different amounts of AKD emulsion were added to prepare CNF suspensions with the AKD to CNF (dry weight) mass ratios of 5%, 10% 15% and 20%. The obtained AKD-CNF suspensions were frozen by liquid nitrogen and then freeze-dried for 48 hours. After the removal of water, the obtained CNFs with AKD were heated to 110 °C for 60 min to enable the chemical bonding between AKD and CNF to be completed.

5.2.3 CNF-PLA composite fabrication by film casting

The thermal treated AKD-CNFs were re-dispersed in DCM by sonification. PLA was previously dissolved in DCM to form a homogenous solution with the concentration of 5wt%. Then charged PLA solution was added into the CNF re-dispersed DCM suspension with different CNF (not including the weight of AKD) to PLA ratios of 2%, 5%, 10% and 15%. Stirring for 10 min to form a homogeneous suspension and then film casting was conducted with the prepared suspension. The solvent evaporation was controlled at a low rate by using ambient temperature.

5.2.4 The AKD modification efficiency measurement and calculations

The AKD modification efficiency, which is defined as the ratio of the bound amount of AKD to the total added amount of AKD, was investigated. The unbound amount of AKD in CNF films was extracted by solvent and measured by the spectrophotometric method which is based on the reaction of AKD with 4-dimethyl aminopyridine (DMAP)[209]:

The AKD modified CNFs obtained in 5.2.2 were firstly extracted with the solvent tetrahydrofuran at the solvent boiling point for 2 hours to extract the unreacted AKD. Then the extracted solution was reacted with DMAP giving an orange colored product. The obtained samples were analyzed by UV spectrophotometer at 338nm. Different amounts of pure AKD were dissolved in tetrahydrofuran and were used as the standard solution for the calibration curve.

The AKD modification efficiency and AKD loading fraction were calculated based on the following equation:

$$\text{Modification Efficiency} = \frac{m_b}{m_{AKD}} \times 100\,\% \quad (5.1)$$

$$\text{AKD loading fraction } (w_{AKD}) = \frac{m_b}{m_{cell} + m_b} \times 100\,\% \quad (5.2)$$

where m_b is the mass of bonded AKD on cellulose backbone, m_{Cell} is the mass of dry solid CNF, and m_{AKD} is the mass of AKD added in the reaction.

5.2.5 Characterizations.

The surface morphology of AKD modified CNFs was examined via LEO 1530 thermally assisted field emission scanning electron microscope (**FE-SEM**) with an acceleration voltage of 10 kV. Samples were gold-sputtered prior to SEM images.

Fourier transform infrared (**FT-IR**) spectra of AKD modified CNF samples were measured by KBr pellets on a Bruker Vertex 80V spectrometer in the scan range of 4000-400 cm^{-1} of 32 scans with resolution 4 cm^{-1}.

Thermogravimetric Analysis (**TGA**) and Derivative Thermogrametric (DTG) were performed using Perkin Elmer STA600 simultaneous thermal analyzer to evaluate thermal degradation of original and sulfonated sample in the range of 40-600°C at a rate of 10°C min^{-1} under a nitrogen flow rate of 20 ml min^{-1}.

Static water contact angle (**WCA**) measurements of hydrophobic modified CNFs were performed at ambient environment using the First Ten Angstrom contact angle analyzer with FTA32 software. A droplet of 8 μL deionized water was placed on the prepared CNF surface for the measurement.

Dynamic mechanical analysis (**DMA**) tester (Q800, TA Instruments, New Castle, DE, USA) was used in the measurements of Young's modulus, strain at break, and ultimate strength of CNFs composites. The measurements were performed under the uniaxial tensile mode. The CNF-PLA composite films were cut into a rectangle shape (length, width, and thickness of approximately 30 by 5 by 0.1 mm, respectively). Each sample was tested three times, and the averages with standard deviations were reported.

The X-ray diffraction (**XRD**) patterns of the CNF-PLA composite samples were analyzed by X'Pert PRO diffractometer. The instrument is equipped with a Cu Kα radiation source (λ=0.154 nm) with a 2θ range of 10-45° and the operation voltage and current was maintained at 40 kV and 40 mA respectively.

The crystallinity index (C.I.) of nanocellulose based on the XRD pattern was determined as[210]:

$$C.I. = \frac{I_{002} - I_{am}}{I_{002}} \times 100\% \qquad (5.3)$$

where, I_{002} is the intensity of (002) peak at $2\theta = 22.5°$ and I_{am} is the intensity of the amorphous region (at 18.3°) between the two crystalline peaks.

The apparent crystallite size (D) for the main (110) and (203) reflections in the XRD pattern of PLA was calculated using the Scherrer's equation:

$$D = \frac{k\lambda}{\beta_c cos\theta} \quad (5.4)$$

where K is the Scherrer constant (0.94), λ is the X-ray wavelength(λ = 0.154056 nm for Cu Kα radiation), β_c is the full width at half maximum value of the diffraction peak (FWHM), and θ is Bragg's angle.

The interplanar distances (d) was calculated using Bragg's relationship:

$$d = \frac{\lambda}{2sin\theta} \quad (5.5)$$

where λ and θ are the same as described in equation (5.4).

5.3 Results and Discussion

5.3.1 AKD in situ modification of CNF in water suspension

5.3.1.1 In situ modification of CNFs by AKD emulsion

The industrial produced AKD water emulsion was directly added in the CNF water suspension for modification and in the following, water was removed by freeze-drying to obtain AKD modified CNFs. Figure 5.2 (A) shows the photographs of AKD modified CNF samples with the AKD addition from 0% to 20% (based on the dry weight of AKD to CNF). The AKD emulsion is critical for the hydrophobic modification. Firstly, AKD is highly hydrophobic and cannot be dissolved in water suspension for effective modification. This is because the AKD molecule has two long alkyl chains (a C_{12}-C_{16} alkyl group in the 3-position and a C_{13}- C_{17} alkylidene group in the 4-position) although the chain length varies with the manufacturing resources[210-212]. In AKD emulsion, the AKD is highly dispersed as nano-sized particles in the water solution which can provide a large contact area with CNF fibrils. After the vigorous homogenizing with CNF suspension, the AKD emulsion particle size even further reduced from the initial 550 nm (on average) to about 200-300 nm, as shown in Fig. 5.2 B (b) and (d). This could be ascribed to that the cellulose nano fiber works as the emulsifier or emulsion stabilizer that stabilizes the nano AKD-emulsion[213-215]. As shown in Fig. 5.2 B (b), AKD nano particles deposited on the surface of CNF fibers, which can largely reduce the fiber hornification and aggregation during the water removal process.
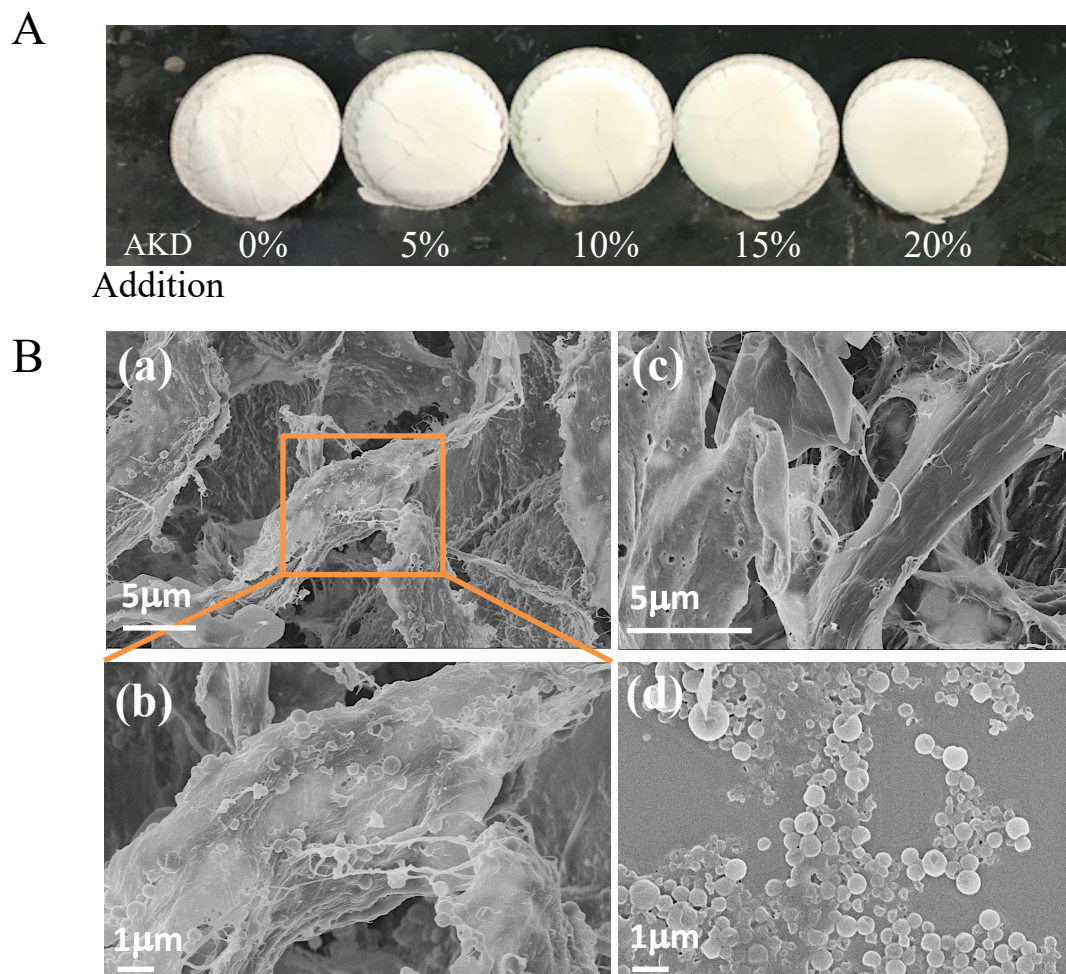
Figure 5. 2 (A) Photographs of prepared AKD modified CNFs with the AKD addition from 0% to 20%. (B) SEM images of the AKD modified CNFs ((a) and magnified image (b)), the CNFs after thermal treatment (c) and the initial AKD emulsion (d) used in the modification.

On the other hand, the emulsion modification avoids the deactivation of AKD. AKD is a kind of lactone that can react with the hydroxyl group of cellulose via esterification. However, the esterification is competitive with the hydrolysis of AKD in aqueous medium[216, 217]. The AKD emulsion encapsulates the AKD molecules inside the oily droplets, which protects it from hydrolysis with water before the fiber modification. After the water removal by freeze-drying, the

AKD particles are anchored on the fiber surface so that hydrogen bonding interactions between CNF fibrils and the hornification were reduced.

After freeze-drying, the AKD emulsion modified CNFs were heat-treated at 110 °C for 60 min[218, 219]. During the process, AKD particles were melted and spread on the nanocellulose surface (as shown in Fig. 5.2 B (c)). At the same time, the covalent ester bonding with hydroxyl groups of nanocellulose occurred.

5.3.1.2 The hydrophobicity of modified CNFs and AKD modification efficiency measurement

As shown in Fig. 5.3 (A), under elevated temperature, the 4-membered oxetane ring of the AKD molecule was opened and bound with the surface hydroxyl group to form a beta-ketocarboxylic ester[218, 219]. By this way, the two long hydrocarbon chains were covalently grafted on the CNF fibers, which changes the nanocellulose fibrils from hydrophilicity to hydrophobicity. The water contact angles of modified CNFs with different AKD additions were measured. The photographs of water droplets sitting on the AKD modified CNFs and the water contact angle values were shown in Fig. 5.3 (B). The CNF without AKD modification is hydrophilic, as the water contact angle is 44° at the initial time. In fact, the native CNF gradually absorbed the water droplet as the time prolonged. However, after the AKD modification and thermal treatment, the water contact angels increased to 101.3° with the AKD addition of 5 wt% based on the dry weight of CNF. The water contact angle further increased with the rise of the addition of AKD. The highest water contact angle reached 110° with the AKD addition of 20%. These results show the hydrophobic property of modified CNFs, which could be more compatible with PLA matrix (water contact angle is 80.5° for smooth PLA surface).
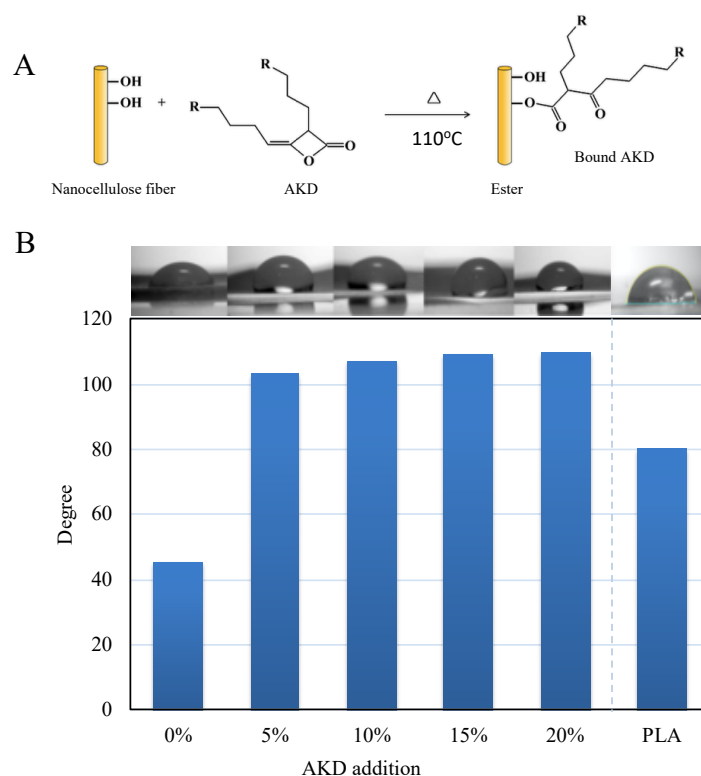
Figure 5. 3 (A) The chemical reaction between AKD and hydroxyl group of CNF[219]. (B) Measurements of the water contact angles and photographs of water droplets sitting on the AKD modified CNFs. The percentage of AKD additions are based on the dry weight of CNF.

The efficiency of AKD modification was investigated in this study. The unbound AKD was extracted by tetrahydrofuran and measured by spectrophotometry. Table 5.1 summarized the modification efficiency and AKD loading fraction for modified CNFs. The highest modification efficiency reached 79.8% at the AKD initial addition of 15%. However, the efficiency decreased to 63.8% when the AKD addition raised to 20%. By simple heating, the AKD was successfully bound to the hydroxyl group of CNF surface and changed it to hydrophobic. It should be noted that the unbound AKD could be absorbed on the CNF fibrils and also contributed to the increase of hydrophobic property.

Table 5. 1 The calculation of modification efficiency and AKD loading fraction for modified CNFs.

AKD addition to CNF (wt%)	Modification efficiency (%)	AKD loading fraction (%)
5	72.5	3.5
10	78.2	7.3
15	79.8	10.7
20	63.8	11.3

5.3.1.3 Characterizations of AKD modified CNF aerogels

The chemical bonding between AKD and hydroxyl groups of CNF was characterized by FT-IR. As shown in Fig 5.4, the characteristic IR band for native CNF (red line) is the -OH stretching at 3,345 cm^{-1}, C-H symmetrical stretching at 2,899 cm^{-1}, C=O stretching vibration at 1,640 cm^{-1} and C-O-C asymmetrical stretching at 1,060 cm^{-1}[195, 220]. After the modification and thermal treatment, the obvious changes is the occurrence of the peaks at 2,850 and 2,920 cm^{-1}, which can be ascribed to the C-H stretching vibration of CH_2 groups in the long alkyl tails of AKD molecules[196, 197]. The C-H stretching vibration bands also exhibited in the modified CNF IR spectrum (blue line) at 1468 and 721 cm^{-1}. The absorption peak located at 721 cm^{-1} was considered as the characteristic vibration band of the molecular structure which contains at least four CH_2 groups[221]. This result verified the existence of the long-chain alkyl groups, which generally contain 12-20 carbon atoms, in the prepared modified CNF aerogel. This could also be explained to the good hydrophobicity of obtained CNF aerogel after modification.
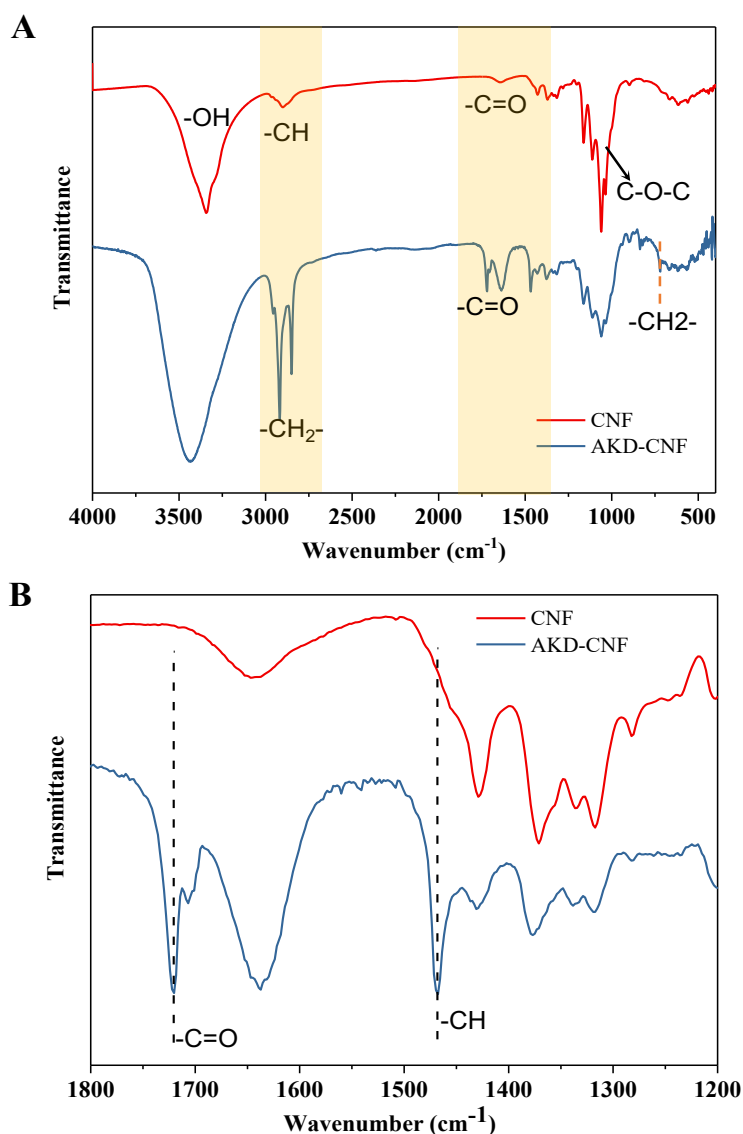
Figure 5. 4 (A) FT-IR spectra of native CNF and AKD modified CNF (addition 10%) after thermal treatment. (B) The magnified spectra in the range of wavelength from 1,200 to 1,800 cm⁻¹.

The other obvious change is C=O stretching vibration band between 1,600-1,700 cm⁻¹. Besides the native nanocellulose C=O band at 1,640 cm⁻¹, the relative absorption peaks at 1,721 and 1,707 cm⁻¹ were ascribed to the C=O stretching vibrations of introduced β-ketoester groups[222, 223], as shown in the magnified FT-IR spectra in Fig. 5.4 B. These results supported the covalent chemical bonding between AKD molecules and CNFs.
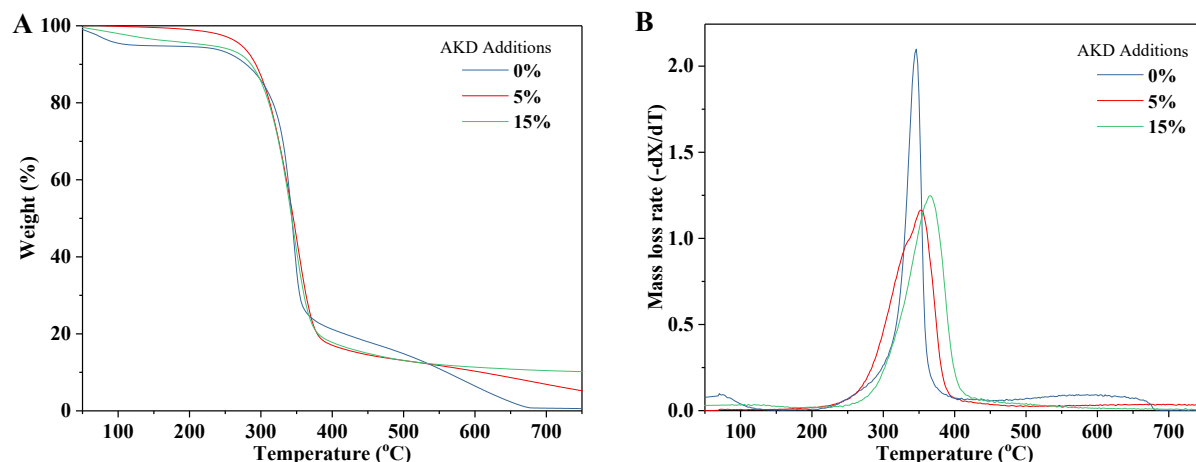
Figure 5. 5 (A) Thermogravimetric analysis (TGA) curves and (B) derivative thermogravimetric (DTG) curves of native CNF and AKD modified CNFs under nitrogen atmosphere.

The thermogravimetric analyses (TGA) of prepared CNF samples were conducted. The results were shown in Fig. 5.5, and the thermal characteristics extracted from the TGA and derivative thermogravimetric (DTG) curves were summarized in Table 5.2. The temperature at the mass loss of 5% ($T_{5\%}$) is recognized as the onset temperature for the CNFs thermal degradation[224, 225]. The onset temperature for native CNF is 121.3 °C which is the loss of absorbed water at this temperature. This result suggests that the native nanocellulose is highly hydrophilic and easily to absorbs moisture from the air. For the sample with 5% AKD addition in the modification, the onset temperature increased to 272.9 °C. However, the onset temperature of the sample with 15% AKD addition is 225.3 °C, which is lower than that of 5% AKD addition sample. This could be attributed to the loss of unbound AKD in the 15% AKD addition sample.

Table 5. 2 The data of $T_{5\%}$, $T_{50\%}$, T_{max} and char residue summarized from TGA curves.

Samples	$T_{5\%}$* (°C)	$T_{50\%}$†(°C)	T_{max}‡(°C)	Char residue/% (at 600 °C)
Native CNF	121.3	343.1	346.3	6.4
CNF with 5% AKD modification	272.9	345.4	353.4	10.3
CNF with 15% AKD modification	225.3	343.1	365.7	11.2

* The temperature at the weight loss of 5%. †The temperature at the weight loss of 50%. ‡The temperature at the maximum decomposition rate.

The temperature of native CNF at the maximum decomposition rate is 346.3 °C and only 6.4% residue char left at the temperature of 600 °C. With the increase of the addition of AKD in the modification, the temperature at the maximum decomposition rate slightly increased to 365.7 °C for 15% AKD modified CNF. The char residue increased as well after the AKD modification. These changes could be attributed to the AKD modification for the CNF fibrils.

5.3.2 Redispersion of modified CNFs in CH$_2$Cl$_2$

After AKD modification and thermal treatment, the obtained CNF aerogels were re-dispersed in organic solvent CH$_2$Cl$_2$. This process was conducted by mechanical homogenizing and sonification. Generally, the dried CNF redispersion in organic solvent is difficult because of the fibrils bonding and hornification during the drying process. Due to the AKD emulsion modification before the water removal in this study, the redispersion performance of the AKD modified CNF was improved. Figure 5.6 shows the photographs of CNF dispersion in the solvent CH$_2$Cl$_2$. It can be seen that the native CNF formed a flocculent precipitant in CH$_2$Cl$_2$, but the AKD modified CNFs obtained much more homogeneous suspensions.

As shown in Fig. 5.6 right column, different amounts of PLA was added into the CNF suspensions to form viscose suspensions with the final PLA concentration 2.5wt%, which were used as the precursor solution for the CNF-PLA composite film fabrication. Because of the high viscosity of the suspension, the CNF fibrils dispersed in it are not observed to be precipitated in 24 hours. This performance helps to make the homogeneous composite films.
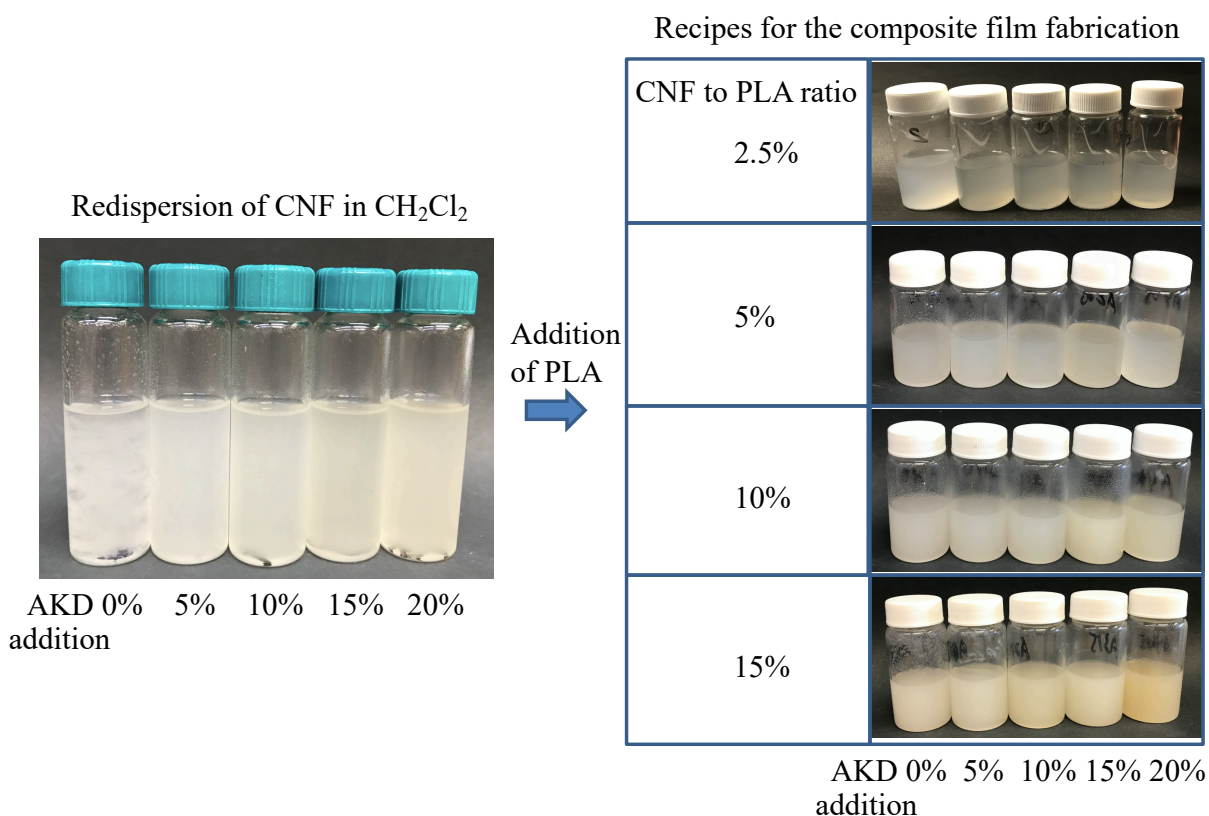
Figure 5. 6 Photographs of CNF dispersions in CH_2Cl_2 and the recipes for the composite film fabrication with different AKD additions and CNF to PLA ratios.

5.3.3 Fabrication of AKD modified CNF-PLA composite films

5.3.3.1 Photographs and SEM images of the prepared composite films

The obtained CNF-PLA composite films with different AKD additions were shown in Fig. 5.7. The ratio of CNF weight (not included the weight of AKD) to that of PLA is 5%. It can be

seen that with the increase of AKD additions in the CNF modification, more homogeneous composite films were obtained. For example, the sample labeled with "AKD 0%" (means the AKD addition of 0% in the modification) in Fig. 5.7 shows the CNF aggregation after the film casting; however, the obtained composite film labeled "15%" and "20%" (means the AKD addition of 15% and 20% respectively) shows more smooth and homogeneous surface. This is because of the improvement of hydrophobicity and the compatibility with the polymer matrix PLA after the AKD modification.
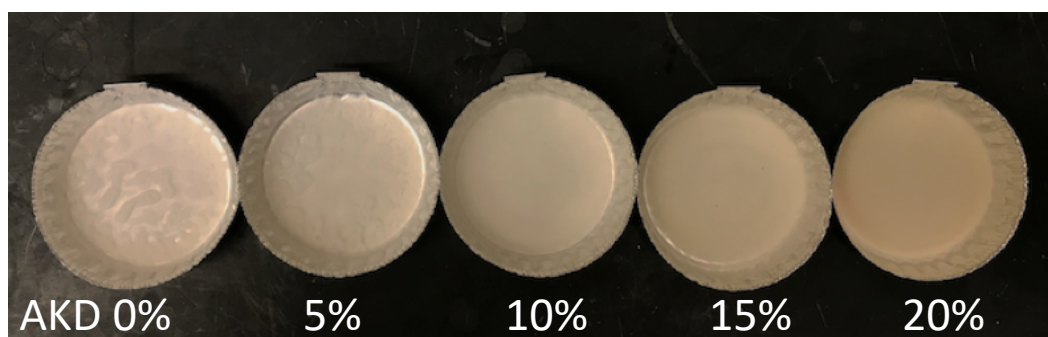
Figure 5. 7 The photographs of CNF-PLA composite films with different AKD additions (the ratio of CNF weight to PLA is 5%).

The CNF content in the composite film is another important fact to improve the composite performances. In this study, different ratios of CNF weight to PLA (0%, 2.5%, 5%, 10% and 15%) were used for the fabrication of composite films. Figure 5.8 shows the SEM images of the composite film with different CNF to PLA ratios (the AKD addition is fixed at 10%). The SEM image of CNF 2.5% shows the smooth surface of the composite film. However, with the increase of CNF to PLA ratio, the CNF fibers can be seen from the film surfaces. For example, from the SEM images of sample CNF 15%, we can see the nanocellulose bundles on the film surface, and some nanocellulose fibrils can be seen from the magnified top-view image and the image of cross-section at the breakage.
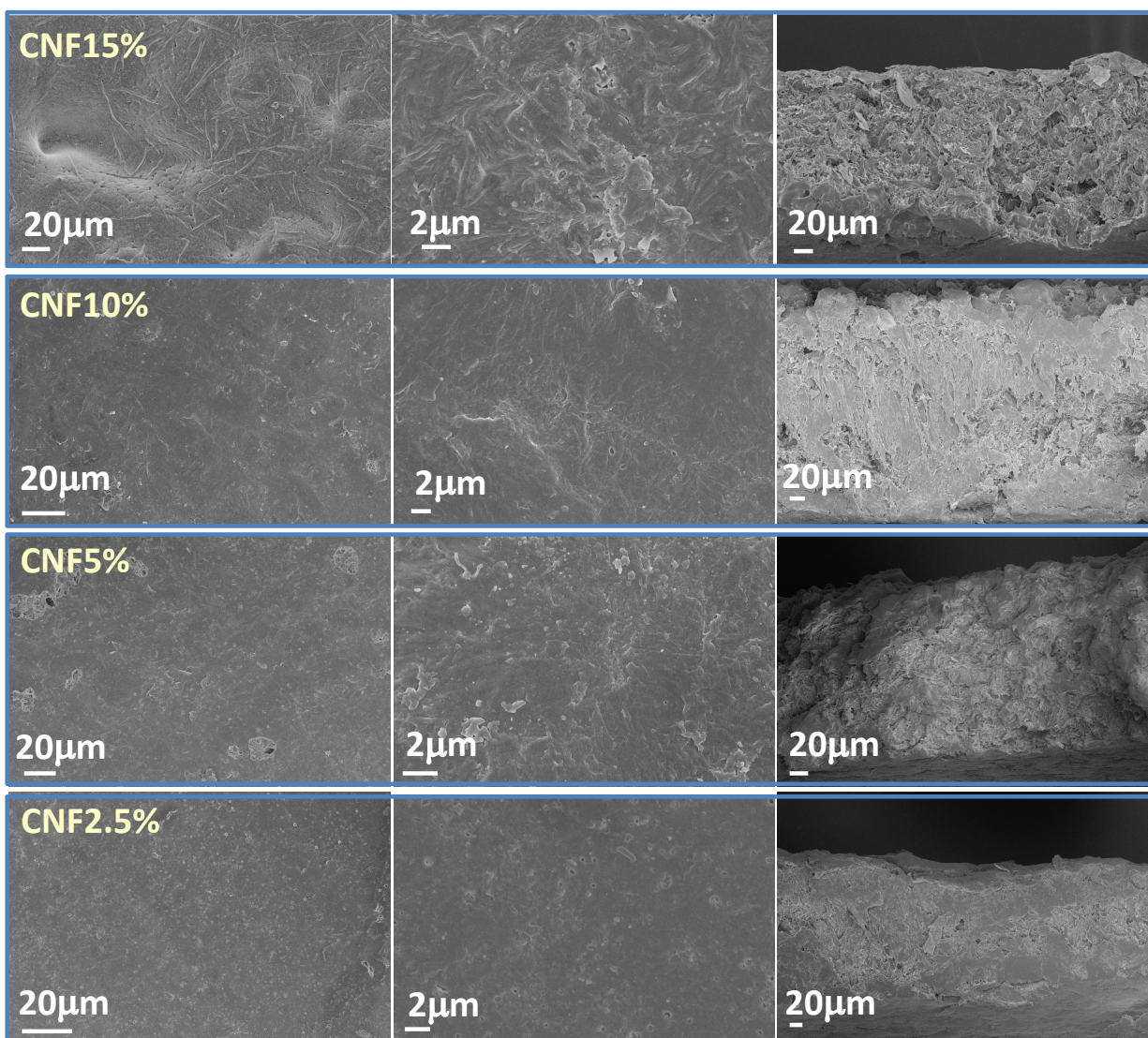
Figure 5. 8 SEM images of the CNF-PLA composite film with the ratio of CNF to PLA from 2.5% to 15%. The AKD addition in the CNF modification is 10%. The left column is the top-view images; the middle column is the magnified top-view images; and the right column is the images of cross-section view at the breakage of the composite film.

The SEM images show the CNF fibrils distributed well in the composite films. These results show that we have successfully prepared the CNF-PLA composite by the AKD emulsion in situ modification CNF fibrils and solvent casting method.

5.3.3.2 XRD and TGA characterizations of prepared composite films

The obtained CNF-PLA composite films were characterized by XRD and TGA. Figure 5.9 shows the XRD patterns of composite films with different CNF contents. The pattern of the sample with CNF content 0% (orange line) shows the characteristic peaks of neat polymer PLA. The two diffraction peaks at $2\theta = 16.3°$ and $18.8°$ were ascribed to (110)/(200) and (203) lattice planes of the α and α' crystalline form of PLA[226, 227]. In the XRD patterns of the CNF-PLA composites, two crystalline peaks at $15.8°$ and $22.5°$, assigned to the characteristic peaks of crystalline cellulose[228, 229], were gradually increased with the rise of CNF content in the composites. But the peaks were weak and broad, indicating the amorphous phase existed in the composites.
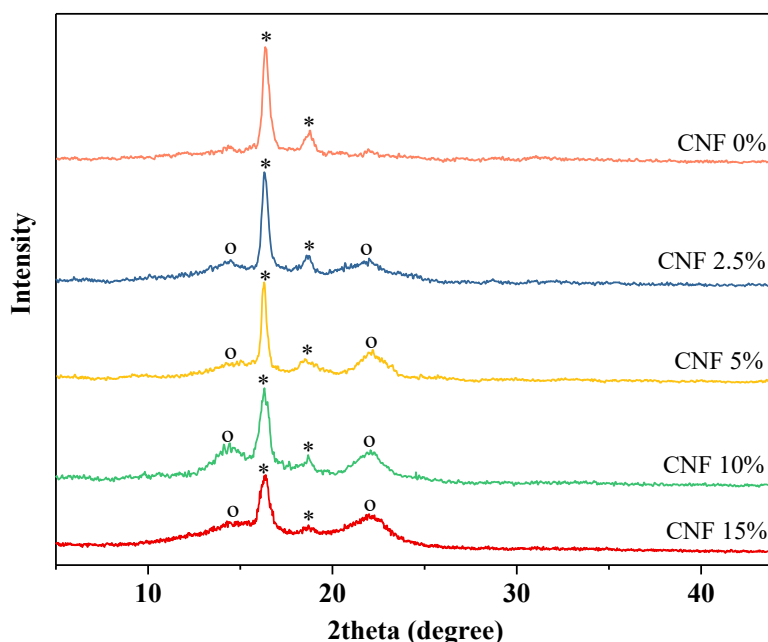
Figure 5. 9 XRD patterns of CNF-PLA composite film with different CNF contents. * noted as the PLA phases and o noted as the phases of nanocellulose.

Table 5. 3 Summary of interplanar distances ($d_{110/200}$) and crystallite sizes (D_{110}) for the PLA phase in the composite films

Samples	CNF 0%	CNF 2.5%	CNF 5%	CNF 10%	CNF 15%
$d_{110/200}$ (Å)	5.45	5.43	5.43	5.43	5.42
D_{110} (nm)	21.1	17.9	16.7	15.4	14.0

The sizes and interplanar distances of the crystalline PLA in the composites were analyzed based on the Scherrer's and Bragg's equations, as shown in Table 5.3. With the increase of CNF content in the composite film, the crystallite size for the PLA phase decreased from 21.1 nm in the native PLA film to 14.0 in the 15% CNF-PLA composite. But the interplanar distances were almost the same in different composites. These results show that the crystalline process is possibly obstructed and restricted by nanocellulose fibrils, resulting in the reduced crystallite sizes of PLA.
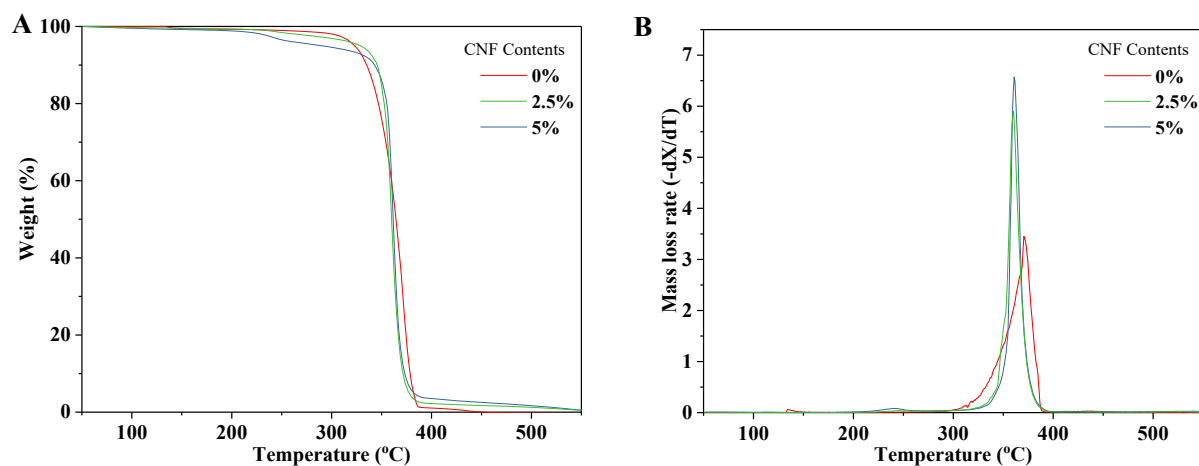
Figure 5. 10 (A) Thermogravimetric analysis (TGA) curves and (B) derivative thermogravimetric (DTG) curves of CNF-PLA composite with different CNF contents.

Table 5. 4 The data of $T_{5\%}$, $T_{50\%}$, T_{max} and char residue summarized from TGA curves.

Samples	$T_{5\%}$ (°C)	$T_{50\%}$(°C)	T_{max}(°C)	Char residue/% (at 550 °C)
CNF 0%	323.9	364.5	371.5	0.12
CNF 2.5%	324.5	360.1	361.0	0.18
CNF 5%	291.3	361.5	360.2	0.22

Thermogravimetric analyses of the composite films were conducted, as shown in Fig. 5.10 and Table 5.4. The T_{max} of pure PLA sample is 371.5 °C, but it decreased to about 360 °C when CNFs were added into the PLA matrix to form composites. This is because the AKD modified nanocellulose has a low T_{max} which is about 350-360 °C, as described above. $T_{5\%}$ values for all CNF-PLA composite films were higher than 290 °C, which suggests the prepared material is thermally stable below 290 °C.

5.3.3.3 Mechanic performances of CNF-PLA composite films

Figure 5.11 and Figure 5.12 show the mechanic performances of prepared CNF-PLA composite films. The neat PLA film is a plastic material with the ultimate tensile strength at the breakage of 22 MPa, Young's modulus about 400 MPa and the elongation at the break about 27.5%, as shown in Fig. 5.11 F. By using nanocellulose as fillers, the mechanical performances of the CNF-PLA composites were improved. The typical tress-strain curves for the composite with different CNF contents and different amounts of AKD modification were shown in Fig. 4.11 A-E. The ultimate tensile strength and modulus were summarized in Fig. 5.12.
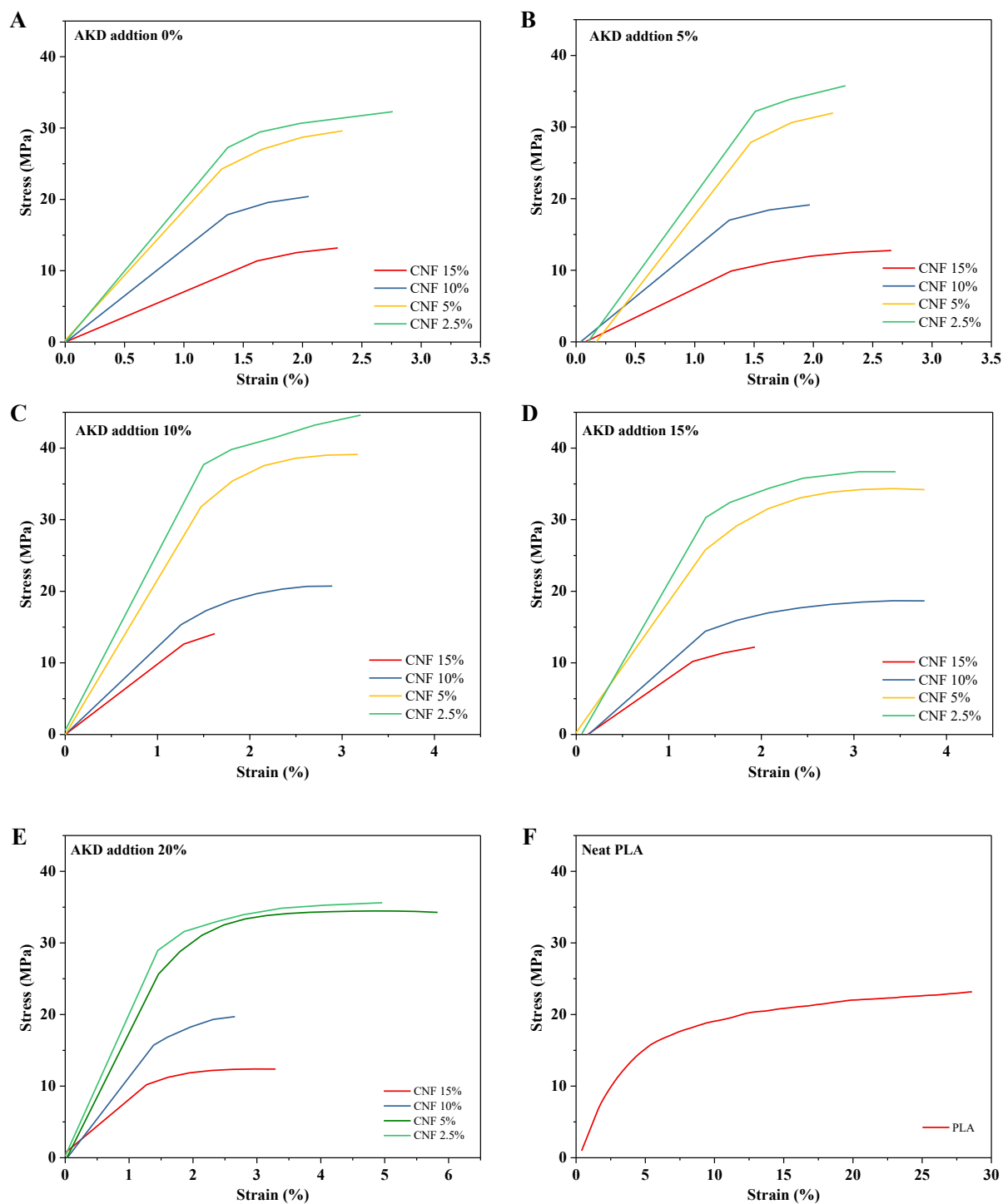
Figure 5. 11 Stress-strain curves for prepared CNF-PLA composite films with different AKD additions in the CNF modification and different CNF contents in the composites.

The results of mechanical tests showed the reinforcement of nanocellulose in the PLA matrix. By 2.5% weight of CNF (without AKD modification) addition in the composite, the ultimate tensile strength increased to 32 MPa, which increased by 50% compared with the neat PLA film. With the AKD modification, the surfaces of nanocellulose fibrils were converted to hydrophobicity, which was shown above. The ultimate tensile strength was further increased by using AKD modified CNF as reinforcing fillers. The optimized AKD addition for the tensile strength improvement is 10% weight of CNF. The highest value reached 45 MPa, which increased by 105% based on the value of initial PLA film. However, with the addition of AKD higher than 10%, the tensile strength decreased, which could be attributed to the reason that the increased unbound AKD in the composite which functions as plasticizer reduced the strength of the material. The changes of Young's modulus were similar to that of the ultimate tensile strength. The highest Young's modulus achieved 2.52 GPa, which is 6 times higher than that of the initial PLA film. The CNF content in the composite film is an important factor to mechanic performance. As shown in Fig. 5.12, when the CNF content was lower than 10%, the mechanic performances of the composite film were improved. The tensile strength decreased with the further increase of CNF content, but the modulus still slightly improved.
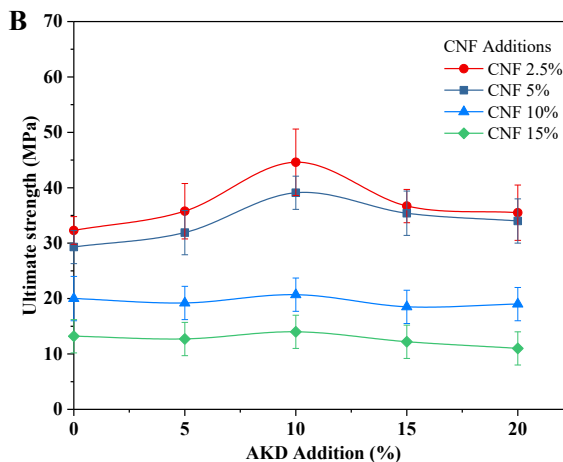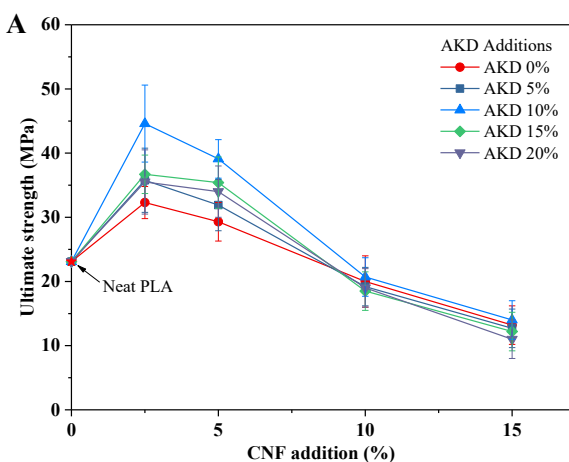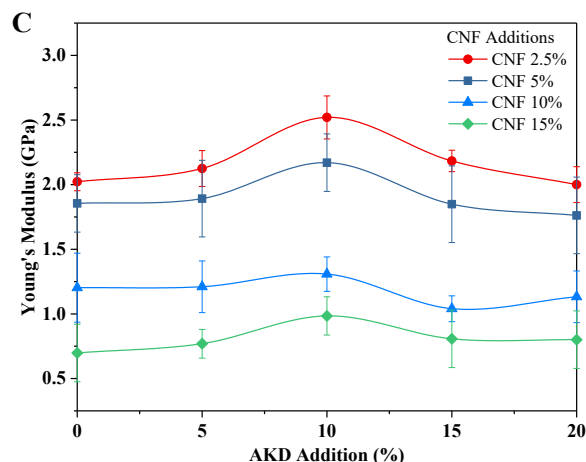
Figure 5. 12 Summary of the ultimate tensile strengths and Yong's moduli with different AKD additions and CNF contents.

5.4 Conclusion

In this study, we have prepared the CNF-PLA composite film in which nanocellulose was used as mechanical reinforcing fillers. To increase the compatibility of CNF with PLA, in situ hydrophobic modification was conducted in CNF water suspension by using AKD emulsion which is a cheap and widely used industrial product. The AKD emulsion modification reduced the CNF fibril's hornification and improved the dispersibility in a polymer matrix. In the composite film preparation, different amounts of AKD addition for the CNF modification and different CNF contents in the composite film were investigated in detail. The AKD modified CNFs and final obtained CNF-PLA composite films were systematically characterized by SEM, IR, XRD and TGA. The mechanical testing verified the reinforced performance of the composite film. The highest tensile strength of 45 MPa with Young's modulus 2.52 GPa was obtained, which are 2 times and 6 times higher than pure PLA respectively.

CHAPTER VI Nano-structure control of nanocellulose frameworks for PLA composite reinforcement

6.1 Introduction

In recent years, poly lactic acid (PLA) received great attention because of its well-established biodegradability and biocompatibility[230, 231]. PLA is generally produced by the ring-open polymerization of lactide or directly polymerized from lactic acid[232]. Both of the two monomers can be 100% derived from renewable resources, such as wheat, maize, corn, wood residues or other biomass. PLA has wide application in many fields due to the good thermoplasticity and processability. However, PLA is a very brittle biopolymer under tensile and bending loads. The fabrication of reinforced PLA composite is a common approach to solve the mechanical issues. Cellulose nanofibril (CNF) is such a filler that can be applied in the PLA composite for mechanical improvement because nanocellulose has a high aspect ratio, high surface area and high mechanical performance[233, 234]. More importantly, CNF is the most abundant natural polymer on Earth and it is completely renewable and biodegradable. Therefore, reinforcements of PLA by nanocellulose fibrils to make the sustainable 'green-composites' are currently widely researched[233, 235-237].

The natural hydrophilic properties of nanocellulose, however, are a big challenge to uniformly distribute in the hydrophobic PLA matrix. The discontinuity of interfacial interaction between nanocellulose fillers and PLA, caused by the non-homogeneous dispersion and aggregation of nanocellulose, weakens the mechanical properties of resultant nanocomposites[238]. One of the strategies is the hydrophobic surface modification of CNF to increase its compatibility with PLA. For example, surface silylation of cellulose nanocrystals with alkyl coupling agents has been validated to stabilize the dispersion in the suspension in organic solvent and also as the filler in

bulk polymeric matrices[239, 240]. Esterifications with different fatty acids were also reported to render the interactions between PLA polymer chain and nanocellulose fillers[241, 242]. Various methods such as etherification, oxidation and usage of compatibilization agents have been extensively explored[242-246]. However, the mechanical performance improvement could not be significant after the tedious and time-consuming chemical oriented treatments and modifications. This could be for several reasons, for example, the low substitute degree (DS) or the degradation of crystalline of nanocellulose during the chemical treatment.

This study focuses on the nano-structure control of cellulose nanofibrils for the PLA composite reinforcement. Herein, we combined different dry methods, i.e. room-temperature drying, heat-drying and freeze-drying, to fabric the high strength and high porous 3D nanocellulose films as the frameworks for PLA composites reinforcement. Firstly, room-temperature drying was conducted for water evaporation to form nanocellulose films from the nanocellulose water suspension, while the heat-drying could strengthen the irreversible intermolecular hydrogen bonding to obtain the strong hydrogen-bonding networks. Next, re-wetting of the obtained CNF film was used to re-open the reversible hydrogen bonding and then freeze-drying was used for water removal and pores formation. As a result, the nanocellulose framework reinforced PLA composites could be fabricated by filling PLA into the pores. High tensile strength could be expected because the nanocellulose fibrils, which function as fillers, are bonded together to form a continuous nanocellulose framework. On the other hand, the interaction between nanocellulose framework and PLA matrix are highly improved because of high porosity and large specific surface area of the CNF framework. With isocyanate as the chemical bonding agent, the nanocellulose framework was covalently bound together with PLA polymeric matrix, which further improved the mechanical performances of the composite.
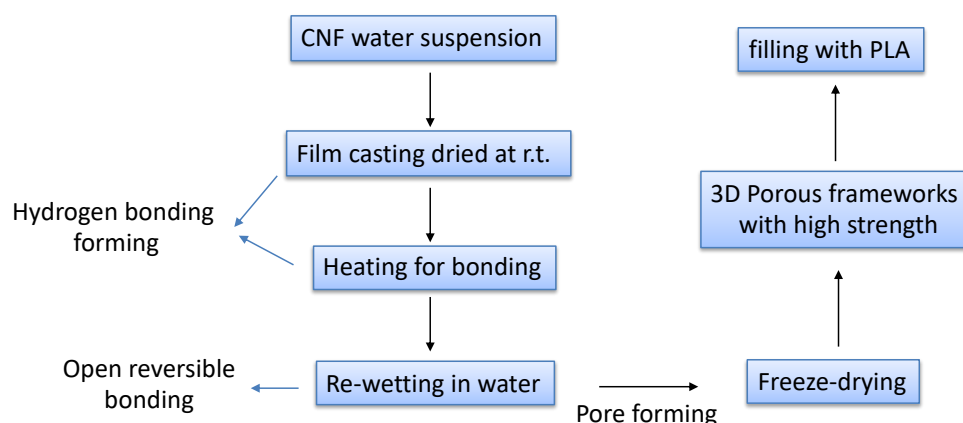
Figure 6. 1 Schematic diagram of 3D porous nanocellulose frameworks preparation in the CNF-PLA composite fabrication.

6.2 Experimental Section

6.2.1 Materials

Cellulose nanofibril slurry (CNF, fiber content 3.4%) prepared from mechanically refined bleached softwood Kraft pulp was purchased from the University of Maine Process Development Center. TOCNF was made by the U.S. Forest Service Forest Products Laboratory pilot plant at Madison and distributed by the University of Maine (1.5 mmol-COONa/g dry TOCNF). Toluene diisocyanate (TDI) was purchased from TCI America. Hexamethylene diisocyanate (HDI) and dichloromethane (DCM) were purchased from Alfa Aesar.

6.2.2 Preparation of high-strength and high-porous CNF films

Charged CNF slurry was diluted with DI water to form a suspension with a solid content of 0.5wt%. The CNF suspension was placed in an aluminum pan with a cover and a nanocellulose film was obtained by natural water evaporation under ambient temperature for several days. The obtained nanocellulose film was placed in the oven and heated to 100 °C for 2 hours. After cooled

to room temperature, the heated film was soaked in DI water at room temperature overnight. The wet films taken out from water were frozen by liquid nitrogen and freeze-dried for several days to obtain the target film.

TOCNF was used to increase the pore size and porosity was added into the initial CNF water suspension for nanocellulose film fabrication. In this study, different TOCNF fractions in CNF suspension (0%, 5%, 10%, 20%, 40%, 60% and 100 wt%, based on dry solid weight) were used to make the porous CNF films.

6.2.3 Chemical cross-linking of PLA with isocyanates

Toluene diisocyanate (TDI) and hexamethylene diisocyanate (HDI) were used for the cross-linking of PLA in the composite fabrication. PLA was dissolved in dichloromethane to form a clear solution. TDI or HDI (1wt% weight of PLA) was added into the solution. Then the mixture was heated to 80 °C with a cover.

6.2.4 Fabrication of CNF framework and PLA composite

The PLA composite was made by impregnation of prepared porous nanocellulose framework in PLA and TDI or HDI crosslinked PLA solutions. The impregnation was performed for a long time, overnight in this study, to ensure full penetration of the PLA solution into the pores of nanocellulose frameworks.

6.2.5 Characterizations

The water retention value (**WRV**) during the re-wetting of nanocellulose films in water was measured. After overnight DI water rewetting, the samples were removed from water and excess

surface water was carefully absorbed with filter paper. The WRV value was calculated using then eqn (6.1):

$$\text{VWR(\%)} = \frac{W_{wet} - W_{dry}}{W_{dry}} \times 100\% \quad (6.1)$$

The surface morphology of obtained samples was examined via LEO 1530 thermally assisted field emission scanning electron microscope (**FE-SEM**) with an acceleration voltage of 10 kV. Samples were gold-sputtered prior to SEM images.

Fourier transform infrared (**FT-IR**) spectra of samples were measured by KBr pellets on a Bruker Vertex 80V spectrometer in the scan range of 4000-400 cm^{-1} of 32 scans with resolution 4 cm^{-1}.

Thermogravimetric Analysis (**TGA**) and Derivative Thermogrametric (DTG) were performed using Perkin Elmer STA600 simultaneous thermal analyzer to evaluate thermal degradation of original and sulfonated sample in the range of 40-600°C at a rate of 10°C min^{-1} under a nitrogen flow rate of 20 ml min^{-1}.

Dynamic mechanical analysis (**DMA**) tester (Q800, TA Instruments, New Castle, DE, USA) was used in the measurements of Young's modulus, strain at break, and ultimate strength of CNFs composites. The measurements were performed under the uniaxial tensile mode. The CNF-PLA composite film was cut into a rectangle shape (length, width, and thickness of approximately 30 by 5 by 0.1 mm, respectively). Each sample was tested three times, and the averages with standard deviations were reported.

The X-ray diffraction (**XRD**) patterns of the CNF-PLA composite samples were analyzed by X'Pert PRO diffractometer. The instrument is equipped with a Cu Kα radiation source (λ=0.154 nm) with a 2θ range of 10-45° and the operation voltage and current was maintained at 40 kV and 40 mA respectively.

The crystallinity index (C.I.) of nanocellulose based on the XRD pattern was determined as[210]:

$$C.I. = \frac{I_{002} - I_{am}}{I_{002}} \times 100\% \qquad (6.2)$$

where, I_{002} is the intensity of (002) peak at 2θ =22.5° and I_{am} is the intensity of the amorphous region (at 18.3°) between the two crystalline peaks.

The degree of crystallinity of PLA or isocyanates (HDI and TDI) modified PLA was computed according to the area of amorphous halo and crystalline peaks in XRD pattern using the equation:

$$\chi_C = \frac{A_C}{A_C + A_a} \qquad (6.3)$$

where χ_c is the degree of crystallinity, and A_c and A_a are the areas of crystallized and amorphous region in the XRD pattern, respectively. The multi-peaks resolution over a diffraction angle of 10° to 30° was performed in Jade to calculate the area.

The apparent crystallite size (D) for the main (110) and (203) reflections in the XRD pattern of PLA was calculated using the Scherrer's equation:

$$D = \frac{k\lambda}{\beta_c \cos\theta} \qquad (6.4)$$

where K is the Scherrer constant (0.94), λ is the X-ray wavelength(λ = 0.154056 nm for Cu Kα radiation), β_c is the full width at half maximum value of the diffraction peak (FWHM), and θ is Bragg's angle.

The interplanar distances (d) was calculated using Bragg's relationship:

$$d = \frac{\lambda}{2sin\theta} \quad (6.5)$$

where λ and θ are the same as described in equation (6.4).

Mercury porosimetry was performed on Autopore IV 9500 instrument (Micromeritics, USA) to measure the pore size distribution and surface area of the materials.

The porosity was defined based on the values of bulk density and true density:

$$\varepsilon\% = \frac{\rho_{true} - \rho_{bulk}}{\rho_{true}} \times 100\% \quad (6.5)$$

where ε is the porosity; ρ_{bulk} is bulk density of the film from its dimensions; ρ_{true} is the skeletal density of the film.

6.3 Results and discussion

6.3.1 The conception for pores construction of CNF framework and composite preparation with polymer PLA

Different drying approaches including room-temperature drying, heat-drying and freeze-drying were combined in the pore construction of the CNF framework. The room-temperature drying results in the production of CNF membranes due to the formation of 3D hydrogen bonding networks. Heating can further strengthen the hydrogen bonding interactions and even the self-crosslinking between CNF fibrils (Fig. 6.2). The hydrogen bonding includes irreversible hydrogen bonding, which is known as the hornification of nanocellulose fibrils, and reversible hydrogen bonding. The reversible hydrogen bonding, just as it implies, can be reversibly formed during the water removal and also broken by the water swelling[62]. Therefore, as shown in Fig. 6.2, the formed reversible hydrogen bonding will reopen and the bonded nanocellulose fibrils swell when the membrane is in contact with water. After the freeze-drying, the water inside the CNF membrane is removed again by freeze-drying so the 3D porous CNF framework is formed.

Different from the CNF aerogels obtained by directly freeze-drying CNF suspensions, the 3D porous framework is highly porous but could remain reasonable high-strength because of the presence of irreversible hydrogen bonding. Without heat-drying, the CNF membrane is disintegrated easily in water. Therefore, both heat-drying and freeze-drying after reswelling are essential for the fabrication of porous CNF framework.
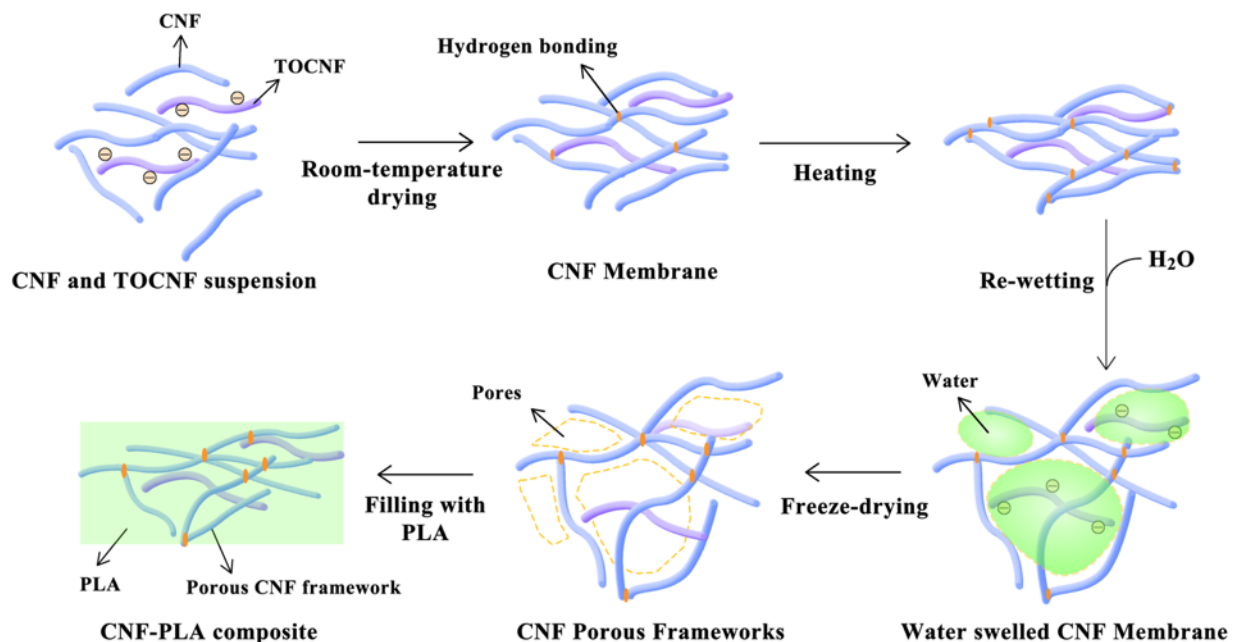
Figure 6. 2 The mechanism of pore formation during the CNF framework fabrication and the composite preparation with PLA.

The CNF-PLA composites can be obtained by filling PLA into the pores of CNF framework. Different from the traditional CNF polymer composite that the CNF fibrils are separately distributed in the polymer matrix, the fibrils used as reinforcement materials in this study are partially bound together via irreversible hydrogen bonding to form a continuous and porous 3D framework. Therefore, it is expected that the mechanical strength of the composite can be highly improved.

6.3.2 Fabrication of porous nanocellulose films
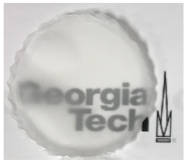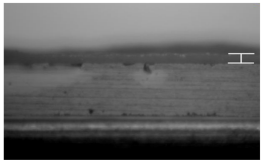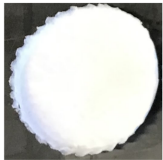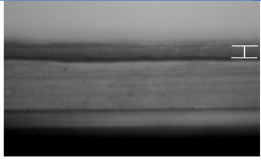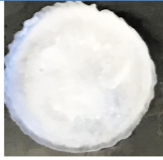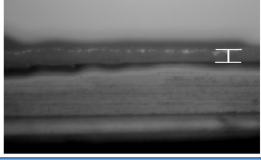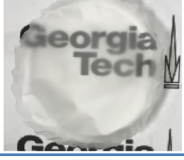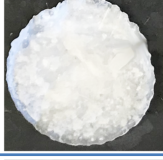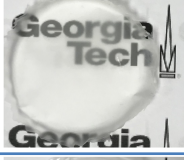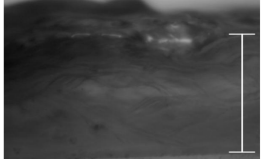
6.3.2.1 Pore structure adjusting with TOCNFs

TOCNF was used in the nanocellulose porous framework fabrication because TOCNF has a high water retention value (WRV) (Fig. 6.3). Different amounts of TOCN were mixed with CNF to form the suspension with the TOCNF fractions of 0%, 5%, 10%, 20%, 40%, 60% and 100%.

After room-temperature water evaporation and heat-drying, different nanocellulose films were obtained, as shown in Table. 6.1. The prepared nanocellulose films are semitransparent because the hornification of nanofibrils occurred during the drying to form a dense and bulk material. With the addition of TOCNF, the transparency of the film increased, which could be attributed to that the fibrils of TOCNF after the TEMPO oxidation are smaller than mechanically prepared CNF. When the TOCNF fraction increased to 100% (i.e. pure TOCNF), the obtained film was completely transparent. After the heating treatment, the films were rewetted in DI water overnight. As shown in Table. 6.1 the middle column and Fig. 6.3A, the thickness of re-wetted film was increased compared to the initial values before impregnation in water (about 0.15 mm on average). For the sample of 100% TOCNF, the thickness increased to 15 times higher than the value before re-wetting. The water retention values showed similar results to the thickness. These results indicate that the dried nanocellulose films can be swollen by water and re-open part of the hydrogen-bonding locked regions[63]. TOCNF is highly hydrophilic due to the carboxyl groups and active hydroxyl groups produced during the TEMPO oxidation. Therefore, the dried TOCNFs can absorb more water than common CNFs, resulting in increased re-wetting thickness and water retention.

The freeze-drying process can remove water from nanocellulose materials but the shape and wet-stated structures would be maintained because the nanocellulose fibers were frozen during the drying process. Table 6.1, the right column shows the freeze-dried nanocellulose films after the heating and then re-wetting treatments. It can be seen that the transparent or semitransparent nanocellulose films turned opaque, indicating the forming of porous structures.

Table 6. 1 The photographs of prepared nanocellulose films with different TOCNF fractions by the treatment of heat-drying, re-wetting and freeze-drying process. The bars shown in the images of re-wetted samples indicate the thickness of nanocellulose films after the water re-wetting.

TOCNF fraction	Heated film	Re-wetted	Freeze-dried
0%			
5%			
10%			
20%			
40%			
60%			
100%			
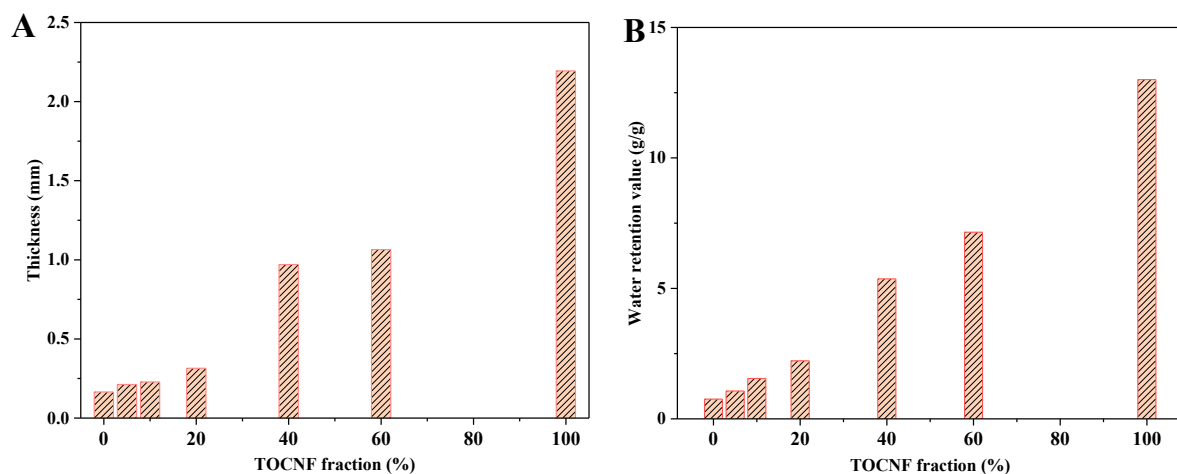
Figure 6. 3 (A) The thickness and (B) the water retention values of re-wetted nanocellulose films

6.3.2.2 Characterizations

The porous nanocellulose frameworks obtained by freeze-drying were characterized via SEM, as shown in Fig. 6.4. The porous part of the material shows a high brightness on the SEM images due to the high electron scattering. However, the dense part or fiber bound part shows a dark color. It can be seen from the SEM images that the porous parts were dispersedly distributed on the nanocellulose film surface. Nanocellulose bundles formed by hydrogen bonding between fibrils remained after the freeze-drying, which constituted the meshing-like frameworks of nanocellulose, shown as dark regions on the SEM images.
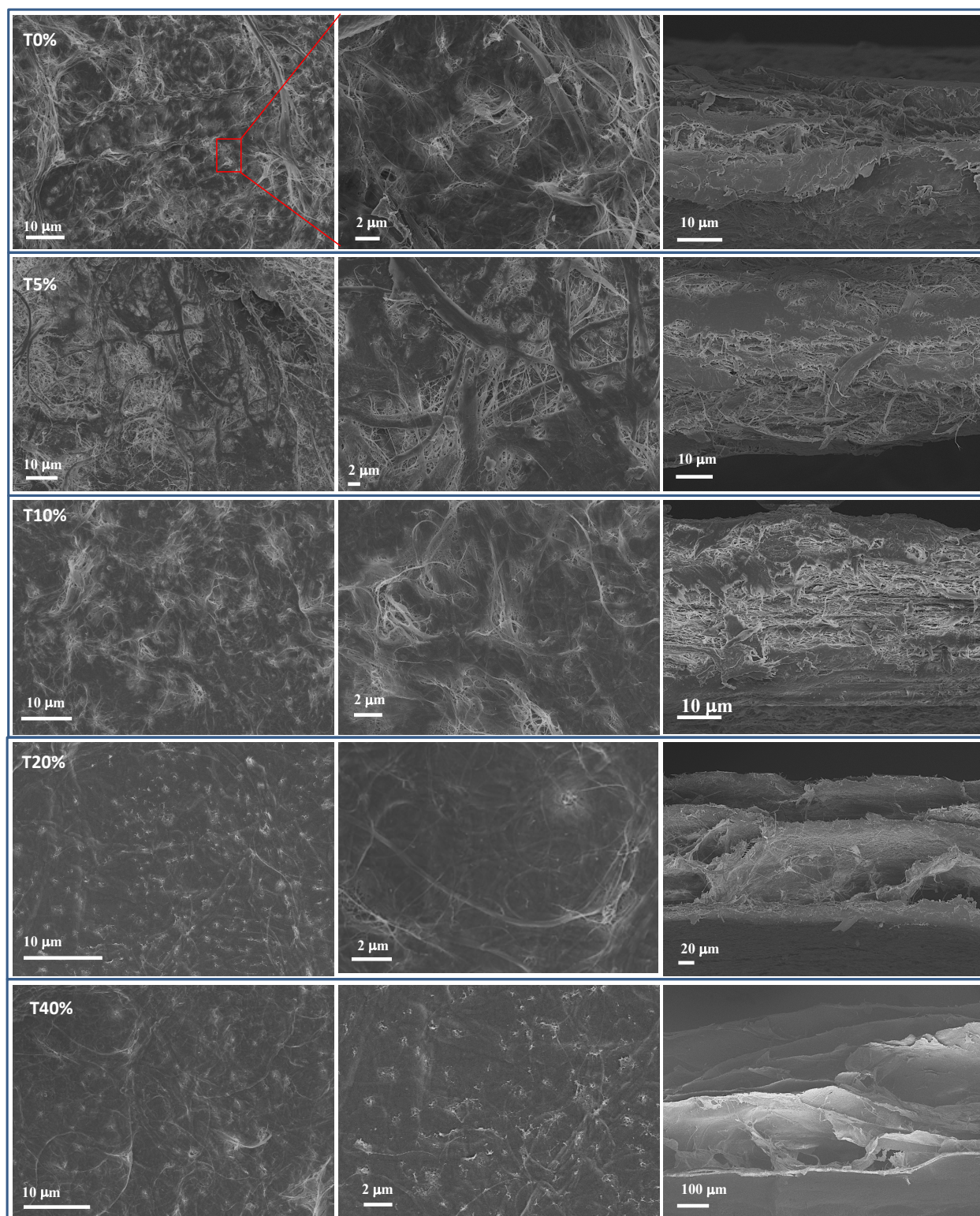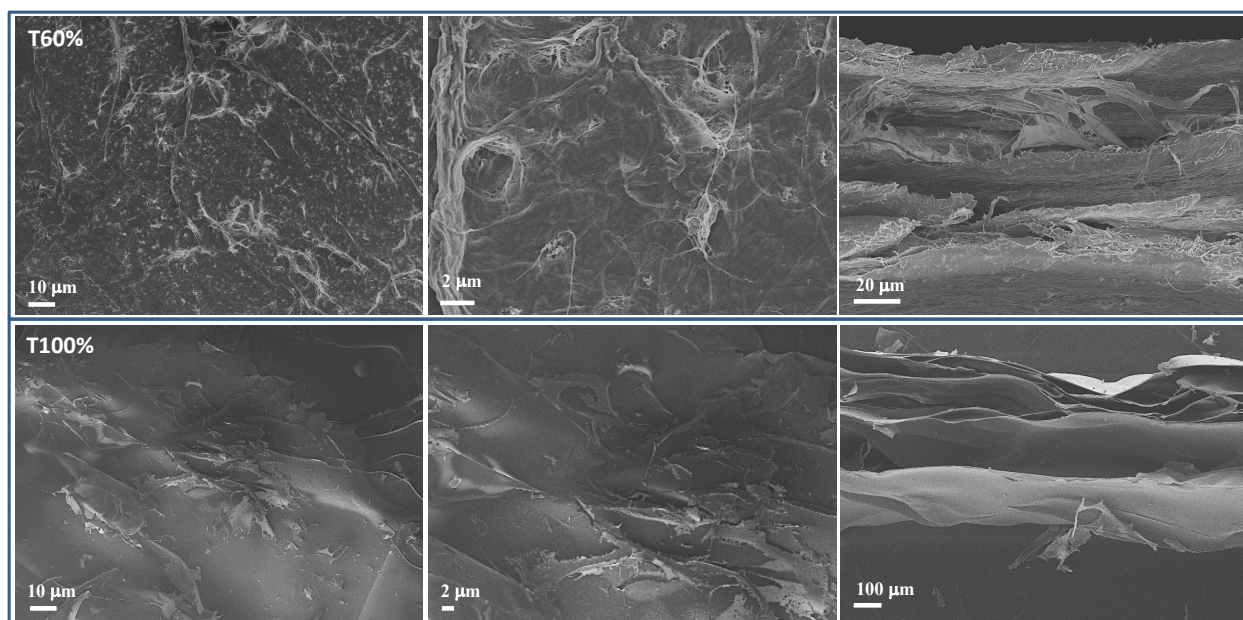
Figure 6. 4 SEM images of freeze-dried nanocellulose films with different TOCNF fractions. T0% noted for the sample with TOCNF fraction of 0% and so on. The columns from left to right are top-view, magnified top-view and cross-section view of freeze-dried nanocellulose films, respectively.

The pore structures were characterized by using mercury porosimetry, as shown in Table 6.2. The porous film made from pure mechanical CNF (T0%) has a specific surface area of 32.45 m^2 g^{-1}, pore diameter of 1.96 μm and porosity 62.96% after the freeze-drying. By adding TOCNFs, the specific area and average pore were increased. For example, by increasing TOCNFs content to 20% (sample T20%), the average pore diameter increased by 0.15μm. At the same time, the specific surface is nearly doubled compared to the pure mechanical CNF sample (T0%). Therefore, the adding of TOCNFs can adjust the porous structures for nanocellulose frameworks due to the highly hydrophilic propertyies and high water retention. However, the specific surface area of 100% TOCNFs film (T100%) is not the highest one, probably because TOCNFs material tends to form layered structures[113], as shown in Fig. 6.4.

Table 6. 2 Hg-porosity data for freeze-dried nanocellulose films.

Samples	Specific Surface Area m^2 g^{-1}	Average Pore Diameter μm	Bulk density g cm^{-3}	Porosity %
T0%	32.45	1.96	0.40	62.96
T5%	41.57	2.08	0.38	64.33
T10%	44.42	2.16	0.29	66.56
T20%	61.58	2.21	0.29	66.40
T40%	60.94	3.59	0.21	66.55
T60%	60.68	7.71	0.14	81.29
T100%	57.66	11.07	0.05	82.40

The FT-IR spectra of porous nanocellulose films made by mechanical CNF (T0%), TOCNF (T100%) and their mixture (T20%) were shown in Fig. 6.5. The most significant difference between them was the vibration of C=O groups at the wavelength 1600 cm^{-1}. TOCNF has a strong vibration absorption at 1600 cm^{-1} because TOCNF fibrils are partially oxidized, and this can explain the high hydrophilic properties of TOCNFs.

XRD patterns show the semi-crystalline structure of the prepared 3D nanocellulose frameworks (Fig. 6.6). The comparisons of the XRD patterns and corresponding crystallinity indices (C.I.) before water re-wetting and after freeze-drying were conducted, as shown in Table 6.3 and Fig. 6.6. The crystallinity of the nanocellulose before re-wetting decreased with the addition of TOCNFs because TOCNFs itself has been slightly degraded during the TEMPO oxidation process. After freeze-drying, the C.I. value of porous CNF frameworks slightly increased compared to the value before re-wetting. Also, C.I. value after freeze-drying decreased with the addition of TOCNFs.
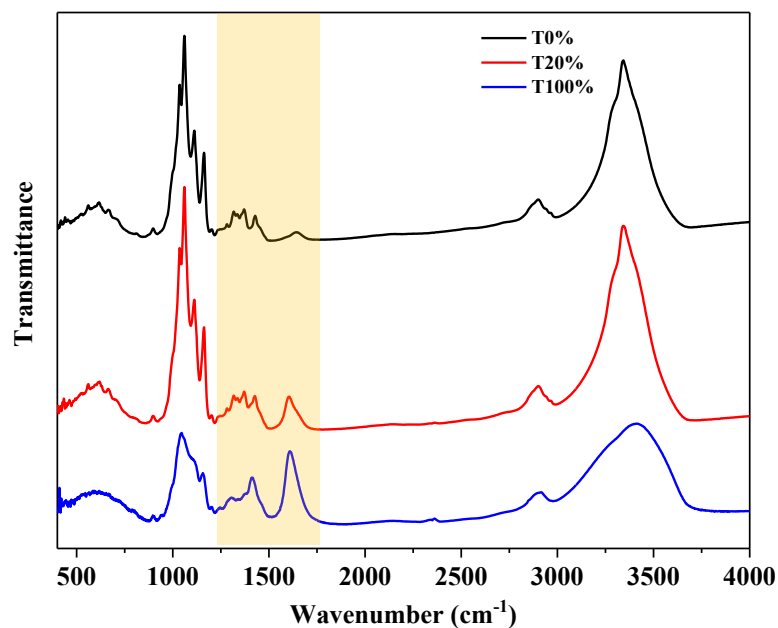
Figure 6. 5 FT-IR spectra of nanocellulose films with different TOCNF fractions after the freeze-drying.
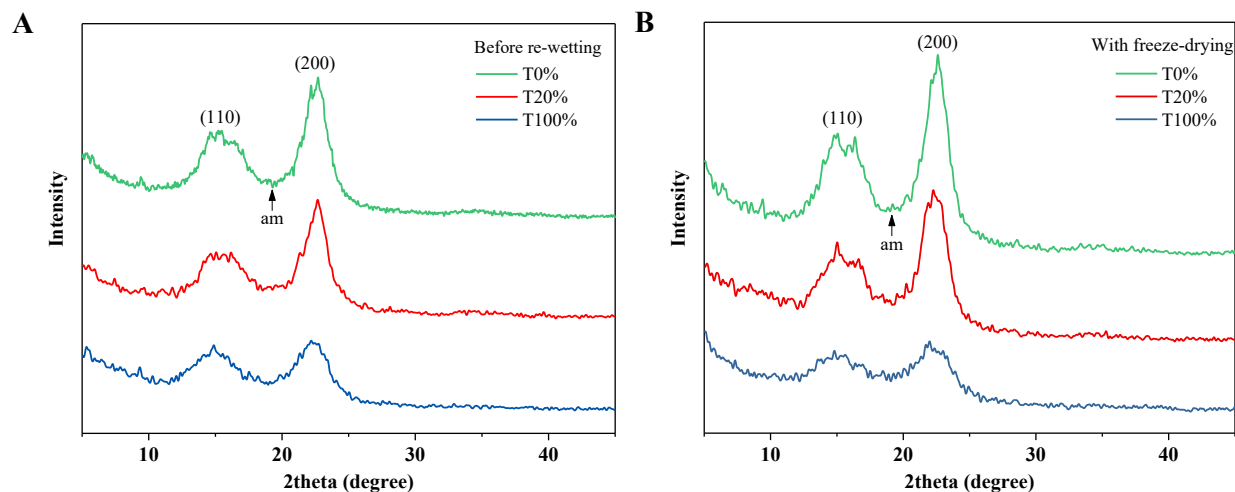
Figure 6. 6 XRD patterns of nanocellulose films with different TOCNF fractions before (A) and after (B) the freeze-drying. The "am" noted the diffraction background of amorphous phase for the crystallinity index calculation.

Table 6. 3 Crystallinity index (C.I.) of nanocellulose films with different TOCNF fractions

Samples before re-wetting	C.I.	Samples With freeze-drying	C.I.
T0%	74.09%	T0%	72.39%
T20%	71.85%	T20%	70.89%
T100%	58.20%	T100%	49.37%

6.3.2.3 Mechanical properties of porous nanocellulose frameworks

The mechanical performances of the porous structures are crucial for composite fabrication. Figure 6.7 shows the comparison of the stress-strain plots, ultimate tensile strength and modulus of the prepared nanocellulose films with different TOCNFs fractions. It can be seen that all the nanocellulose films with heat-drying before the re-wetting have good mechanical properties with the ultimate tensile strength of 200-250 MPa and modulus of 6-7 GPa. These results are in accordance with the published literature which reported that the mechanical strength of both CNFs and TOCNFs are high due to the ordered strong hydrogen bonding interactions[247, 248]. In this study, the mechanical behaviors of prepared porous nanocellulose films after the re-wetting and freeze-drying were investigated. The films of pure mechanical CNF (sample T0%) and mixed with 5% TOCNF (T5%) have shown a high tensile strength and modulus which are almost the same as that of initial films. This suggests that by combining different drying methods in this study, the high porosity of the nanocellulose structures (porosity 63-67%) and high mechanical performances (tensile strength 230-250 MPa) were simultaneously reached. With the increase of TOCNFs fraction in the nanocellulose films, the tensile strength decreased. However, with the TOCNFs fraction of 20% (sample T20%), the tensile strength still reached 150 MPa, which still can be considered as a good reinforcement framework.
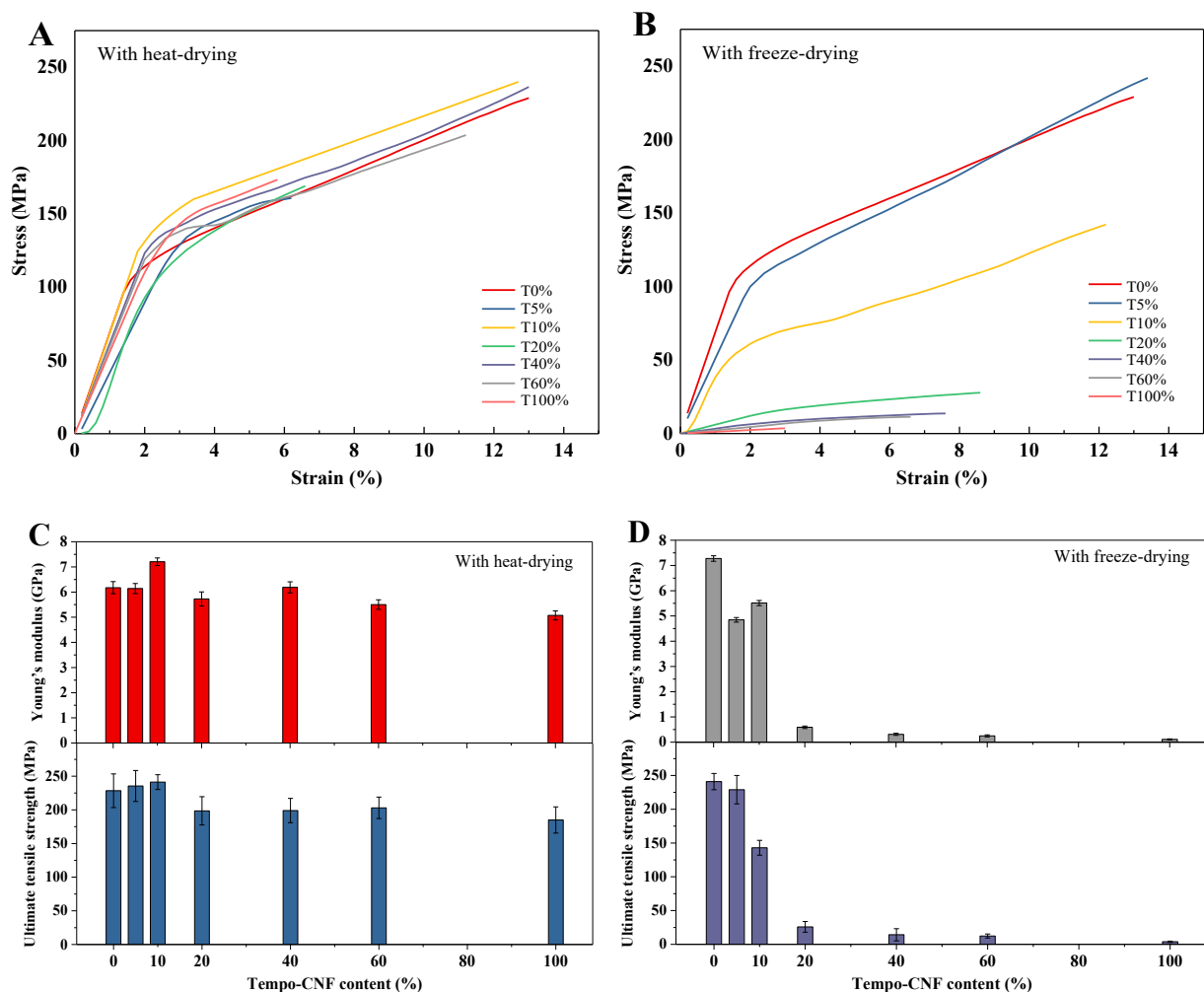
Figure 6. 7 (A) Stress-strain curves of nanocellulose films before and (B) after the re-wetting and freeze-drying. (C) Summarization of the ultimate tensile strength and Yong's modulus of nanocellulose films before and (D) after the re-wetting and freeze-drying.

6.3.3 Chemical crosslinking of PLA using isocyanates

To increase the interactions between the PLA polymer chains and the interaction between PLA and CNFs fibrils, chemical crosslinking was introduced. In this study, the bi-functional isocyanates, toluene diisocyanate (TDI) and hexamethylene diisocyanate (HDI), were used as bridge molecules in the crosslinking reactions, as shown in Fig. 6.8. On one hand, TDI or HDI can

react with the hydroxyl groups or carboxyl groups at the end of PLA chains, so that the PLA can be crosslinked. On the other hand, TDI or HDI could bond the PLA molecules with the surface hydroxyl groups of CNF fibrils, as shown in Fig. 6.7 C. TDI and HDI are two molecules with different configurations. TDI connects molecules through the benzene ring which is a ridged connection; however, HDI is a linear molecule with 6 carbons C-C bond chain, which is more flexible than TDI.
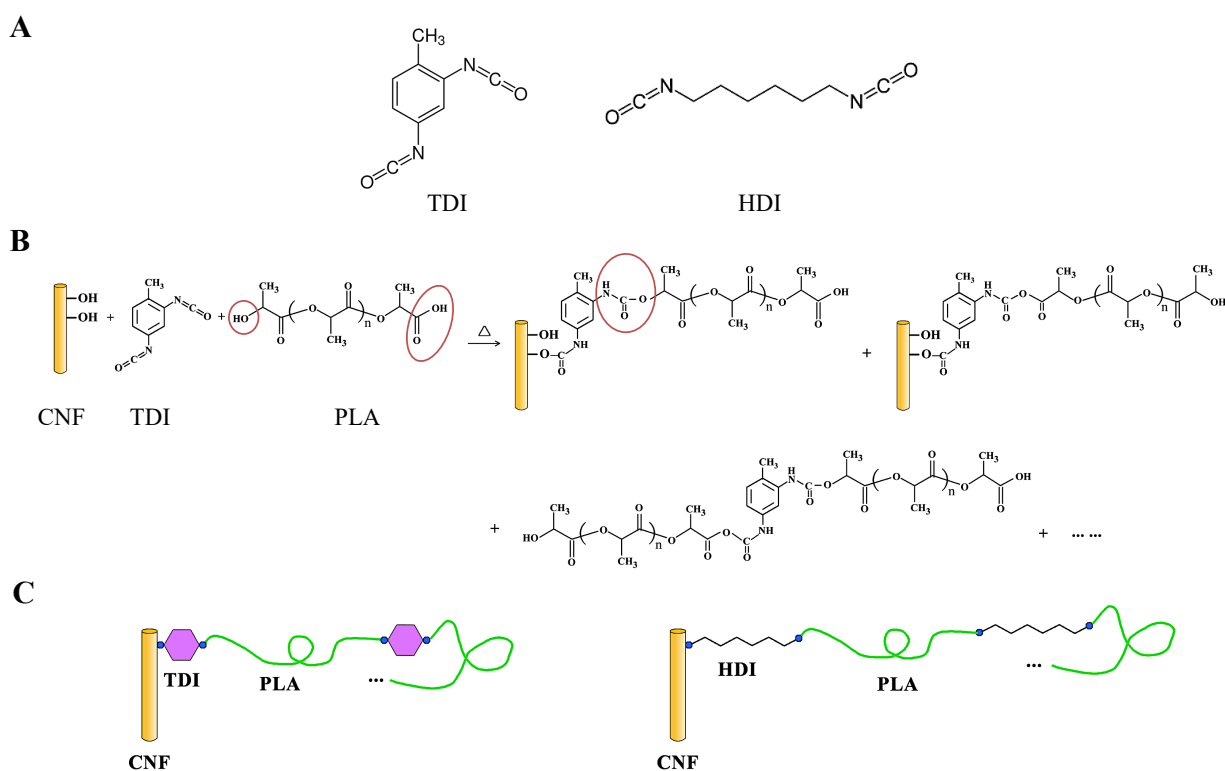
Figure 6. 8 (A) The chemical structure of isocyanates TDI and HDI. (B) The molecular structure of chemical bondings between PLA polymer chains, and PLA and CNF fibrils. (C) The connection model for TDI and HDI crosslinked PLA-CNF composites.

This study first researched the crosslinking of PLA polymer with TDI and HDI. The crosslinking reactions were conducted in the PLA solution at 80°C. Figure 6.9 shows the FT-IR

characterizations of PLA and PLA with the modification of TDI and HDI. The peaks at the wavenumber of 1691 cm^{-1} (shown in Fig. 6.9 B) can be ascribed to the stretching vibration of C=O of PLA[249]. In the spectra of TDI-PLA and HDI-PLA, small peaks appear beside the C=O vibration peak of PLA. This could be ascribed to the C=O group vibration in carbamates formed by the reaction of PLA and isocyanates, indicating the successful crosslinking of PLA.
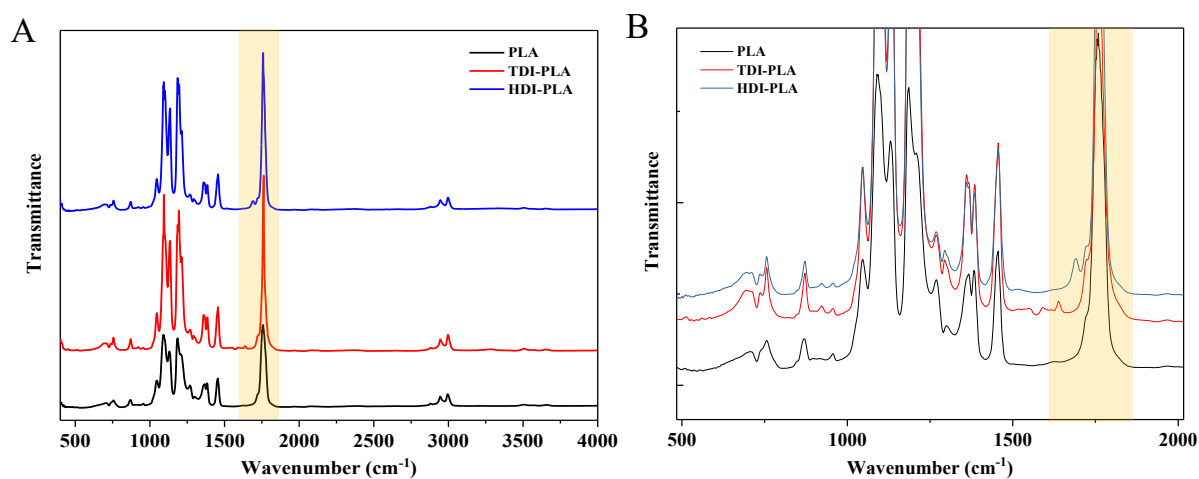
Figure 6. 9 (A) FT-IR spectra of pure PLA, HDI and TDI modified PLA. (B) The magnified FT-IR spectra in the range of 500-2000 cm^{-1}.

To investigate the chemical and physical properties of crosslinked PLA, PLA films were prepared by the casting method under ambient temperature. XRD patterns show the PLA and crosslinked PLA films have crystalline and also amorphous structures (Fig. 6.10). The crystallinities were calculated according to the results of peak resolving. The results indicate that after the TDI and HDI crosslinking, the crystallinity of the PLA increased from initial value of 41.8% to 55.2% and 45.7% respectively (Table 6.4). The increase of the crystallinity suggests the modified PLA would have improved mechanical properties.
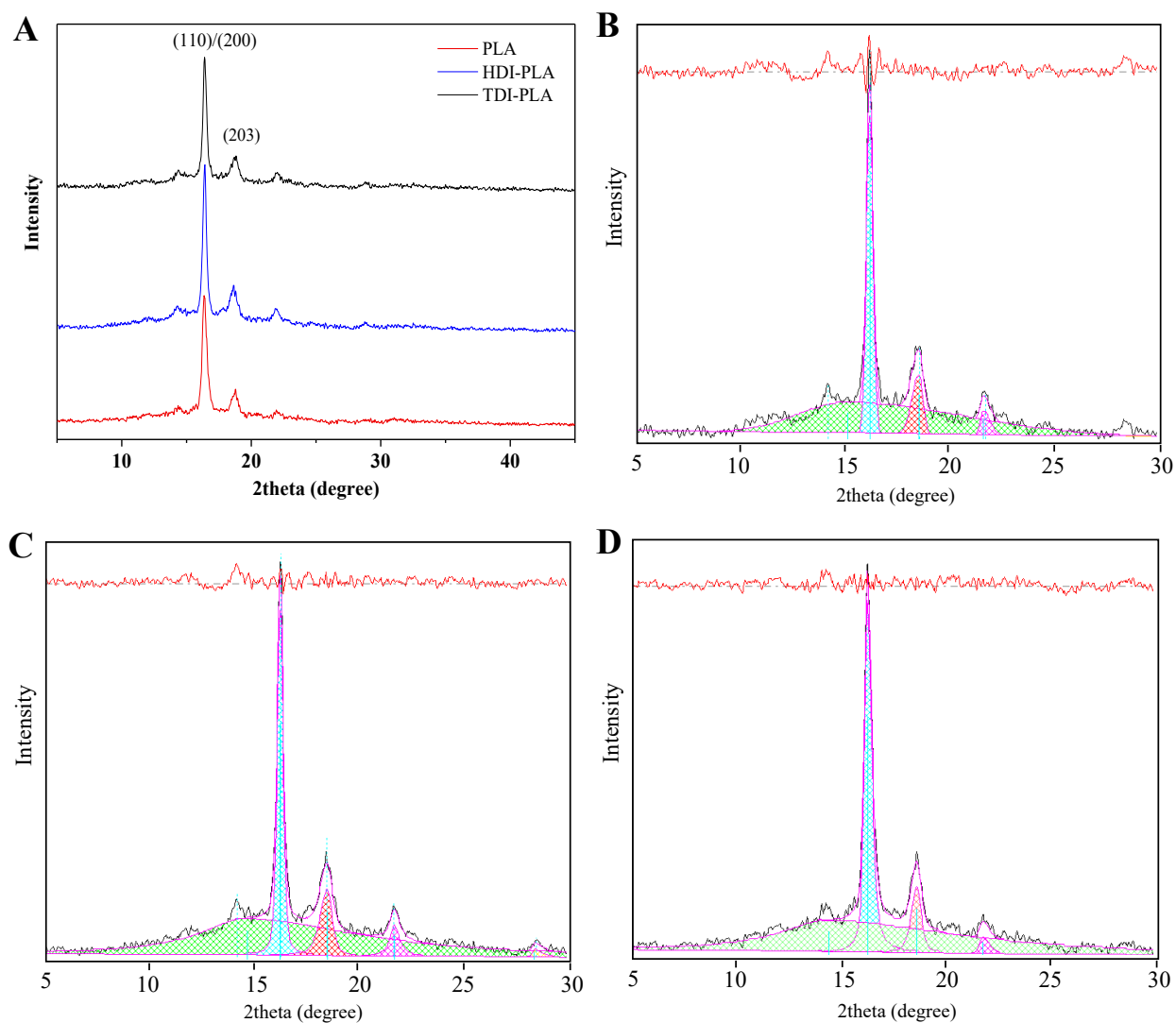
Figure 6. 10 (A) XRD pattern of PLA and isocyanates crosslinked PLA. (B), (C) and (D) Peak-resolving of the XRD pattern for crystallinity calculation of TDI, HDI modified PLA and pure PLA, respectively.

Thermogravimetric analyses (TGA) of the PLA samples show that the thermal stability has improved after the isocyanate crosslinking (Fig. 6.11 and Table 6.4). The onset temperature ($T_{5\%}$) of thermal decomposition for the initial PLA is 322.9 °C. The value increased by 5 °C and 20 °C with reacted with HDI and TDI respectively. The temperature at 50% weight of loss ($T_{50\%}$) and the temperature at the maximum decomposition rate (T_{max}) also have increased after the chemical

crosslinking. These results show that crosslinking by isocyanate is an effective method to improve the performance of PLA matrices and the operation for the reactions is very simple.
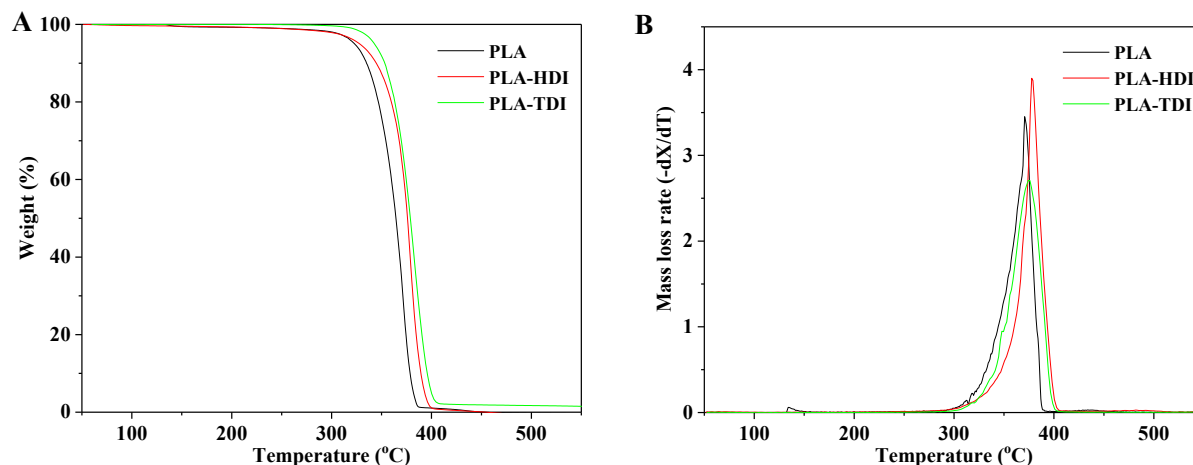
Figure 6. 11 (A) Thermogravimetric analysis (TGA) curves and (B) derivative thermogravimetric (DTG) curves of TDI, HDI modified PLA and pure PLA.

Table 6. 4 The calculated crystallinity (χ_c) and crystalline sizes (D_{110}) from the XRD patterns and $T_{5\%}$, $T_{50\%}$, T_{max} values summarized from TGA curves.

Samples	$T_{5\%}{}^*$ (°C)	$T_{50\%}{}^\dagger$(°C)	$T_{max}{}^\ddagger$(°C)	Crystallinity χ_c(%)	D_{110} (nm)
PLA	322.9	364.3	370.8	41.8%	21.1
PLA-HDI	327.7	376.1	375.2	45.7%	25.1
PLA-TDI	342.5	378.7	378.2	55.2%	24.9

* The temperature at the weight loss of 5%. †The temperature at the weight loss of 50%. ‡The temperature at the maximum decomposition rate.

The mechanical properties of the PLA and isocyanate crosslinked PLA films have been investigated (Fig. 6.12). As expected, after the TDI and HDI modification, the tensile strength and

modulus were increased. TDI crosslinking increased the ultimate tensile strength from the initial value of 23.2 MPa to 40 MPa and the modulus from initial 0.4 GPa to 1.7 GPa. Moreover, the elongation at break reduced from initially 28.5% to 6.3%, which means the modified PLA is rigid. HDI modification is different from TDI. The ultimate tensile strength and modulus were not as high as that of TDI modified PLA, but the elongation was highly improved to 60.9%, indicating the increase of plasticity. This can be attributed to the flexible linear configuration of the HDI molecules which is described above.
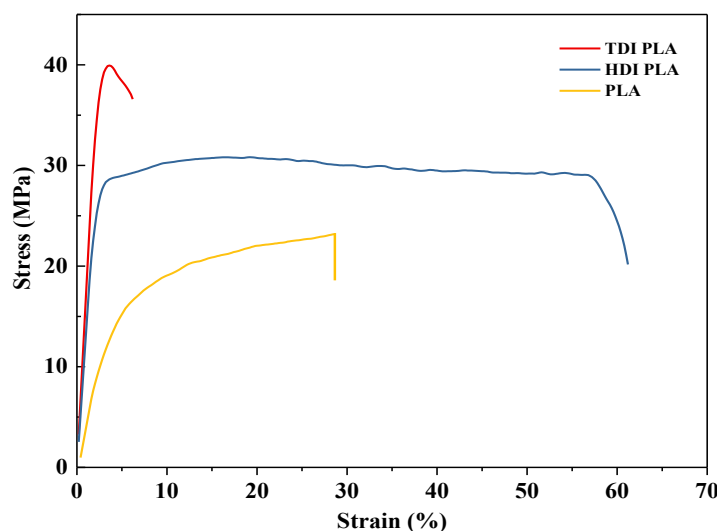
Figure 6. 12 Stress-strain curves for PLA and isocyanates crosslinked PLA films.

6.3.4 Fabrication of nanocellulose frameworks reinforced CNF-PLA composite

6.3.4.1 CNF-PLA composite film preparation

By impregnation approach, the porous nanocellulose frameworks were filled with PLA to form the CNF-PLA composite films. Simultaneously, isocyanate was added into the PLA solution for in-situ crosslinking of CNF fibrils and PLA. Different from the traditional filler reinforced composite that the fillers are separately distributed in the polymer matrix, the fibrils of the porous

nanocellulose frameworks used here were bound together to form continuous 3D networks. Moreover, the nanocellulose frameworks are highly porous and have a high specific area, which provides good contact and strong interaction with PLA polymeric matrix. With the crosslinking by the bridge molecules TDI or HDI, the covalent bonding between CNF porous frameworks and PLA polymeric matrix was formed. Therefore, we could expect that the mechanical performances of the composite material will be highly improved. SEM images (Fig. 6.13) show the surface and fracture morphology of the prepared CNF-PLA composite film.
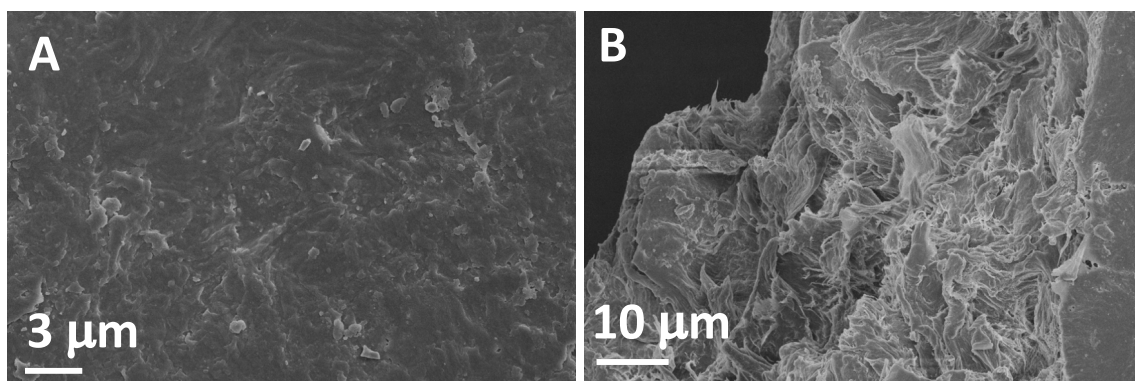
Figure 6. 13 SEM images of porous nanocellulose framework reinforced PLA composite membrane. (A) and (B) show the film crosslinked with TDI.

6.3.4.2 Characterizations

The prepared CNF-PLA composite films were characterized by XRD. Figure 6.14 shows the XRD patterns of the composites with different TOCNF fractions in the porous frameworks. The peak at $2\theta = 16.3°$ and $18.8°$ were assigned to the reflection from the crystallographic plane of (110)/(200) and (203) in PLA phase (noted with *) and the peaks for crystalline phase of nanocellulose were located at the $15.8°$ and $22.5°$ (noted with o)[226, 227]. The crystalline sizes and interplanar distances of PLA in the composites were analyzed according to the Scherrer's and

Bragg's equations, as shown in Table 6.5. In the composite film, the PLA crystallite size slightly decreased to in the range of 11.9-17.5 nm, but the interplanar distances were almost the same in different composites.
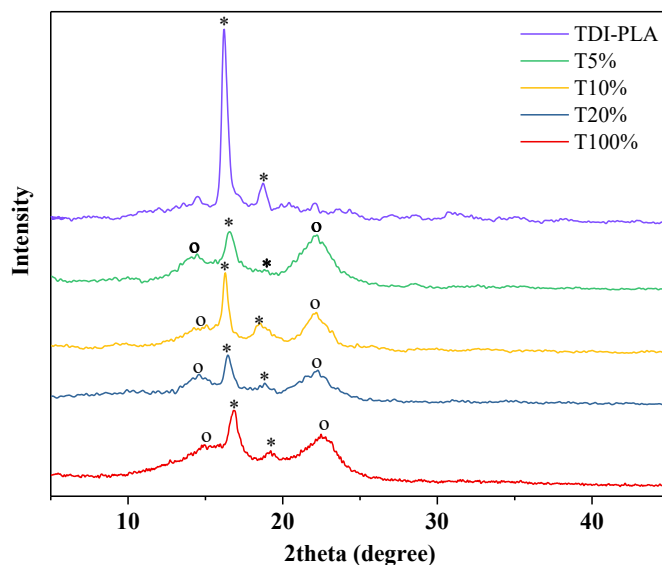
Figure 6. 14 XRD patterns of PLA composites reinforced by the porous nanocellulose frameworks with different TOCNF contents (crosslinked with TDI). PLA content is 50wt% in the composites. * noted as the PLA phases and o noted as the phases of nanocellulose.

Table 6. 5 Summary of interplanar distances ($d_{110/200}$) and crystallite sizes (D_{110}) for the PLA phase in the composite films

Samples	TDI-PLA	T5%	T10%	T20%	T100%
$d_{110/200}$ (Å)	5.44	5.35	5.44	5.38	5.27
D_{110} (nm)	24.9	11.9	17.5	15.7	12.0

The composite films with different PLA contents (~50% and ~70%) were prepared by repeating the impregnation process. The obtained films were characterized by thermogravimetric analyses, as shown in Fig. 6.15 and Table 6.6. With the increase of the PLA content in the composites, the onset decomposition temperature ($T_{5\%}$), the temperature at 50% weight loss ($T_{50\%}$) and the temperature at the maximum decomposition rate (T_{max}) were increased. This indicates that thermal stability improved with increased of PLA content because the isocyanate crosslinked PLA matrix has better thermal stability than nanocellulose.
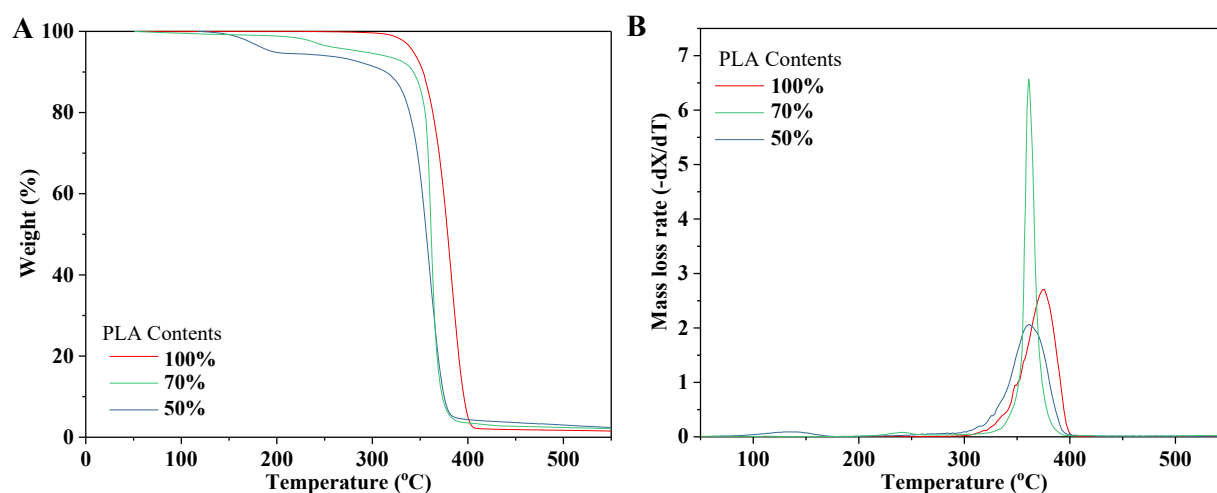
Figure 6. 15 (A) Thermogravimetric analysis (TGA) curves and (B) derivative thermogravimetric (DTG) of the porous CNF frameworks reinforced PLA composites with different CNF to PLA weight ratios (crosslinked with TDI).

Table 6. 6 The data of $T_{5\%}$, $T_{50\%}$, T_{max} and char residue summarized from TGA curves.

Composites	$T_{5\%}$ (°C)	$T_{50\%}$(°C)	T_{max}(°C)	Char residue (%) (at 550 °C)
100% PLA	342.5	378.7	378.2	1.45
70% PLA	308.4	361.6	360.5	2.12
30% PLA	239.6	356.2	361.9	2.41

6.3.4.3 Mechanical measurement

The mechanical performances of the composite films were investigated in detail. Figure 6.16 shows the stress-strain curves and summarized data of HDI crosslinked PLA composite films reinforced with porous 3D nanocellulose frameworks that contain different TOCNF fractions. The obtained composite materials show high ultimate tensile strengths and moduli. As shown in Fig.6.16 (A) and (B), with 50% PLA content in the composites, the highest value of the ultimate tensile strength reached 160 MPa which is nearly 8 times higher than that of the native PLA film, and the modulus reached 3.5 GPa. The highest results were achieved when the nanocellulose framework made by 10% TOCNF and 90% mechanical CNF. At this ratio, the obtained 3D porous nanocellulose framework has a high porosity and simultaneously high strength. With the further addition of TOCNFs in the framework, the tensile strength and modulus decreased because the TOCNFs have relatively lower tensile strength than that of mechanical CNFs. By repeating the impregnation process, the composite films with a higher PLA content (~70%) were obtained. The mechanical strength testing curves were shown in Fig. 6.16 C and D. With the high content PLA in the composite, the tensile strengths and moduli were slightly decreased but the values still achieved in the range of 80-120 MPa and 1.5-2.8 GPa which are high compared with the reported results in literatures[250-252].
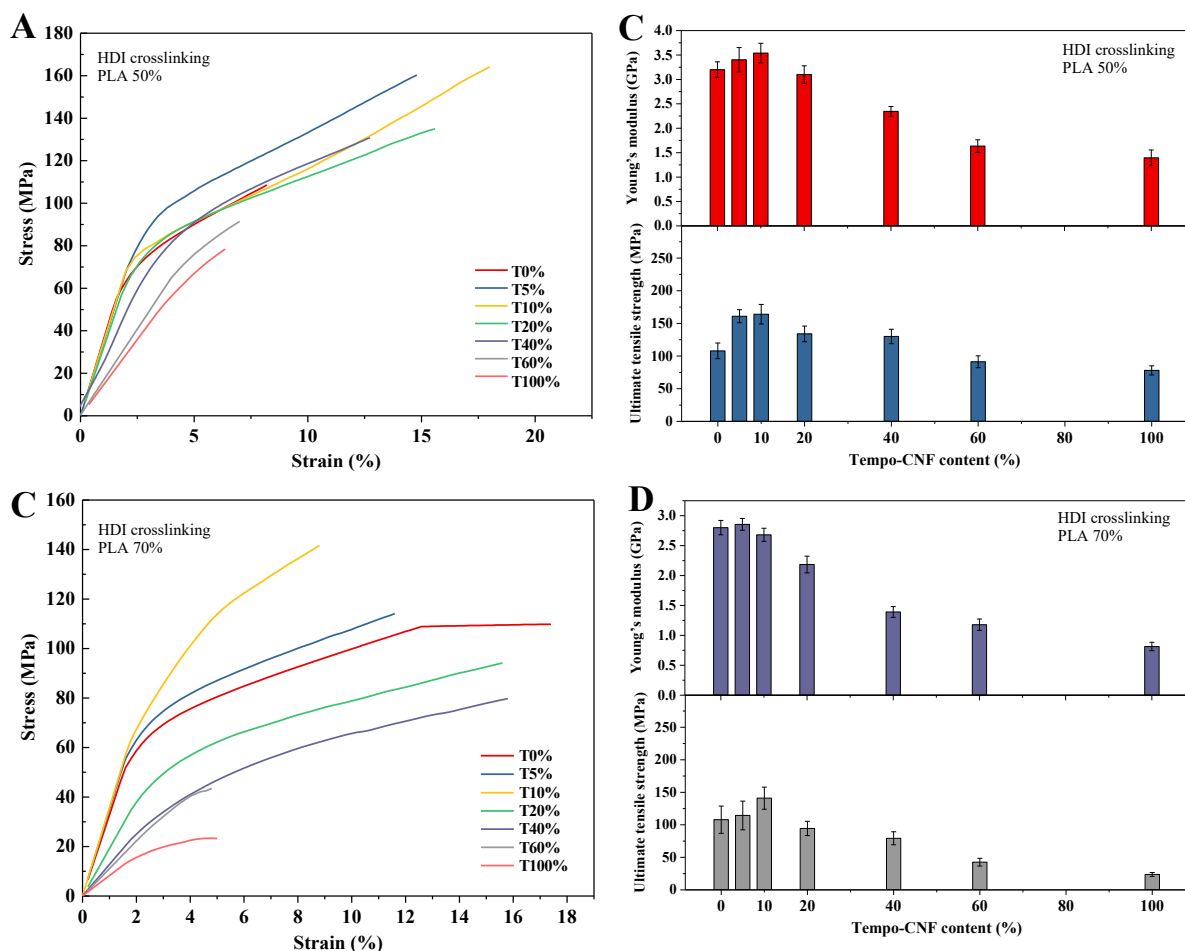
Figure 6. 16 (A) Typical stress-strain curves for the CNF-PLA composite films with different TOCNF content in the porous nanocellulose frameworks (crosslinked by **HDI** and PLA content 50%). (B) Data summary of the ultimate tensile strengths and Yong's moduli in (A). (C) Stress-strain curves for the samples with PLA content 70%. (D) Data summary of (C).

By crosslinking with TDI, the mechanical performances were further improved, as shown in Fig. 6.17. The highest tensile strength and modulus reached 205 MPa and 5.8 GPa respectively, which increased by nearly 10 times compared with that of native PLA films. It should be noticed that the elongations at the break for TDI crosslinked composite films were reduced compared with that of HDI crosslinked films, which were caused by the connection of rigid benzene rings in TDI.
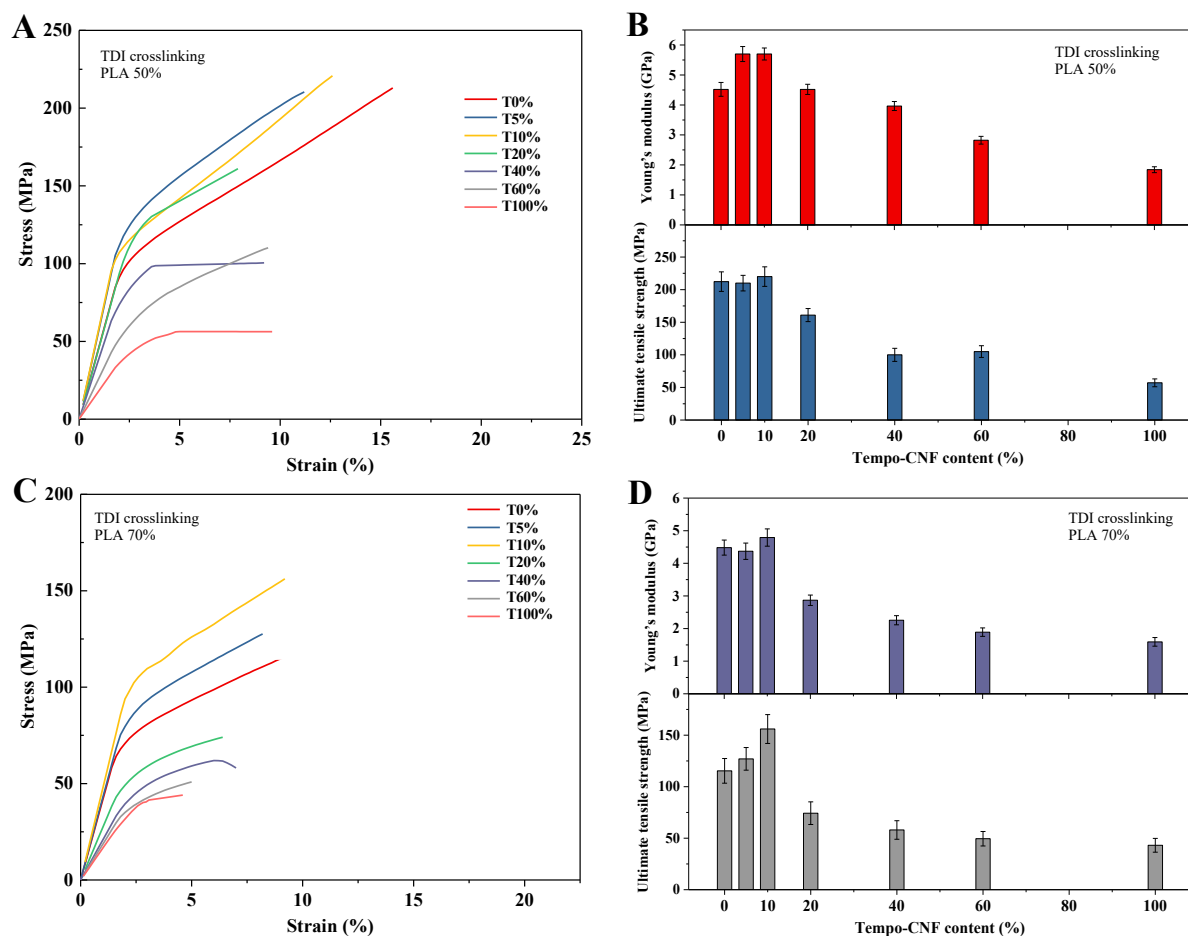
Figure 6. 17 (A) Typical stress-strain curves for the CNF-PLA composite films with different TOCNF content in the porous nanocellulose frameworks (crosslinked by TDI and PLA content 50%). (B) Data summary of the ultimate tensile strengths and Yong's moduli in (A). (C) Stress-strain curves for the samples with PLA content 70%. (D) Data summary of (C).

6.4 Conclusion

In summary, high mechanical performance CNF-PLA composites were fabricated by reinforcing the PLA polymeric matrix with 3D porous nanocellulose frameworks. The nanocellulose frameworks were made by re-wetting of dried nanocellulose films in water to open

the reversible hydrogen-bonding regions, and then freeze-dried to remove water and form pores. Therefore, the high strong irreversible hydrogen-bonding regions still remain in the porous frameworks to create it high strength. In the pore forming process, TOCNFs were used as structure adjusting agents that can increase the porosity of the material. Furthermore, to increase the interactions between the PLA matrix and nanocellulose frameworks, isocyanates, TDI and HDI, which can covalently bond with CNFs and PLA together, were introduced in the composite film preparation. The highest tensile strength and modulus of 205 MPa and 5.8 GPa respectively were achieved in the final obtained CNF-PLA (TDI modified, PLA content 50 wt%) composite films.

CHAPTER VII Nanocellulose filaments fabrication by alternative chemical and

mechanical approaches

7.1 Introduction

High-strength and long filaments are widely used in a vast array of commercial applications including automotive parts, aerospace, energy applications, building construction and even wearable electronics. The synthetic polymer-based and mineral-material-based filaments, such as aramid Kevlar fibers, thermal treated carbon fibers and glass fibers, are typical products in current markets. In recent years, high-performance filaments from renewable resources have attracted tremendous interest in both scientific and industrial fields.

Cellulose nanofibrils (CNFs, or called nanocellulose) have been of great interest to make filaments due to their low weight, high aspect ratio, and excellent theoretical mechanical strength properties. Nanocellulose can be environmentally friendly, extracted from the cellulose, which is the most abundant natural polymer on earth and widely sourced from lignocellulosic biomass, algae and bacteria. The elementary fibers of nanocellulose are generally 3-4 nm wide and highly crystallized by the intra- and intermolecular hydrogen bonding networks. Therefore, individual fibrils of nanocellulose show excellent mechanical properties, e.g., estimated elastic modulus of 29-36 GPa and tensile strength of 1-3 GPa along the fibril axis[12, 22]. However, the extraordinary performances of individual nanofibers have a significant loss if they are fabricated into the practical applied continuous nanocellulose filaments with the diameter of tens to hundreds of micrometers. Compared with individual nanocellulose fibers, nanocellulose fabricated filaments are commonly reported with the tensile strength of 100-400 MPa and Young's modulus of 10-20 GPa[20, 156-158]. Indeed, the loss in mechanical properties during the practical macroscale fiber

fabrication from nano-sized individual fiber is a general problem in engineering. For example, the tensile strength of individual carbon nanotubes reach as high as 63 GPa, while carbon nanotube fabricated fibers can only have moderate mechanical properties (~200-300 MPa in tensile strength)[12, 22]. The significant performance loss could possibly be caused by several reasons, such as intrinsic defects existed in nano-cellulose materials, the length limitation of highly crystallized individual cellulose fibers, the boundaries, voids and week bonding between nano cellulose fibers and mis-alignment of the nanofibers[159].

Various strategies have been proposed to improve the mechanical performances of nanocellulose filaments. The alignment of cellulose nanofibers in filaments is usually used because alignment can improve the fiber orientation and reduce voids or pores in fabricated filaments. Also, alignment increases the contact area among fibers, which will lead to increase of bonding force between fibers; and the generated long period stacking structure further improves the stress performances of filaments. Magnetic and electric fields are early applied in the fiber alignment control[160, 161]. However, considering the sophisticated operation of magnetic and electric fields, hydrodynamic shear orientation is a simple method that can be achieved to improve the fibril alignment. Nanofibrils in the hydrodynamic flow will tend to orient themselves perpendicular (deceleration) or parallel (acceleration) to the flow direction[162]. The improved toughness or strength related nanostructures can be controlled by operation parameters such as the extrusion capillary length, nozzle diameter and flow rate[156, 253, 254]. Besides the orientation, the structure and inter-fiber bonding may be the other factors affecting the mechanical properties[166, 167]. Due to the abundant hydroxyl groups on the surface of nanocellulose fibrils, various chemical modifications involving covalent or ionic crosslinking of cellulose fibers could be used to enhance inter-fibril bonding and reduce voids among fibers[20].

In this study, a wet-spinning method was used to fabricate the nanocellulose filaments. Firstly, to prepare continuous and uniform nanocellulose filaments, operation conditions such as the solid contents of nanocellulose spinning dope, spinning rate and nozzle diameter were investigated. To increase the fiber-fiber interaction, chemical bonding of nanocellulose fibers by different chemical bonding agents, including organic crosslinkers, polymer binders and inorganic fillers, were researched. In addition, physical post-treatments by wet stretching or wet-twisting were conducted to further improve mechanical properties.

7.2 Experimental Section

7.2.1 Materials

Cellulose nanofibril slurry (CNF, fiber content 3.4 wt%) was provided by American Process International LLC. Citric acid, boric acid, glutaraldehyde, polyvinyl alcohol (PVA, M_w 106,000-110,000), sodium carboxymethyl cellulose (CMC, M_w 250,000) and LUDOX® AS-30 colloidal silica were purchased from Sigma-Aldrich. Ameroxide® TiO_2 P25 was purchased from Nippon Aerose. Co., LTD. Kymene™ was an industrial product.

7.2.2 Wet-spinning of nanocellulose filaments

CNF filaments were prepared by using wet-spinning method at room temperature. The spinning dope, nanocellulose paste (with different solid concentrations of 2%, 3% 4% and 6%), was carefully transferred to the syringe to avoid air bubbles in it. A syringe pump was used to extrude the spinning dope through a nozzle. The extruded CNF filaments were completely dried at room temperature and then dried at 80 °C for 2 hours in the oven. Different nozzles with diameters of 0.41, 0.6 and 1.0 mm were used and different spinning rates of 0.5 ml min^{-1}, 2.5 ml min^{-1} and 2.5 ml min^{-1} were performed in the nanocellulose spinning.

119

7.2.3 Chemical modification of the nanocellulose filaments

The bonding agent (10wt% based on the dry weight of nanocellulose) was directly added into nanocellulose fibril slurry and mixed with mechanical stirring. Then the obtained nanocellulose paste was used in the wet-spinning. After completely drying at room temperature, the extruded CNF filaments were heated at elevated temperature for 2 hours in oven. The bonding agents used here included citric acid, glyoxal, glutaraldehyde, PVA, CMC, Kymene, boric acid, P25 and colloidal silica. For Kymene, citric acid and glutaraldehyde modified filament, the drying temperature was 100 °C after the room-temperature drying, and other samples were dried at 80 °C.

7.2.4 Wet stretching or wet-twisting treatment

To improve the fibril alignment, wet-stretching and wet-twisting were applied before drying. The stretching was conducted by hanging the filament on a shelf. One end of the filament was fixed and the other end attached a weight (5 gram) until the filament was completely dried. To further increase the mechanical properties, the half-dried filaments were twisted and dried at room temperature.

7.2.5 Characterizations

The surface morphology of filaments was examined via LEO 1530 thermally assisted field emission scanning electron microscope (**FE-SEM**) with an acceleration voltage of 10 kV. Samples were gold-sputtered prior to SEM images.

Optical microscopic images were obtained using a Leica DMLM light microscope connected to a color video camera. The diameters were measured based on the cross-section images and a scale.

Fourier transform infrared (**FT-IR**) spectra of both original and modified samples were measured by KBr pellets on a Bruker Vertex 80V spectrometer in the scan range of 4000-400 cm^{-1} of 32 scans with resolution 4 cm^{-1}.

Dynamic mechanical analysis (**DMA**) tester (Q800, TA Instruments, New Castle, DE, USA) was used in the measurements of Young's modulus, strain at break, and ultimate strength of nanocellulose filament. The measurements were performed under the uniaxial tensile mode. Each sample was tested three times, and the averages with standard deviations were reported.

The degree of orientation of the spun fibers will be characterized using **wide-angle X-ray diffraction (WAXD)**. The orientation parameter of the spun filaments was characterized using Herman's orientation factor (f_H):

$$f_H = \frac{3(cos^2\varphi)_{hkl} - 1}{2} \; ; \; where \; (cos^2\varphi)_{hkl} = \frac{\int_0^{\pi/2} I(\varphi)cos^2\varphi sin\varphi d\varphi}{\int_0^{\pi/2} I(\varphi)sin\varphi d\varphi}$$

Here, I(φ) is the scattering intensity along the azimuthal angle, φ. The azimuthal intensity distributions of the diffraction patterns were determined along the (200) planes.

7.3 Results and discussion

7.3.1 Filaments preparation under different operation conditions

The hydrodynamic alignment which can improve the fibril orientation and the mechanical properties of resulting filaments could be controlled by different operating parameters in the fibrils wet-spinning. When CNF fibril dispersion was injected into a flow channel, the shear stress can be expressed using the definition of Darcy's friction:

$$\tau = \frac{1}{8} f_D \rho (\upsilon)^2$$

where τ is the shear stress, υ is the spinning speed, ρ is the density and f_D is the friction factor.

By using the Hagen-Poiseuille equation, the shear stress can be rewritten as:

$$\tau = \frac{8\mu\upsilon}{d}$$

where d is the inner diameter of nozzle, μ is the viscosity of CNF suspension and υ is the spinning speed.

Therefore, the operation parameters, the inner diameter of nozzle (d), the viscosity of CNF suspension (μ) and the spinning speed (υ), were investigated firstly in this study.

7.3.1.1 Solid contents

The solid content of the CNF suspension is an important parameter that affects the viscosity and rheology of the CNF paste used for the wet-spinning. We have investigated the performances of different CNF solid contents of 2%, 3%, 4%, 5% and 6% (weight percent) in the CNF filament preparations. The low CNF solids content easily leads to breaking during the spinning of filaments. However, the high CNF solid content paste easily causes nozzle clogging and leads to low tensile

strength of prepared filaments. Figure 7.1 shows the optical microscopic images of nanocellulose filaments prepared by different solid contents of nanocellulose pastes. It can be seen that the filaments prepared by the solid contents of 3%, 4% and 5% have more uniform shapes in side-view than that prepared from the highest (6%) or the lowest (2%) CNF solids content.
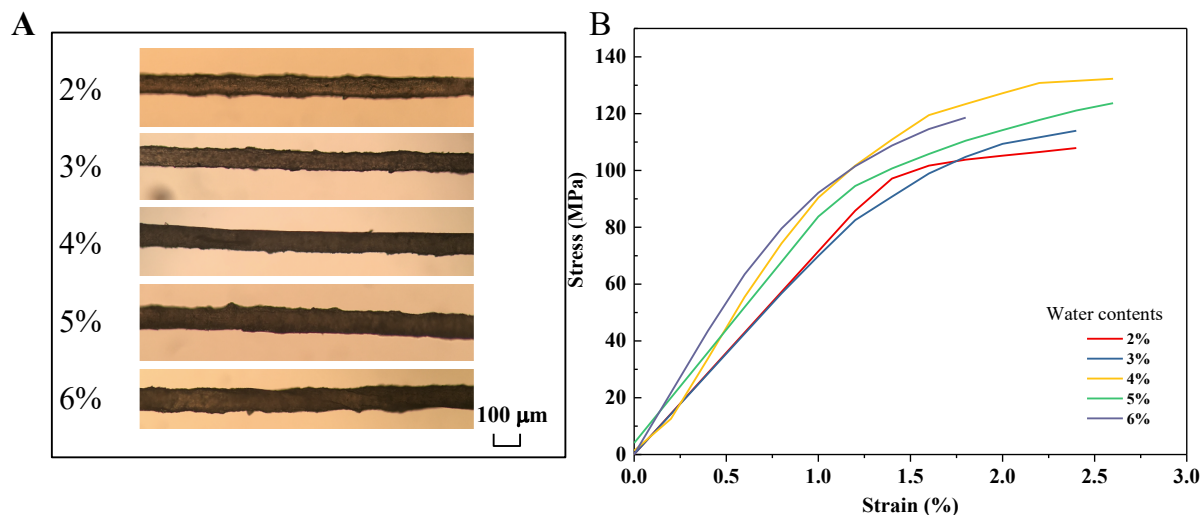
Figure 7. 1 (A) Optical microscopic images of nanocellulose filaments prepared by different solid contents of nanocellulose pastes. (B) Typical stress-strain curves for the nanocellulose filaments.

The cross-section view of SEM images shows different shapes of the nanocellulose filaments prepared by different solid contents of CNF pastes, as shown in Fig. 7.2. It should be noted that the filaments prepared by wet-spinning should have a circular section. However, the shape was deteriorated due to the low viscosity of CNF pastes. It should be noted that in this environmentally-friendly filament preparation, the coagulation bath with organic solvent for wet filaments dewatering was not used. The drying process was directly conducted by placing wet filaments on a plastic film under room-temperature. As shown in Fig. 7.2 (A), the trapezoid cross-section formed for 2% CNF sample because the low viscosity paste cannot maintain the shape during the drying process which usually requires 24 hours. Increasing of CNF solid contents would remedy

the shape deterioration during the drying process. As shown in Fig. 7.2 (C), the cross-section maintained a semi-circular shape with the CNF solid content 6%. The typical stress-strain curves of nanocellulose filaments prepared with different solid contents pastes are shown in Fig. 7.1 (B) and the values of tensile strength and modulus are summarized in Table 7.1. The results indicated the 3% or 4% is an appropriate concentration for the CNF filaments spinning.
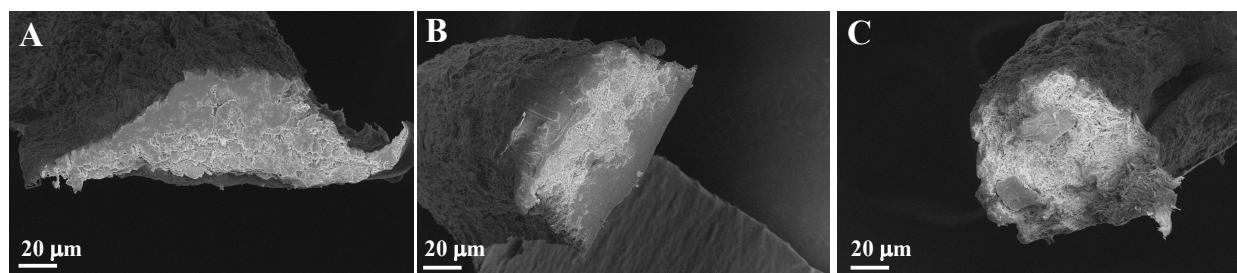
Figure 7. 2 The cross-section view SEM images of nanocellulose filament prepared with (A) 2% (B) 3%, (C) 6% solid content of CNF paste.

7.3.1.2 diameter of nozzle

Different types of needles (22G, 20G and 17G) were used as nozzle in the CNF filaments wet-spinning (solid content 4%). Fig. 7.3 shows the optical microscopic images (side-view and cross-section view) of nanocellulose filaments prepared by different diameters of nozzles. The width and the cross-section shape were changed by different diameter nozzles. The mechanical measurements of resulting filaments show that the smaller the diameter of the needle we used, the higher the tensile strength can be obtained. However, the smaller nozzle is easy to be clogged during the wet-spinning.

124

Nozzle diameter

1.0 mm

0.6 mm

0.41 mm

100 μm
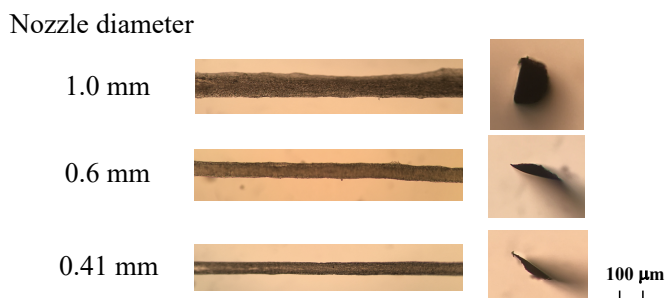
Figure 7. 3 Optical microscopic images (side-view and cross-section view) of nanocellulose filaments prepared by different diameters of nozzles (solid content 4%).

7.3.1.3 Spinning speed

Theoretically, the higher spinning speed generates a higher shear force for the CNF fiber alignment during the fiber extrusion, but the high spinning speed is not easy for practical operation. Three different wet-spinning speeds of 0.5, 2.5 and 5 ml min^{-1} were performed by using a syringe pump. SEM images of nanocellulose filaments prepared with different spinning speeds (0.5 and 2.5 ml min^{-1}) were shown in Fig. 7.4. The side-view images show that CNF fibrils are bundled along the axis direction. The diameter of the fibril bundle is 1-2 μm. From the magnified SEM images, we can see the CNF fibril orientation on the filament surface. Compared with Fig. 7.4 (C) and (G), it can be seen that the filament prepared with a high spinning speed of 2.5 ml min^{-1} has better fibrils orientation than that of the low spinning speed of 0.5 ml min^{-1}. The fibril orientation can also be observed from the SEM images at the filament breakages, as shown in 7.4 (D) and (H). The values of tensile strength are shown in Table 1, which suggests that the speed of 2.5 ml min^{-1} is enough for the fabrication.

Based on optimal conditions, it could be preliminarily concluded: the solid content of 4% reached the highest tensile strength; for the nozzle diameter, the smaller the better; while the spinning speed, the higher the better. By considering the operation feasibility, we choose the

125

operating conditions with the solid content 4%, nozzle diameter 0.60 mm and spinning speed 2.5

ml min^{-1} in further researche.
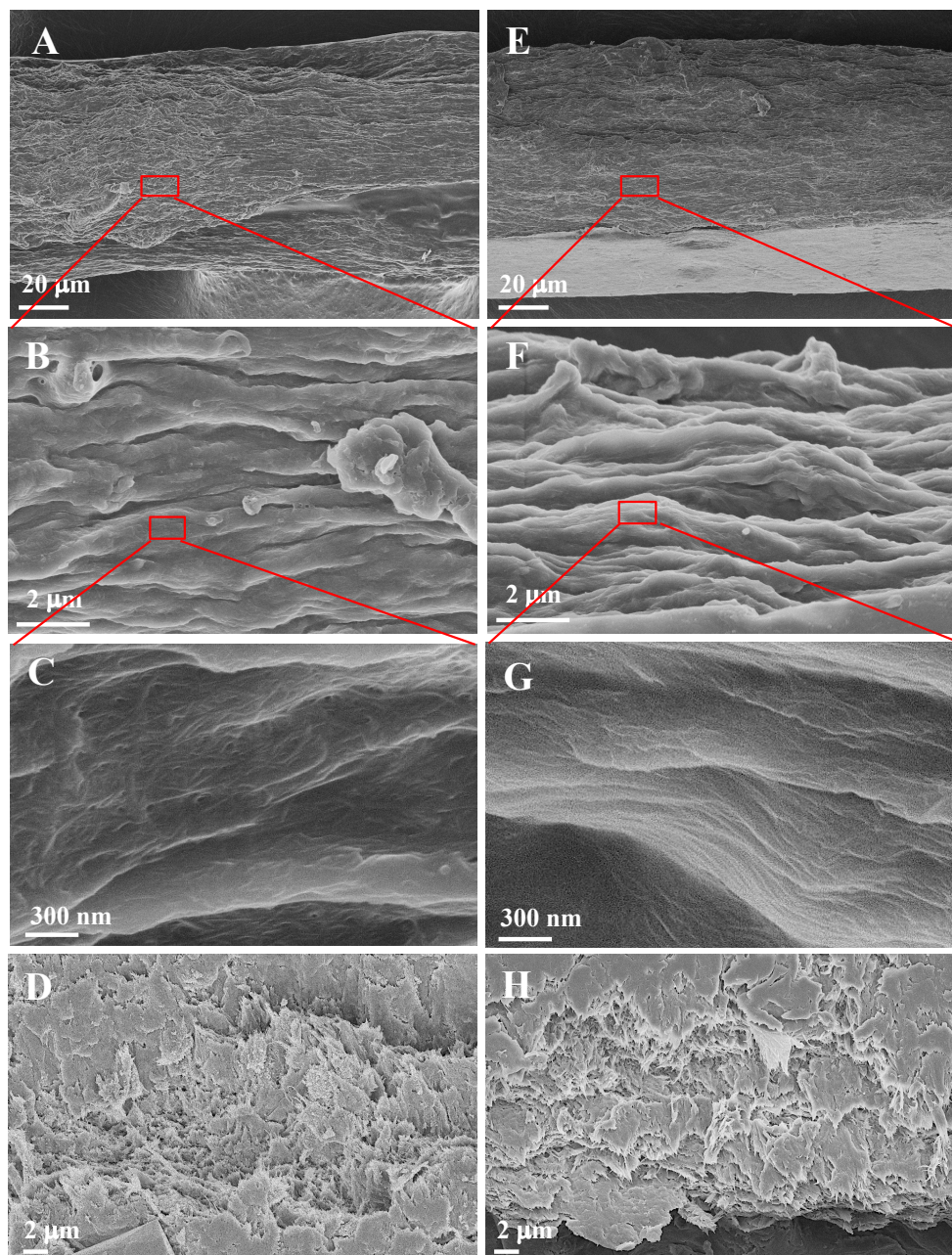
Figure 7. 4 SEM images of nanocellulose filaments prepared with different spinning speeds.

(A)-(D): spinning speed 0.5 ml min^{-1}; (E)-(H): spinning speed 2.5 ml min^{-1}; (D) and (H) are

cross-section view SEM images at the breakage.

Table 7. 1 Data summary of nanocellulose filaments prepared with different operating parameters.

	Conditions	Tensile strength (MPa)	Modules (GPa)
	2% solid content	105±3	7.2±0.5
	3% solid content	110±2	7.1±0.5
CNF concentration	4% solid content	135±3	9.4±0.4
	5% solid content	121±2	8.4±0.4
	6% solid content	119±3	10.0±0.4
	0.5 ml min^{-1}(1.75 m/min)	125±2	8.5±0.3
Spinning speed	2.5 ml min^{-1} (8.84 m/min)	135±3	9.4±0.4
	5 ml min^{-1} (17.69 m/min)	140±1	10.9±0.3
	22G, 0.41 mm	144±4	10.8±0.5
Diameter of needle	20G, 0.60 mm	135±3	9.4±0.4
	17G, 1.00 mm	125±2	8.1±0.5

7.3.2 Screening of additives for the strength improvement

Increasing the bonding force between nanocellulose fibers is one of the important ways to improve the tensile strength of prepared nanocellulose filaments. The nanocellulose fibril bonding can be improved by using bonding agents. The original bonding between nanocellulose fibers is mainly intermolecular hydrogen bonding which is a relatively week bonding force. After treatment with chemical bonding agents, the covalent bonding could be formed via esterification, etherification and amidation reactions etc.

Based on the different chemical reactions with nanocellulose fibers, we have chosen the organic and inorganic bonding agents: (1) Boric acid to improve the hydrogen bonding; (2) citric acid for forming of ester group bonding; (3) glutaraldehyde or glyoxal for forming of ether group bonding; and (4) Kymene which is a polymer that can introduce amide groups into nanocellulose fibers. In addition, the chemicals which can physically absorb on the surface of nanocellulose fibrils to improve the interaction other than chemical bonding were also applied in the filament fabrication, such as polymers (sodium carboxymethyl cellulose (CMC) and polyvinyl alcohol

(PVA)) and inorganic nanoparticles (TiO$_2$ P25 and colloidal silica). These chemicals were mixed with nanocellulose slurry to form a homogeneous paste for the following wet-extrusion process. Figure 7.5 schematically illustrated the chemical bonding of nanocellulose fibrils.

A Esterification: Citric acid
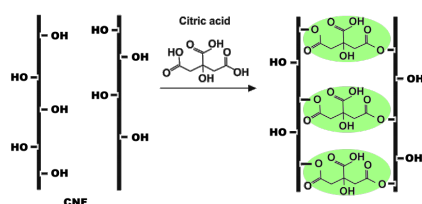
C Acetalation: Glutaraldehyde
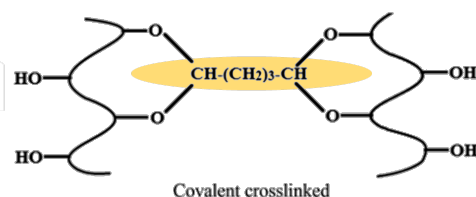
B Hydrogen bonding: Boric acid
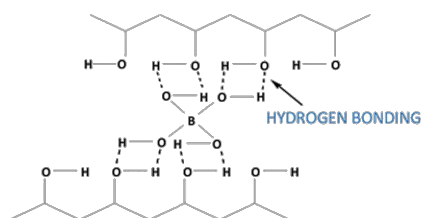
D Polymer : Kymene
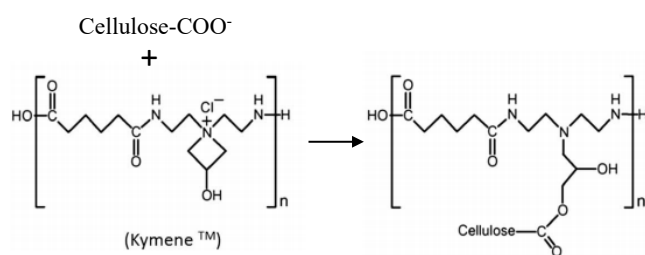
Figure 7. 5 Schematic illustrations of Chemical bonding of nanocellulose fibrils.

7.3.2.1 Chemical bonding additives

Figure 7.6 shows the FT-IR spectra of nanocellulose filaments modified with different chemical bonding additives. The peaks that are different from the native CNF spectrum are highlighted with yellow color. As shown in Fig. 7.6 (A), after the citric acid modification, the ester group can be formed with the surface hydroxyl group of nanocellulose fibrils, which corresponds to the changes and increases of vibration adsorption of carboxyl bonds at 1740 cm^{-1} and C-O bond at 1040 cm^{-1} [255, 256]. For the modification with boric acid, the obvious changes occur at the region of 1250-1500 cm^{-1} which can be ascribed to the vibration of the C-O bond of cellulose molecules. This is because the extensive hydrogen bonding networks between hydroxyl groups of nanocellulose can be generated with the bonding of boric acid[257].
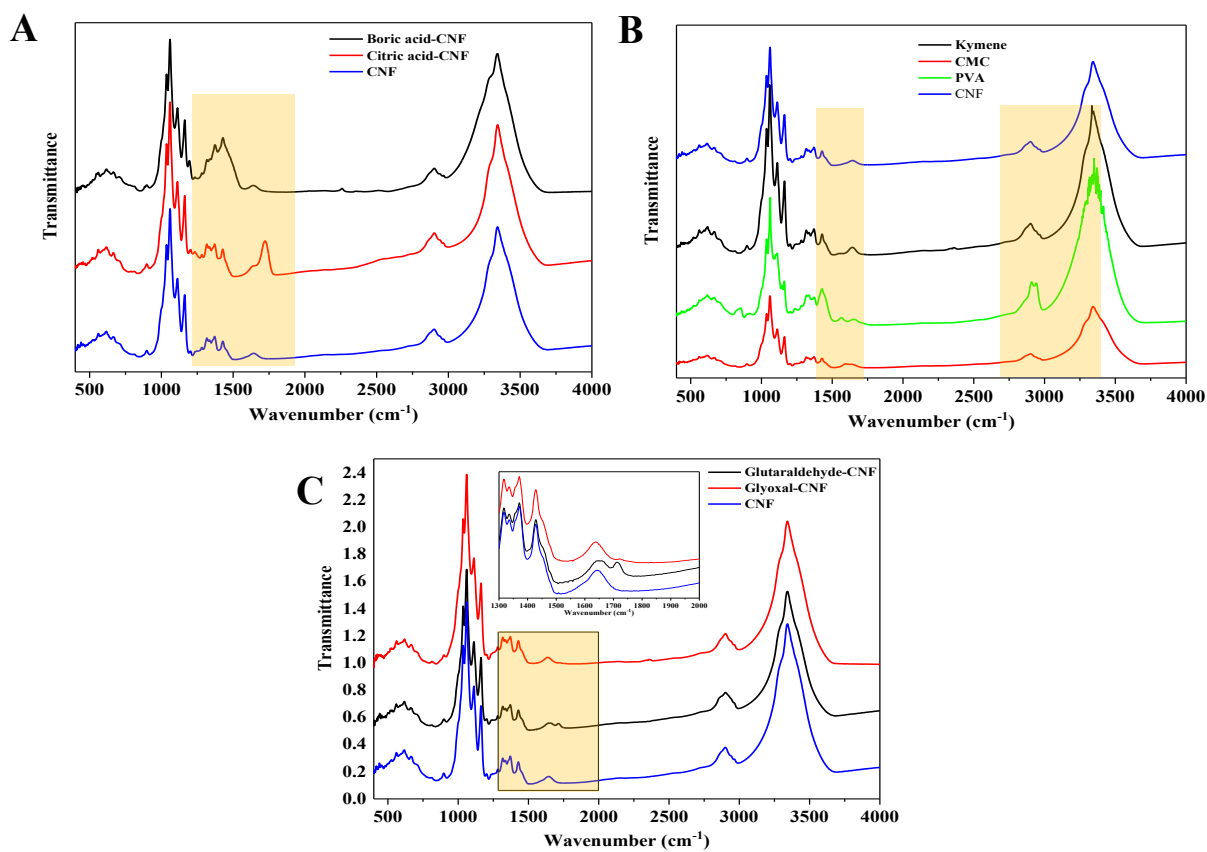
Figure 7. 6 FT-IR spectra of nanocellulose filament modified with different chemical bonding additives.

Kymene is a polyamide-epichlorohydrin (PAE) resin[258]. Papermaking industry usually uses it as a wet-strength agent to improve the strength of paper in water. Because of the chemical cross-linking with cellulose fibrils, Kymene has also been applied to strengthen dry cellulose membranes and aerogels[259, 260]. The cross-linking mechanism is based on the formation of covalent ester bonds between the carboxyl groups of cellulose and the azetidinium groups of PAE during the curing process[261]. This was verified with the increase of peak adsorption at 1650 cm^{-1} which is attributed to the stretching of carboxylated groups and amide C=O groups in the FT-IR spectrum[261].

Although the polymer PVA and CMC cannot directly chemically bond with nanocellulose fibrils, the addition of these polymers can increase the viscosity of the nanocellulose paste and thus improve the operation feasibility. Moreover, PVA and CMC abound in hydroxyl groups which can form hydrogen bonding with the nanocellulose fibrils. The minor changes of vibration adsorption of C-O groups show the interactions between nanocellulose and polymers[262, 263]. SEM images of the filament modified with polymer PVA are shown in Fig. 7.7. By mixing with polymer, the resulting filaments have a smooth surface without obvious cellulose bundles shown above. This could be attributed to the binding effect of polymers. From the SEM image at the breakage, the cross-section has less deterioration compared to filaments prepared without PVA. This suggests that the addition of polymer could improve the maintenance of the filament shape.
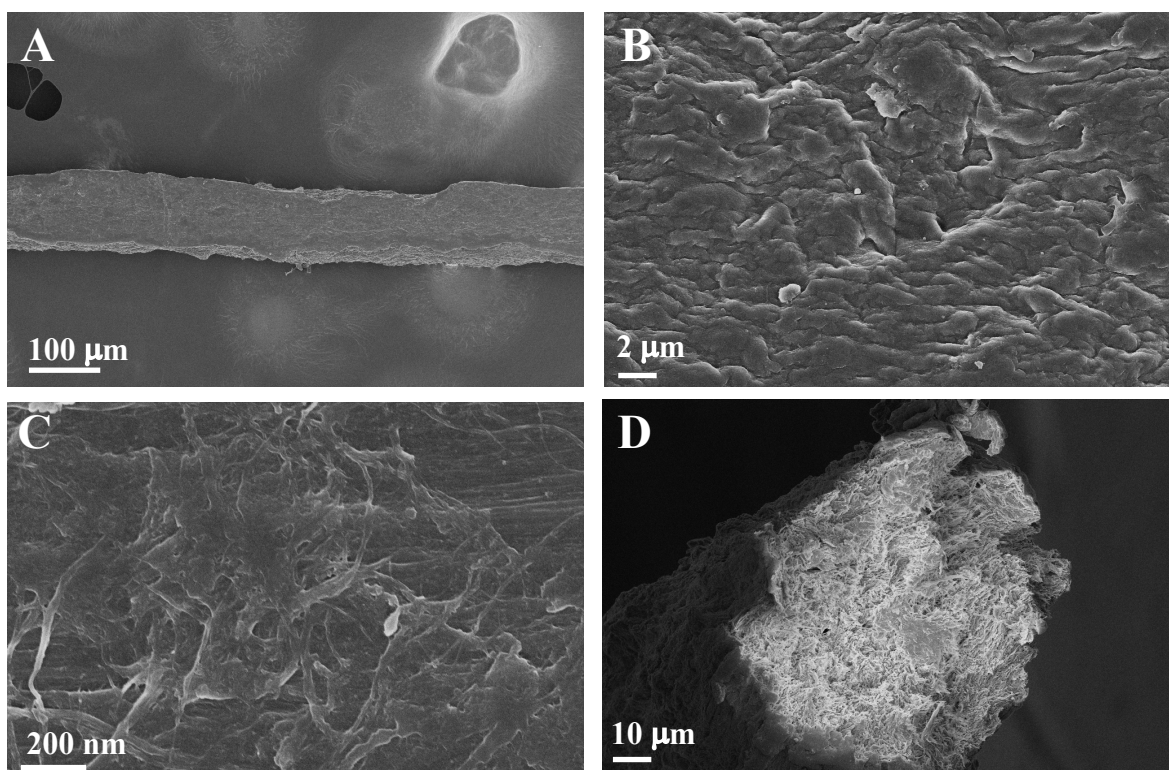
Figure 7. 7 SEM images of the filament modified with polymer PVA.

Glutaraldehyde (GA) is a widely used cross-linker for biopolymers through the reaction with hydroxyl groups. The acidic condition can catalyze the cross-linking reaction of GA with the CNF fibrils. The GA treatment has been reported to remarkably improve the tensile strength of CNF films and water resistance and stability[264-266]. The obvious change of the FT-IR spectrum is the presence of the C=O vibration at 1710 cm^{-1}, which indicates that the cross-linking of the CNF film with GA was formed successfully.
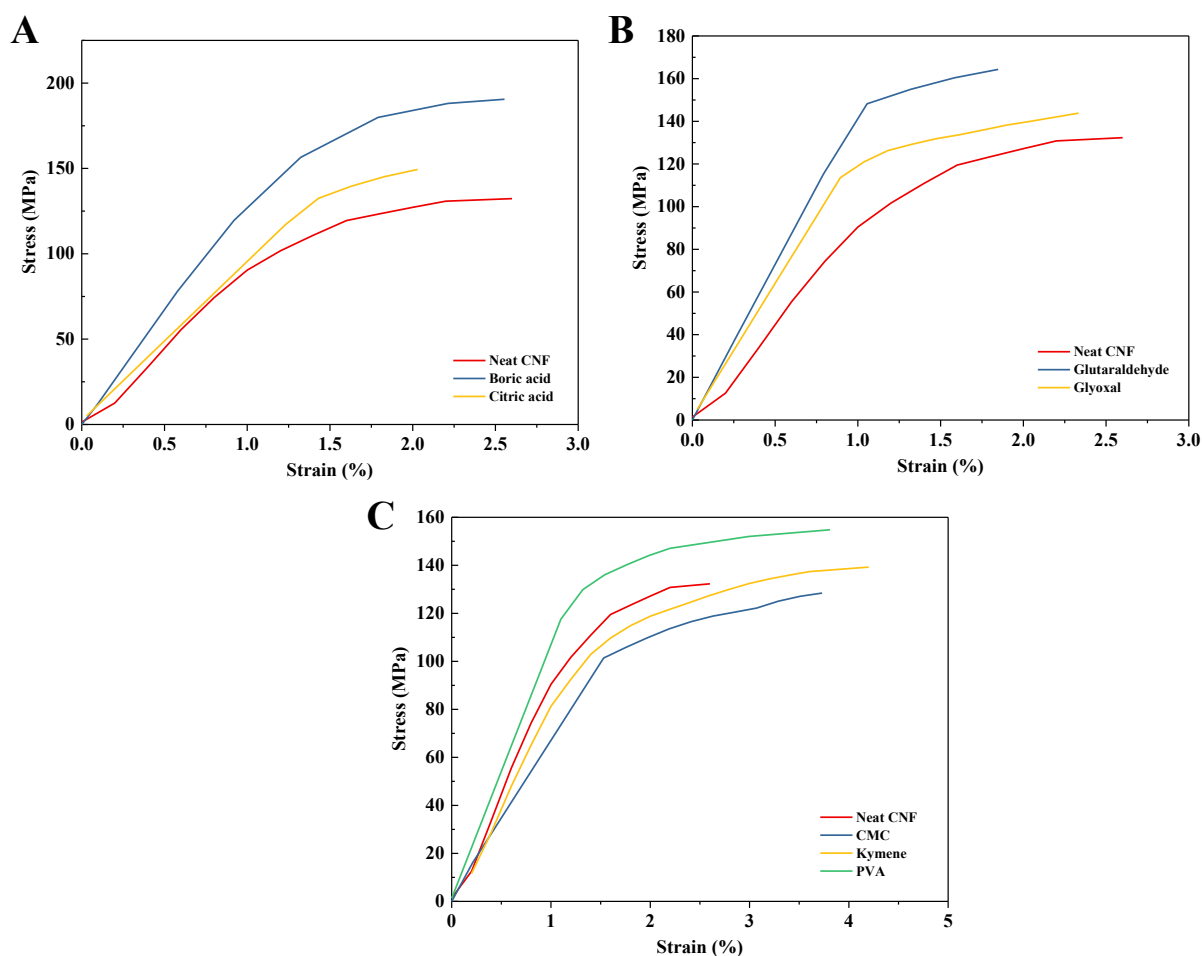
Figure 7. 8 Typical stress-strain curves for the nanocellulose filaments modified with chemical bonding additives.

The tensile strength of different bonding agent treated filaments were measured and repeated at least 3 times. Typical stress-strain curves for the nanocellulose filaments modified with chemical

bonding additives are shown in Fig. 7.8. The average values of tensile strength are summarized in Table 7.2. The results show that: (1) Kymene only slightly improved the tensile strength. The value is almost the same as initial pure nanocellulose filaments, which is around 135 MPa; (2) glutaraldehyde and citric acid that formed covalent bonding between nanocellulose fibers increased 25% of initial tensile strength, to 150-160 MPa; (3) boric acid which forms the hydrogen bonding with nanocellulose fibers increased 67% of the initial tensile strength. The value reached 190-200 MPa; (4) polymer PVA increased the tensile strength to ~150 MPa; however, CMC slightly decreased the strength, especially decreasing the modulus but the elongation was increased as expected.

7.3.2.2 Inorganic nanoparticles as additives

Inorganic nanoparticles were applied in the CNF filaments wet-spinning. The nanoparticles, on one hand, function as fillers that can increase the tensile strength and modulus of prepared filaments. On the other hand, nanoparticles can fill in the voids of prepared filaments and thus reduce the defects and increase the mechanical properties. We investigated P25 (nano TiO_2 with diameter 25 nm) and colloidal silica as the inorganic particle additives. The results show that TiO_2 and boric acid increase the mechanic properties of obtained filaments while colloidal silica slightly decreased the tensile strength.

The SEM images of nanocellulose filament with modified when TiO_2 P25 and colloidal silica are shown in Fig. 7.9. Comparing the two different particles, the fibrils in TiO_2 nano particles modified filament are more densely packed and it can be clearly seen that TiO_2 nano particles were filled in the voids of the filament. Colloidal silica modified filaments show more defects and voids

that formed in the filament preparation. Therefore, it can be expected that TiO_2 modified filaments could have a higher tensile strength than colloidal silica modified filaments.
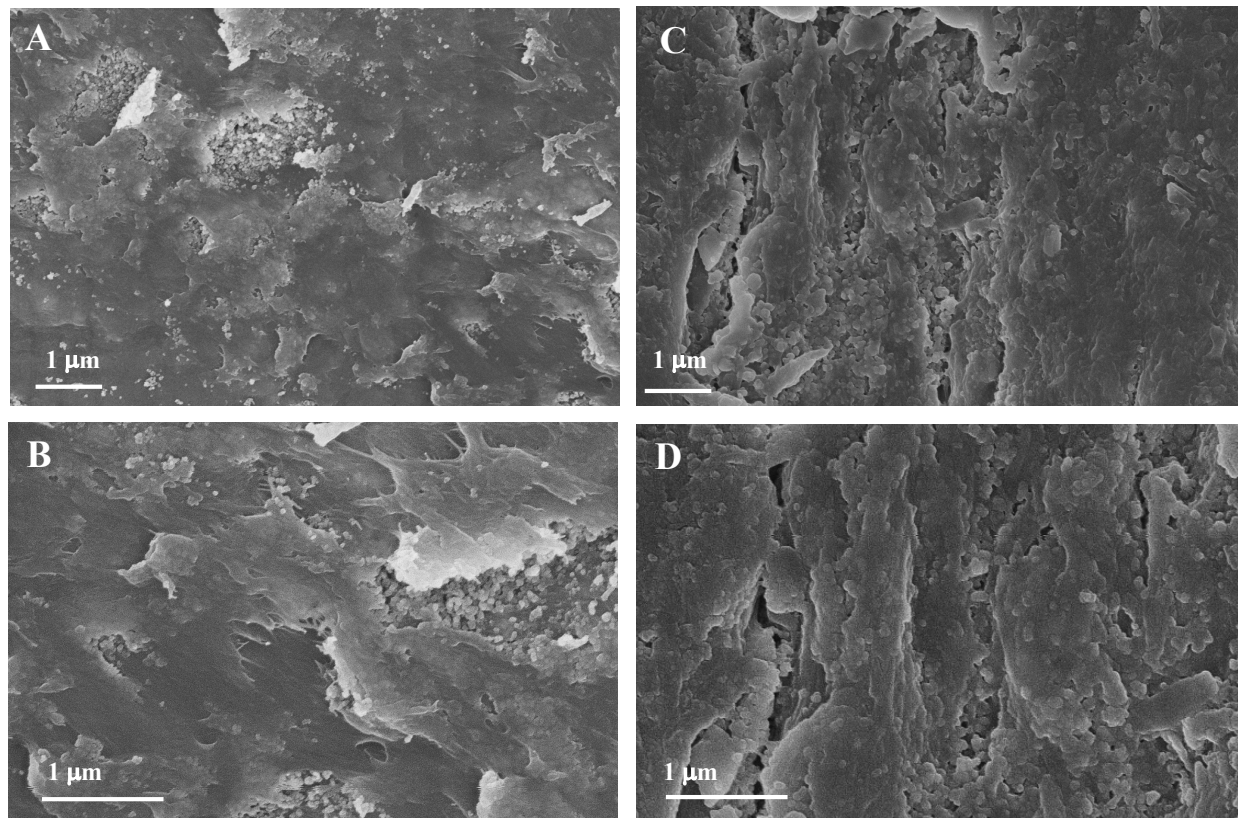
Figure 7. 9 SEM images of nanocellulose filament with modified with TiO_2 P25 ((A) and (B)) and colloidal silica ((C) and (D)).

FT-IR spectra of nanocellulose filament modified with TiO_2 P25 and colloidal silica are shown in Fig. 7.10. In the spectra of a TiO_2 P25 modified filament, the peaks around 750 to 500 cm^{-1} could be assigned to the characteristic absorption of the Ti-O bond[267]. While for silica modified filament, the peak at 470 cm^{-1} is assigned to bending vibrations of Si-O-Si bonds[268, 269]. The main characteristic peaks of the cellulose, such as C=O absorption at 1634 cm^{-1}, O-H stretching vibration at 3440 cm^{-1} and the C–O stretching vibration at 1060 cm^{-1}, are almost the

same as that of native nanocellulose[270], which indicates the physical mixing of the inorganic nanoparticles and nanocellulose.
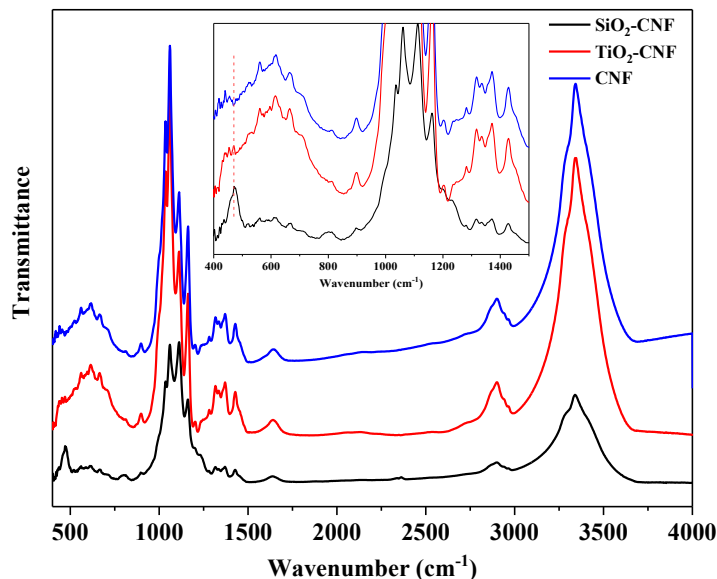
Figure 7. 10 FT-IR spectra of nanocellulose filament with TiO_2 P25 and colloidal silica as fillers

Typical stress-strain curves for the nanocellulose filaments modified with TiO_2 P25 and colloidal silica are shown in Fig. 7.11. The data are summarized in Table 7.2. As expected, the TiO_2 P25 modified filament shows a significant mechanical strength improvement from the initial 120 MPa to around 200 MPa. However, for a colloidal silica modified sample, although the modulus slightly increased, the tensile strength is almost the same compared with the initial value.
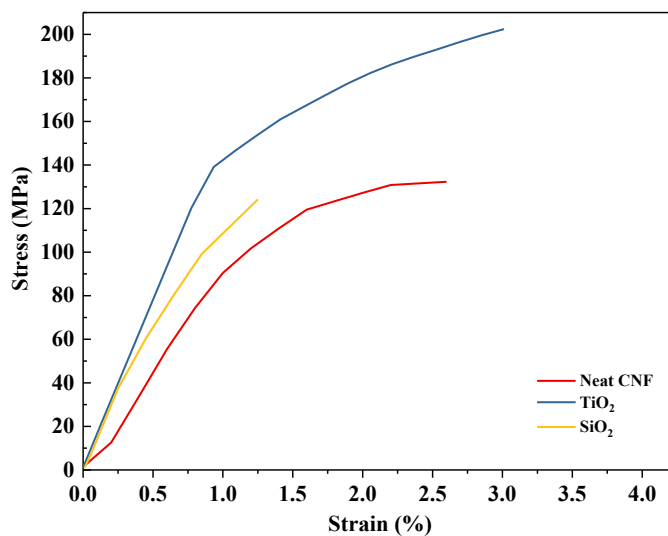
Figure 7. 11 Typical stress-strain curves for the nanocellulose filaments modified with TiO$_2$ P25 and colloidal silica.

Table 7. 2 Data summary of nanocellulose filaments with organic and inorganic additives

Treatments	Additives	Tensile strength (MPa)	Modules (GPa)
Inorganic additives 10wt%	Boric acid	190±5	13.3±0.2
	TiO$_2$ P25	205±4	16.6±0.2
	Colloidal silica	120±3	12.5±0.3
	Citric acid	160±3	10.0±0.2
	Glutaraldehyde	173±4	15.3±0.3
Organic additives 10wt%	Glyoxal	142±4	12.9±0.3
	Kymene	139±3	8.4±0.2
	CMC	125±5	6.6±0.4
	PVA	158±3	10.8±0.3

7.3.3 Wet stretching or wet-twisting treatment

Post-treatments were conducted to further increase the mechanical properties of CNF filaments, including wet-stretching or wet-twisting. The wet-stretching is believed to help the hydrodynamic alignment of fibers and improve the ordered orientation along the fiber axis. In this study, gravity

was used to draw half-dried nanocellulose filaments in the wet-stretching. After the stretching, the elongation of the filaments reached around 10%. Figure 7.12 shows the SEM images of nanocellulose filament with wet-stretching. We can see the densely packed nanocellulose fibril bundles on the surface of filaments. The fracture surface clearly shows the "pull-out" feature of nanofibrils with the gravity stress (Fig. 7.12 D). With wet-stretching, the tensile strength and modulus of resulting filaments are increased, as shown in Table 7.3.
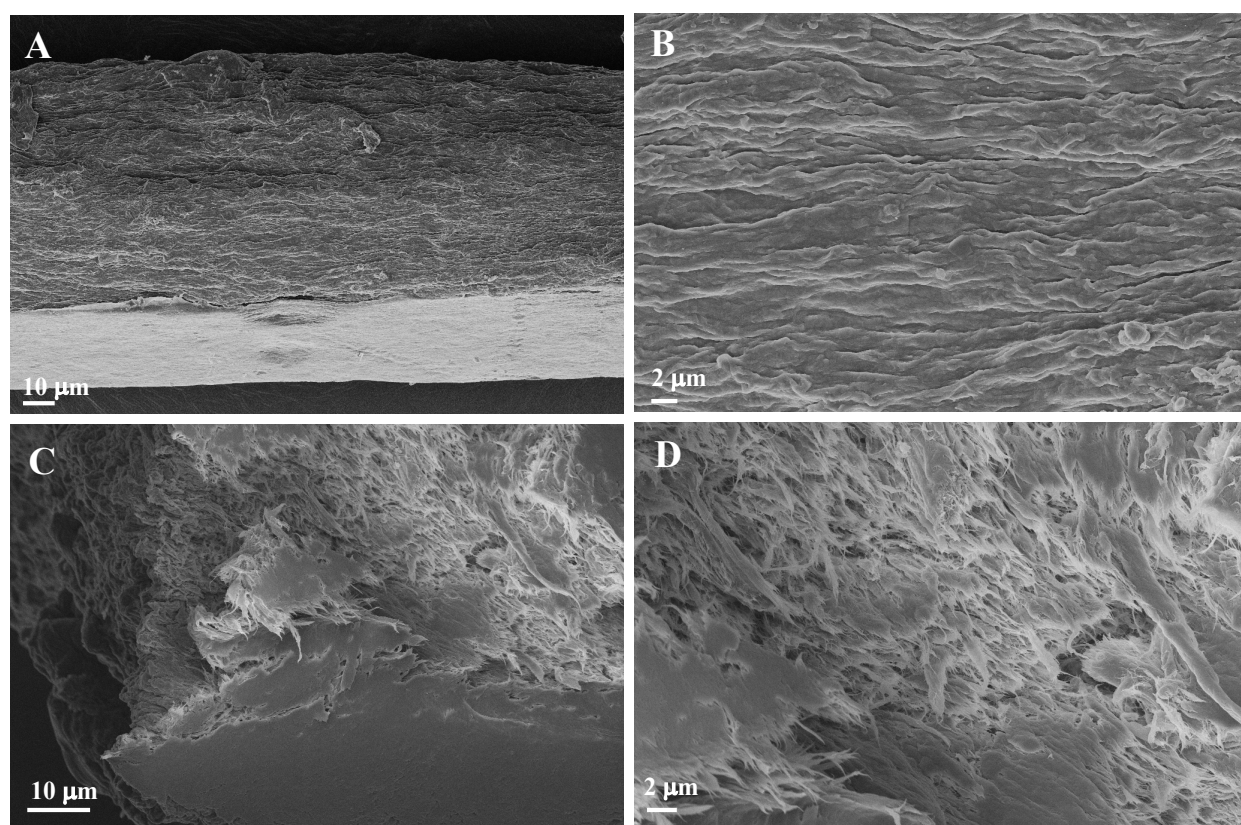
Figure 7. 12 SEM images of nanocellulose filament with wet-stretching. (A) and (B) side-view and magnified image; (C) and (D) cross-section view and magnified image.

Furthermore, wide-angle X-ray diffraction was investigated to determine the Herman's orientation factors (f_H), as shown in Fig. 7.13. The calculated value of f_H increases from initial 0.22 (without stretching) to 0.41 after stretching, indicating the improvement of fibril orientation.

Wet-twisting can increase the bonding force between interacting fibers, like yarns. Figure 7.14 shows the microscopic images of untwisted and twisted CNF filaments. The twisting process led to a smaller diameter of the filament than the untwisted samples, resulting in a more compact structure and therefore a higher mechanical strength. The additive PVA was added in nanocellulose paste for wet-twisting. PVA functions as a binder that could increase the fiber interaction and viscosity of the paste to ensure the successful twisting. As shown in Table 7.3, the modulus of twisted filament is significantly increased but the tensile strength does not show significant improvement.
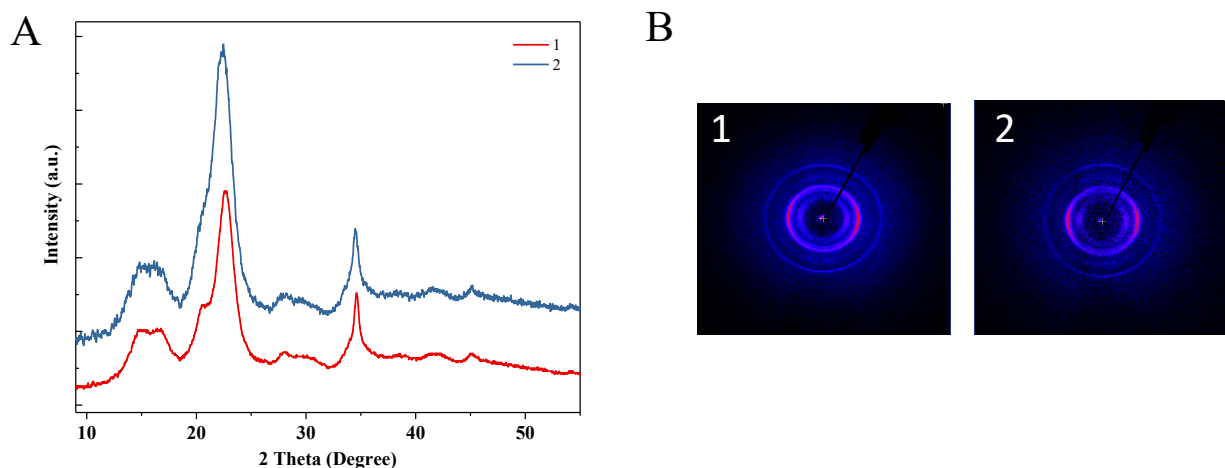
Figure 7. 13 (A) wide-angle X-ray diffraction (WAXD) patterns of filaments with (2) and without (1) wet-stretching. (B) Diffractograms from the WAXD scan of the filaments.
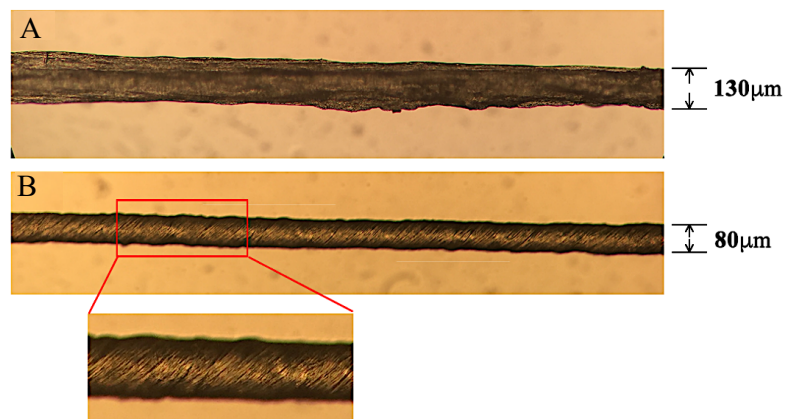
Figure 7. 14 (A) Microscopy images of extruded native nanocellulose filament and wet-twisted filament.

Table 7. 3 Data summary of nanocellulose filaments with wet-stretching and wet-twisting.

Treatments	Additives	Tensile strength (MPa)	Modules (GPa)
Wet-stretching	TiO_2	211±2	18.2±0.2
Wet-stretching	Boric acid	208±2	15.5±0.2
Wet-twisting	PVA	172±5	140±0.3

7.3.4 Continuous preparation of filaments

Continuous nanocellulose filament extrusion was conducted in this study. CNF/TiO$_2$ mixture (weight of TiO$_2$ to dry CNF 1:10) were used as raw material in the extrusion. To extrude the nanocellulose filaments continuously, the experimental setup was designed, as shown in Fig. 7.15 A. Two rollers with a plastic belt were used to hold the wet extruded filament. Heated air was blown from the top of the plastic belt to dry the filaments quickly. A high-pressure syringe pump and a 50 mL volume syringe were used for the extrusion. The solids content of the raw material was 3% based on the dry weight of nanocellulose. Therefore, about 1.5 g nanocellulose filament (estimated total of 400 meters long) was obtained for a one-time extrusion. With the roller and blowing heat-air, the filament could be continuously extruded and dried. At the end of roller, there

was a collecting roller to collect the dried filament together. The actual experimental setup is shown in Figure 7.15 B. The belt was 6 meters long, and the roller could be heated to 90 ºC. Figure 7.16 C shows the continuous filament extrusion from a stainless-steel needle. Figure 7.16 D shows the resulting nanocellulose filaments. In one of our experiments, we obtained 15 g dry nanocellulose filament (estimated total of 4,000 meters) by using the designed instrument.
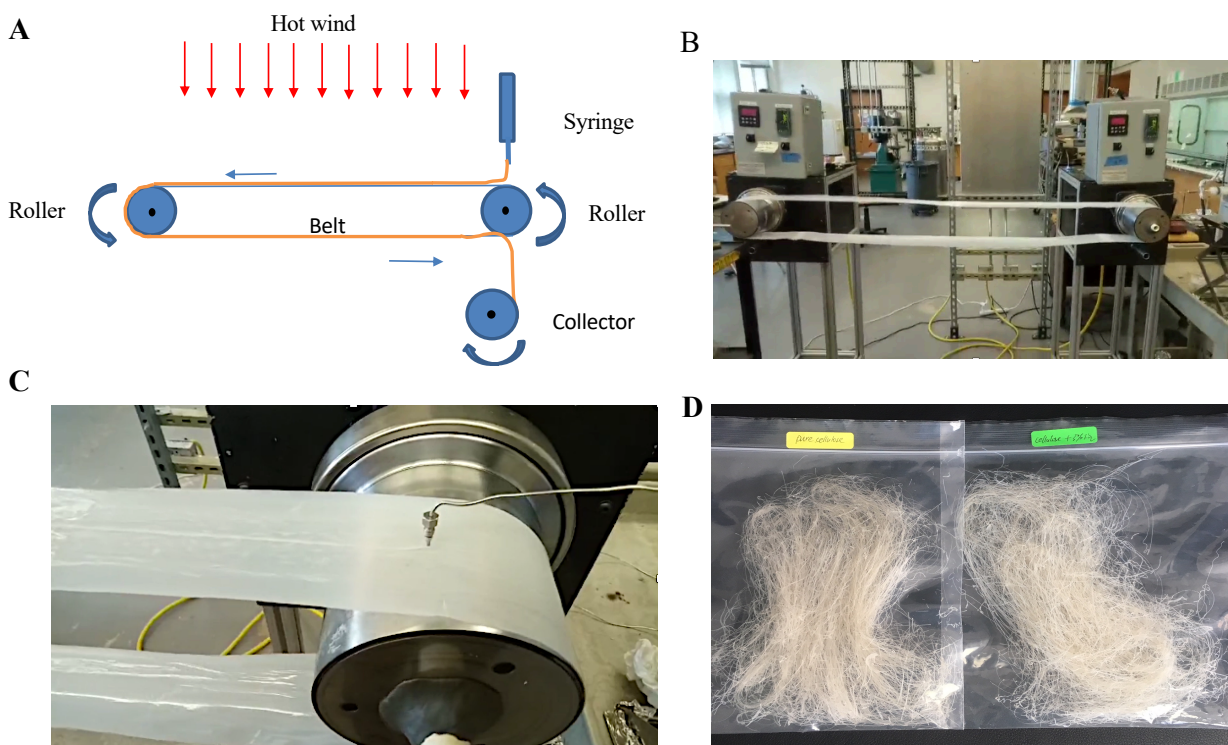
Figure 7. 15 (A) Illustration of continuous CNF ropes preparation. (B) Photographic image of the experimental setup. (C) The photograph of CNF rope extrusion. (D) Obtained CNF ropes.

7.4 Conclusion

In this study, we prepared nanocellulose filaments by a wet-spinning approach. The mechanical strength of the filaments was improved by chemical bonding and fibril alignment. We

have investigated the wet-spinning operation conditions such as solid content of nanocellulose paste, nozzle diameter and spinning rate. Screening of additives was conducted to improve the fibril integrations, including chemical bonding agents, polymers and inorganic nano fillers. Post-treatments including wet-stretch and wet-twisting were performed to increase the fibril orientation. With optimized operations, we have obtained a nanocellulose filament with the highest tensile strength of 211 MPa and modulus of 18.2 GPa in this study. Finally, we have conducted continuous extrusion of nanocellulose filaments with our designed setup. The nanocellulose filaments were produced in total weight of 15 grams.

CHAPTER VIII: OVERALL CONCLUSIONS AND FUTURE WORKS

8.1 Overall Conclusions

This dissertation focuses on the chemical modification and micro/nano structure control of cellulose nanofibrils for composite film and wet-spinning fiber applications. It mainly includes four parts.

The first part of the work demonstrated that the superhydrophobicity of nanocellulose membrane can be reached by a simple templated surface patterning and non-fluorinated chemicals surface modification. The patterning formed hierarchical structure combining of micro-sized surface patterns and nano-sized cellulose fibers, which is very important to the superhydrophobic properties. The pattern size, which is a critical factor to the resulting superhydrophobic property, can be tuned in this study by changing the size of metal or plastic meshes which were used as templates in the surface patterning. The obtained membranes also showed a good repellent ability to the common liquids that create clothing stains in daily life.

The second work focuses on in situ hydrophobic modification of the nanocellulose fibrils with AKD emulsion in water suspension, which can improve the compatibility with PLA matrices to form CNF-PLA composites. The AKD emulsion was used in the modification, which can prevent the de-activation of AKD with water and enable the successful modification of CNF. The AKD addition in the CNF modification was found important to the resulting reinforced mechanical properties of the composites.

The third part of the work is the reinforcement of PLA composite films with nano-structure controlled porous nanocellulose frameworks, to avoid the ununiform nanocellulose fiber

distribution issue in traditional composites. This study examined different drying processes in the fabrication of CNF frameworks. The room-temperature-drying and heat-drying improve the irreversible hydrogen bonding resulting in high strength of the CNF framework, while the re-wetting and freeze-drying process lead to high porosity. TOCNF was used to adjust the pore structure of a formed framework because TOCNF has high water retention in the re-wetting process. Isocyanates such as HDI and TDI crosslinking were applied to improve the chemical bonding between CNF framework. The mechanical strength of the final obtained composite was significantly improved as expected.

In the last part, we focus on the preparation of nanocellulose filaments by a wet-spinning approach. Fibril orientation and chemical modification are two variants applied in this study for mechanical property improvement. Firstly, to improve the fibril orientation, we optimized the wet-spinning operation conditions, i.e., the solid content of nanocellulose paste, the nozzle diameter and the spinning speed. The post-treatments, including wet-stretching and wet-twisting, were also used for the filament mechanical improvement. Secondly, different chemical additives were screened, including chemical bonding agents such as citric acid, boric acid, glutaraldehyde and glyoxal; polymeric binders such as PVA and CMC; and inorganic fillers such as TiO_2 (P25) and colloidal silica. Finally, we have designed an engineering process for continuous extrusion of nanocellulose filament.

8.2 Future Works

In the part of superhydrophobic nanocellulose membrane fabrication, although the surface patterning could be simply and quickly completed in several seconds, the subsequent water removal from the patterned nanocellulose membrane was conducted by freeze-drying, which is an energy-and time-consuming process. A more efficient drying process can be explored in future research, such as room-temperature drying or heat drying. The challenge for the room-temperature drying or heat drying is how to avoid shrinkage and deformation of nanocellulose membranes during the drying process. The control of water evaporation rate would be one of the strategies to solve the problem.

In the part of AKD emulsion in situ modification of CNF for PLA composite reinforcement, the modified CNFs were required to re-disperse into organic solvent and mix with PLA to prepare the composite. To avoid use of organic solvents, screw extrusion would be one of the options that deserve to be researched. However, in the direct extrusion of CNF with PLA, the dispersion of CNF in a PLA matrix would be a problem that needs to be resolved. In addition, the extrusion is usually conducted under the melting point of PLA, which is as high as 160 $^\circ$C. How to avoid the thermal degradation of CNF in the crew extrusion would be another meaningful research topic.

In the part of nanocellulose 3D porous framework reinforced PLA composite, the high performance PLA composite film was prepared by an impregnation method. Another attractive method to prepare the PLA composite film would be hot-pressing of a PLA membrane with the nanocellulose framework to form a sandwiched packed composite film. This method can avoid the use of organic solvent and can be quickly completed. In addition, applying different polymer matrices could be a promising direction. A general engineering polymer such as PE, PP and PVC

could be used for composite fabrication. Therefore, it is meaningful to investigate the modifications of nanocellulose to increase the interaction between nanocellulose frameworks and different polymer matrices.

In the part of the nanocellulose filament fabrication, future research could be focused on the following aspects: firstly, the wet CNF filament is easily broken during the spinning, which highly restricts continuous spinning in the practical operation. How to improve the spinning performance to avoid breakage and defects would be the next steps in the research. Second, drying filaments at a large scale is a high energy consumption and slow process. The CNF solids content in the filament spinning was 4%, which means a huge amount of water was required to be removed. It is meaningful to solve the high cost of energy in the drying process for industrial production. Third, filament shape changes during the drying process. The deformation and non-uniformity of the cross-section size should be resolved in future studies.

REFERENCES

[1]   Geyer R, Jambeck J R, and Law K L. *Production, use, and fate of all plastics ever made.* **Science Advances**, 2017, 3 (7): e1700782.

[2]   Adebiyi-Abiola B, Assefa S, Sheikh K, and García J M. *Cleaning up plastic pollution in Africa.* **Science**, 2019, 365 (6459): 1249-1251.

[3]   Dhawan R, Bisht B M S, Kumar R, Kumari S, and Dhawan S K. *Recycling of plastic waste into tiles with reduced flammability and improved tensile strength.* **Process Safety and Environmental Protection**, 2019, 124 299-307.

[4]   Karan H, Funk C, Grabert M, Oey M, and Hankamer B. *Green Bioplastics as Part of a Circular Bioeconomy.* **Trends in Plant Science**, 2019, 24 (3): 237-249.

[5]   Holbert J, Sudrajat D J, Nurhasybi, and Yulianti. *Alternative methods for reforestation and land rehabilitation to reduce the plastics waste in forest areas.* **IOP Conference Series: Earth and Environmental Science**, 2019, 407 012007.

[6]   Lei Y and Wu Q. *Recycling engine oil containers to prepare wood–plastic composites.* **Journal of Applied Polymer Science**, 2011, 122 (2): 964-972.

[7]   Srivastava L M. *CHAPTER 2 - Cell Wall, Cell Division, and Cell Growth*. Place: Academic Press, 2002.

[8]   Rojas O J. *Cellulose Chemistry and Properties: Fibers, Nanocelluloses and Advanced Materials*. Place: Springer, 2016.

[9]   Klemm D, Heublein B, Fink H-P, and Bohn A. *Cellulose: Fascinating Biopolymer and Sustainable Raw Material.* **Angewandte Chemie International Edition**, 2005, 44 (22): 3358-3393.

[10]   Siró I and Plackett D. *Microfibrillated cellulose and new nanocomposite materials: a review.* **Cellulose**, 2010, 17 (3): 459-494.

[11]   Habibi Y, Lucia L A, and Rojas O J. *Cellulose nanocrystals: chemistry, self-assembly, and applications.* **Chemical reviews**, 2010, 110 (6): 3479-3500.

[12]   Moon R J, Martini A, Nairn J, Simonsen J, and Youngblood J. *Cellulose nanomaterials review: structure, properties and nanocomposites.* **Chemical Society Reviews**, 2011, 40 (7): 3941-3994.

[13]   Kim J-H, Shim B S, Kim H S, Lee Y-J, Min S-K, Jang D, Abas Z, and Kim J. *Review of nanocellulose for sustainable future materials.* **International Journal of Precision Engineering and Manufacturing-Green Technology**, 2015, 2 (2): 197-213.

[14]   Du X, Zhang Z, Liu W, and Deng Y. *Nanocellulose-based conductive materials and their emerging applications in energy devices - A review.* **Nano Energy**, 2017, 35 (Supplement C): 299-320.

[15]   Hoeng F, Denneulin A, and Bras J. *Use of nanocellulose in printed electronics: a review.* **Nanoscale**, 2016, 8 (27): 13131-13154.

[16]   Khan A, Huq T, Khan R A, Riedl B, and Lacroix M. *Nanocellulose-based composites and bioactive agents for food packaging.* **Critical reviews in food science and nutrition**, 2014, 54 (2): 163-174.

[17]   Abdul Khalil H P S, Bhat A H, and Ireana Yusra A F. *Green composites from sustainable cellulose nanofibrils: A review.* **Carbohydrate Polymers**, 2012, 87 (2): 963-979.

[18]   Islam M T, Alam M M, and Zoccola M. *Review on modification of nanocellulose for application in composites.* **Int J Innov Res Sci Eng Technol**, 2013, 2 (10): 5444-5451.

[19]   Kargarzadeh H, Mariano M, Huang J, Lin N, Ahmad I, Dufresne A, and Thomas S. *Recent developments on nanocellulose reinforced polymer nanocomposites: A review.* **Polymer**, 2017, 132 368-393.

[20]   Yao J, Chen S, Chen Y, Wang B, Pei Q, and Wang H. *Macrofibers with High Mechanical Performance Based on Aligned Bacterial Cellulose Nanofibers.* **ACS Applied Materials & Interfaces**, 2017, 9 (24): 20330-20339.

[21]   Hooshmand S, Aitomäki Y, Norberg N, Mathew A P, and Oksman K. *Dry-spun single-filament fibers comprising solely cellulose nanofibers from bioresidue.* **ACS applied materials & interfaces**, 2015, 7 (23): 13022-13028.

[22]   Iwamoto S, Kai W, Isogai A, and Iwata T. *Elastic Modulus of Single Cellulose Microfibrils from Tunicate Measured by Atomic Force Microscopy.* **Biomacromolecules**, 2009, 10 (9): 2571-2576.

[23]   Zhao J, Zhang W, Zhang X, Zhang X, Lu C, and Deng Y. *Extraction of cellulose nanofibrils from dry softwood pulp using high shear homogenization.* **Carbohydrate Polymers**, 2013, 97 (2): 695-702.

[24]   Song J, Tang A, Liu T, and Wang J. *Fast and continuous preparation of high polymerization degree cellulose nanofibrils and their three-dimensional macroporous scaffold fabrication.* **Nanoscale**, 2013, 5 (6): 2482-2490.

[25]   Nair S S, Zhu J Y, Deng Y, and Ragauskas A J. *Characterization of cellulose nanofibrillation by micro grinding.* **Journal of Nanoparticle Research**, 2014, 16 (4): 2349.

[26]   Lee J and Deng Y. *The morphology and mechanical properties of layer structured cellulose microfibril foams from ice-templating methods.* **Soft Matter**, 2011, 7 (13): 6034-6040.

[27]   Hamad W. *On the Development and Applications of Cellulosic Nanofibrillar and Nanocrystalline Materials.* **The Canadian Journal of Chemical Engineering**, 2006, 84 (5): 513-519.

[28]   Chinga-Carrasco G. *Cellulose fibres, nanofibrils and microfibrils: The morphological sequence of MFC components from a plant physiology and fibre technology point of view.* **Nanoscale Research Letters**, 2011, 6 (1): 417.

[29]   Wambua P, Ivens J, and Verpoest I. *Natural fibres: can they replace glass in fibre reinforced plastics?* **Composites Science and Technology**, 2003, 63 (9): 1259-1264.

[30]   Ku H, Wang H, Pattarachaiyakoop N, and Trada M. *A review on the tensile properties of natural fiber reinforced polymer composites.* **Composites Part B: Engineering**, 2011, 42 (4): 856-873.

[31]   Siqueira G, Bras J, and Dufresne A. *Cellulosic Bionanocomposites: A Review of Preparation, Properties and Applications.* **Polymers**, 2010, 2 (4): 728.

[32]   Chinga-Carrasco G. *Cellulose fibres, nanofibrils and microfibrils: The morphological sequence of MFC components from a plant physiology and fibre technology point of view.* **Nanoscale Research Letters**, 2011, 6 (1): 417-417.

[33]   Stenstad P, Andresen M, Tanem B S, and Stenius P. *Chemical surface modifications of microfibrillated cellulose.* **Cellulose**, 2008, 15 (1): 35-45.

[34]   Siqueira G, Bras J, and Dufresne A. *New Process of Chemical Grafting of Cellulose Nanoparticles with a Long Chain Isocyanate.* **Langmuir**, 2010, 26 (1): 402-411.

[35]   Eyley S and Thielemans W. *Surface modification of cellulose nanocrystals.* **Nanoscale**, 2014, 6 (14): 7764-7779.

[36]   Liu J, Wang Y, Wu S, Zhang P, and Zhu Y. *Preparation of poly (glycidylmethacrylate-divinylbenzene) weak acid cation exchange stationary phases with succinic anhydride, phthalic anhydride, and maleic anhydride for ion chromatography.* **Journal of separation science**, 2016, 39 (15): 2970-2977.

[37]   Ma J, Wang X, Fu Q, Si Y, Yu J, and Ding B. *Highly Carbonylated Cellulose Nanofibrous Membranes Utilizing Maleic Anhydride Grafting for Efficient Lysozyme Adsorption.* **ACS applied materials & interfaces**, 2015, 7 (28): 15658-15666.

[38]   Sahin H, Manolache S, Young R, and Denes F. *Surface fluorination of paper in CF4-RF plasma environments.* **Cellulose**, 2002, 9 (2): 171-181.

[39]   Siró I, Plackett D, Hedenqvist M, Ankerfors M, and Lindström T. *Highly transparent films from carboxymethylated microfibrillated cellulose: the effect of multiple homogenization steps on key properties.* **Journal of Applied Polymer Science**, 2011, 119 (5): 2652-2660.

[40]   Shang S-M, Li Z, Xing Y, Xin J H, and Tao X-M. *Preparation of durable hydrophobic cellulose fabric from water glass and mixed organosilanes.* **Applied Surface Science**, 2010, 257 (5): 1495-1499.

[41]   Roy D, Semsarilar M, Guthrie J T, and Perrier S. *Cellulose modification by polymer grafting: a review.* **Chemical Society Reviews**, 2009, 38 (7): 2046-2064.

147

[42] George J, Sreekala M S, and Thomas S. *A review on interface modification and characterization of natural fiber reinforced plastic composites.* **Polymer Engineering & Science**, 2001, 41 (9): 1471-1485.

[43] Kalia S, Dufresne A, Cherian B M, Kaith B S, Av, #233, rous L, Njuguna J, and Nassiopoulos E. *Cellulose-Based Bio- and Nanocomposites: A Review.* **International Journal of Polymer Science**, 2011, 2011

[44] Tobjörk D and Österbacka R. *Paper Electronics.* **Advanced Materials**, 2011, 23 (17): 1935-1961.

[45] Shimizu M, Fukuzumi H, Saito T, and Isogai A. *Preparation and characterization of TEMPO-oxidized cellulose nanofibrils with ammonium carboxylate groups.* **International Journal of Biological Macromolecules**, 2013, 59 (Supplement C): 99-104.

[46] Sone A, Saito T, and Isogai A. *Preparation of Aqueous Dispersions of TEMPO-Oxidized Cellulose Nanofibrils with Various Metal Counterions and Their Super Deodorant Performances.* **ACS Macro Letters**, 2016, 5 (12): 1402-1405.

[47] Saito T, Kimura S, Nishiyama Y, and Isogai A. *Cellulose Nanofibers Prepared by TEMPO-Mediated Oxidation of Native Cellulose.* **Biomacromolecules**, 2007, 8 (8): 2485-2491.

[48] Isogai A, Saito T, and Fukuzumi H. *TEMPO-oxidized cellulose nanofibers.* **Nanoscale**, 2011, 3 (1): 71-85.

[49] Lu P and Hsieh Y-L. *Preparation and properties of cellulose nanocrystals: rods, spheres, and network.* **Carbohydrate Polymers**, 2010, 82 (2): 329-336.

[50] Beck-Candanedo S, Roman M, and Gray D G. *Effect of reaction conditions on the properties and behavior of wood cellulose nanocrystal suspensions.* **Biomacromolecules**, 2005, 6 (2): 1048-1054.

[51] Ramires E C and Dufresne A. *A review of cellulose nanocrystals and nanocomposites.* **Tappi J**, 2011, 10 (4): 9-16.

[52] Mariano M, El Kissi N, and Dufresne A. *Cellulose nanocrystals and related nanocomposites: review of some properties and challenges.* **Journal of Polymer Science Part B: Polymer Physics**, 2014, 52 (12): 791-806.

[53] Author. Suspensions containing microfibrillated cellulose. United States patent US 4,500,546, 1985.

[54] Hasani M, Cranston E D, Westman G, and Gray D G. *Cationic surface functionalization of cellulose nanocrystals.* **Soft Matter**, 2008, 4 (11): 2238-2244.

[55] Nishiyama Y, Sugiyama J, Chanzy H, and Langan P. *Crystal structure and hydrogen bonding system in cellulose Iα from synchrotron X-ray and neutron fiber diffraction.* **Journal of the American Chemical Society**, 2003, 125 (47): 14300-14306.

[56] Watanabe A, Morita S, and Ozaki Y. *Temperature-dependent changes in hydrogen bonds in cellulose Iα studied by infrared spectroscopy in combination with perturbation-correlation moving-*

window two-dimensional correlation spectroscopy: comparison with cellulose Iβ. **Biomacromolecules**, 2007, 8 (9): 2969-2975.

[57] Horikawa Y and Sugiyama J. *Localization of crystalline allomorphs in cellulose microfibril.* **Biomacromolecules**, 2009, 10 (8): 2235-2239.

[58] Festucci-Buselli R A, Otoni W C, and Joshi C P. *Structure, organization, and functions of cellulose synthase complexes in higher plants.* **Brazilian Journal of Plant Physiology**, 2007, 19 (1): 1-13.

[59] Nishiyama Y, Johnson G P, French A D, Forsyth V T, and Langan P. *Neutron crystallography, molecular dynamics, and quantum mechanics studies of the nature of hydrogen bonding in cellulose Iβ.* **Biomacromolecules**, 2008, 9 (11): 3133-3140.

[60] O'Neill H, Pingali S V, Petridis L, He J, Mamontov E, Hong L, Urban V, Evans B, Langan P, Smith J C, and Davison B H. *Dynamics of water bound to crystalline cellulose.* **Sci Rep**, 2017, 7 (1): 11840.

[61] Lindh E L, Terenzi C, Salmén L, and Furó I. *Water in cellulose: evidence and identification of immobile and mobile adsorbed phases by 2H MAS NMR.* **Physical Chemistry Chemical Physics**, 2017, 19 (6): 4360-4369.

[62] Kato K L and Cameron R E. *A review of the relationship between thermally-accelerated ageing of paper and hornification.* **Cellulose**, 1999, 6 (1): 23-40.

[63] Hubbe M A, Venditti R A, and Rojas O J. *WHAT HAPPENS TO CELLULOSIC FIBERS DURING PAPERMAKING AND RECYCLING? A REVIEW.* **BioResources; Vol 2, No 4 (2007)**, 2007,

[64] Ding Q, Zeng J, Wang B, Tang D, Chen K, and Gao W. *Effect of nanocellulose fiber hornification on water fraction characteristics and hydroxyl accessibility during dehydration.* **Carbohydrate Polymers**, 2019, 207 44-51.

[65] Lindman B, Medronho B, Alves L, Costa C, Edlund H, and Norgren M. *The relevance of structural features of cellulose and its interactions to dissolution, regeneration, gelation and plasticization phenomena.* **Phys Chem Chem Phys**, 2017, 19 (35): 23704-23718.

[66] Nair S S, Zhu J Y, Deng Y, and Ragauskas A J. *High performance green barriers based on nanocellulose.* **Sustainable Chemical Processes**, 2014, 2 (1): 23.

[67] Scallan A. *The accommodation of water within pulp fibers.* in *Sixth fundamental Research Symposium, 1977,(Fiber-Water Interactions in Papermaking), London.* Year

[68] Maloney T C. *Network swelling of TEMPO-oxidized nanocellulose.* **Holzforschung**, 2015, 69 (2): 207-213.

[69] Heux L, Chauve G, and Bonini C. *Nonflocculating and Chiral-Nematic Self-ordering of Cellulose Microcrystals Suspensions in Nonpolar Solvents.* **Langmuir**, 2000, 16 (21): 8210-8212.

[70] Bondeson D and Oksman K. *Dispersion and characteristics of surfactant modified cellulose whiskers nanocomposites.* **Composite Interfaces**, 2007, 14 (7-9): 617-630.

[71]   Bonini C, Heux L, Cavaillé J-Y, Lindner P, Dewhurst C, and Terech P. *Rodlike Cellulose Whiskers Coated with Surfactant: A Small-Angle Neutron Scattering Characterization.* **Langmuir**, 2002, 18 (8): 3311-3314.

[72]   Sarwar M S, Niazi M B K, Jahan Z, Ahmad T, and Hussain A. *Preparation and characterization of PVA/nanocellulose/Ag nanocomposite films for antimicrobial food packaging.* **Carbohydrate Polymers**, 2018, 184 453-464.

[73]   Lee S-Y, Mohan D J, Kang I-A, Doh G-H, Lee S, and Han S O. *Nanocellulose reinforced PVA composite films: Effects of acid treatment and filler loading.* **Fibers and Polymers**, 2009, 10 (1): 77-82.

[74]   Gan P G, Sam S T, Abdullah M F b, and Omar M F. *Thermal properties of nanocellulose-reinforced composites: A review.* **Journal of Applied Polymer Science**, 2020, 137 (11): 48544.

[75]   Zhou C, Chu R, Wu R, and Wu Q. *Electrospun Polyethylene Oxide/Cellulose Nanocrystal Composite Nanofibrous Mats with Homogeneous and Heterogeneous Microstructures.* **Biomacromolecules**, 2011, 12 (7): 2617-2625.

[76]   Kim J, Montero G, Habibi Y, Hinestroza J P, Genzer J, Argyropoulos D S, and Rojas O J. *Dispersion of cellulose crystallites by nonionic surfactants in a hydrophobic polymer matrix.* **Polymer Engineering & Science**, 2009, 49 (10): 2054-2061.

[77]   Gunathilake T M S U, Ching Y C, Chuah C H, Illias H A, Ching K Y, Singh R, and Nai-Shang L. *Influence of a nonionic surfactant on curcumin delivery of nanocellulose reinforced chitosan hydrogel.* **International journal of biological macromolecules**, 2018, 118 1055-1064.

[78]   Zhou Q, Brumer H, and Teeri T T. *Self-Organization of Cellulose Nanocrystals Adsorbed with Xyloglucan Oligosaccharide–Poly(ethylene glycol)–Polystyrene Triblock Copolymer.* **Macromolecules**, 2009, 42 (15): 5430-5432.

[79]   Moreau C, Beury N, Delorme N, and Cathala B. *Tuning the Architecture of Cellulose Nanocrystal–Poly(allylamine hydrochloride) Multilayered Thin Films: Influence of Dipping Parameters.* **Langmuir**, 2012, 28 (28): 10425-10436.

[80]   Zhao F, Repo E, Song Y, Yin D, Hammouda S B, Chen L, Kalliola S, Tang J, Tam K C, and Sillanpää M. *Polyethylenimine-cross-linked cellulose nanocrystals for highly efficient recovery of rare earth elements from water and a mechanism study.* **Green Chemistry**, 2017, 19 (20): 4816-4828.

[81]   Li J, Zuo K, Wu W, Xu Z, Yi Y, Jing Y, Dai H, and Fang G. *Shape memory aerogels from nanocellulose and polyethyleneimine as a novel adsorbent for removal of Cu(II) and Pb(II).* **Carbohydrate Polymers**, 2018, 196 376-384.

[82]   Brockman A C and Hubbe M A. *Charge reversal system with cationized cellulose nanocrystals to promote dewatering of a cellulosic fiber suspension.* **Cellulose**, 2017, 24 (11): 4821-4830.

[83]   Roman M and Winter W T. *Effect of Sulfate Groups from Sulfuric Acid Hydrolysis on the Thermal Degradation Behavior of Bacterial Cellulose.* **Biomacromolecules**, 2004, 5 (5): 1671-1677.

[84]   Abitbol T, Kloser E, and Gray D G. *Estimation of the surface sulfur content of cellulose nanocrystals prepared by sulfuric acid hydrolysis.* **Cellulose**, 2013, 20 (2): 785-794.

[85]   Mautner A, Maples H A, Kobkeatthawin T, Kokol V, Karim Z, Li K, and Bismarck A. *Phosphorylated nanocellulose papers for copper adsorption from aqueous solutions.* **International Journal of Environmental Science and Technology**, 2016, 13 (8): 1861-1872.

[86]   Isogai A, Hänninen T, Fujisawa S, and Saito T. *Review: Catalytic oxidation of cellulose with nitroxyl radicals under aqueous conditions.* **Progress in Polymer Science**, 2018, 86 122-148.

[87]   Sun F, Liu W, Dong Z, and Deng Y. *Underwater superoleophobicity cellulose nanofibril aerogel through regioselective sulfonation for oil/water separation.* **Chemical Engineering Journal**, 2017, 330 774-782.

[88]   Spinella S, Samuel C, Raquez J-M, McCallum S A, Gross R, and Dubois P. *Green and Efficient Synthesis of Dispersible Cellulose Nanocrystals in Biobased Polyesters for Engineering Applications.* **ACS Sustainable Chemistry & Engineering**, 2016, 4 (5): 2517-2527.

[89]   Kedzior S A, Graham L, Moorlag C, Dooley B M, and Cranston E D. *Poly(methyl methacrylate)-grafted cellulose nanocrystals: One-step synthesis, nanocomposite preparation, and characterization.* **The Canadian Journal of Chemical Engineering**, 2016, 94 (5): 811-822.

[90]   Pracella M, Haque M M-U, and Puglia D. *Morphology and properties tuning of PLA/cellulose nanocrystals bio-nanocomposites by means of reactive functionalization and blending with PVAc.* **Polymer**, 2014, 55 (16): 3720-3728.

[91]   Habibi Y. *Key advances in the chemical modification of nanocelluloses.* **Chemical Society Reviews**, 2014, 43 (5): 1519-1542.

[92]   Nogi M, Abe K, Handa K, Nakatsubo F, Ifuku S, and Yano H. *Property enhancement of optically transparent bionanofiber composites by acetylation.* **Applied Physics Letters**, 2006, 89 (23): 233123.

[93]   Tomé L C, Pinto R J B, Trovatti E, Freire C S R, Silvestre A J D, Neto C P, and Gandini A. *Transparent bionanocomposites with improved properties prepared from acetylated bacterial cellulose and poly(lactic acid) through a simple approach.* **Green Chemistry**, 2011, 13 (2): 419-427.

[94]   Junior de Menezes A, Siqueira G, Curvelo A A S, and Dufresne A. *Extrusion and characterization of functionalized cellulose whiskers reinforced polyethylene nanocomposites.* **Polymer**, 2009, 50 (19): 4552-4563.

[95]   Lee K-Y, Blaker J J, and Bismarck A. *Surface functionalisation of bacterial cellulose as the route to produce green polylactide nanocomposites with improved properties.* **Composites Science and Technology**, 2009, 69 (15): 2724-2733.

[96]   Lee K-Y, Quero F, Blaker J J, Hill C A S, Eichhorn S J, and Bismarck A. *Surface only modification of bacterial cellulose nanofibres with organic acids.* **Cellulose**, 2011, 18 (3): 595-605.

[97]   Goussé C, Chanzy H, Excoffier G, Soubeyrand L, and Fleury E. *Stable suspensions of partially silylated cellulose whiskers dispersed in organic solvents.* **Polymer**, 2002, 43 (9): 2645-2651.

[98]   Raquez J M, Murena Y, Goffin A L, Habibi Y, Ruelle B, DeBuyl F, and Dubois P. *Surface-modification of cellulose nanowhiskers and their use as nanoreinforcers into polylactide: A sustainably-integrated approach.* **Composites Science and Technology**, 2012, 72 (5): 544-549.

[99]   Follain N, Belbekhouche S, Bras J, Siqueira G, Marais S, and Dufresne A. *Water transport properties of bio-nanocomposites reinforced by Luffa cylindrica cellulose nanocrystals.* **Journal of Membrane Science**, 2013, 427 218-229.

[100]   Chakrabarty A and Teramoto Y. *Recent Advances in Nanocellulose Composites with Polymers: A Guide for Choosing Partners and How to Incorporate Them.* **Polymers**, 2018, 10 (5): 517.

[101]   Li Z Q, Zhou X D, and Pei C H. *Synthesis of PLA-co-PGMA Copolymer and its Application in the Surface Modification of Bacterial Cellulose.* **International Journal of Polymeric Materials and Polymeric Biomaterials**, 2010, 59 (9): 725-737.

[102]   Saba N, Safwan A, Sanyang M L, Mohammad F, Pervaiz M, Jawaid M, Alothman O Y, and Sain M. *Thermal and dynamic mechanical properties of cellulose nanofibers reinforced epoxy composites.* **International Journal of Biological Macromolecules**, 2017, 102 822-828.

[103]   Yang W, Dominici F, Fortunati E, Kenny J M, and Puglia D. *Melt free radical grafting of glycidyl methacrylate (GMA) onto fully biodegradable poly(lactic) acid films: effect of cellulose nanocrystals and a masterbatch process.* **RSC Advances**, 2015, 5 (41): 32350-32357.

[104]   Araki J, Wada M, and Kuga S. *Steric Stabilization of a Cellulose Microcrystal Suspension by Poly(ethylene glycol) Grafting.* **Langmuir**, 2001, 17 (1): 21-27.

[105]   Pei A, Malho J-M, Ruokolainen J, Zhou Q, and Berglund L A. *Strong Nanocomposite Reinforcement Effects in Polyurethane Elastomer with Low Volume Fraction of Cellulose Nanocrystals.* **Macromolecules**, 2011, 44 (11): 4422-4427.

[106]   Lönnberg H, Fogelström L, Berglund L, Malmström E, and Hult A. *Surface grafting of microfibrillated cellulose with poly(ε-caprolactone) – Synthesis and characterization.* **European Polymer Journal**, 2008, 44 (9): 2991-2997.

[107]   Habibi Y, Goffin A-L, Schiltz N, Duquesne E, Dubois P, and Dufresne A. *Bionanocomposites based on poly(ε-caprolactone)-grafted cellulose nanocrystals by ring-opening polymerization.* **Journal of Materials Chemistry**, 2008, 18 (41): 5002-5010.

[108]   Goffin A-L, Habibi Y, Raquez J-M, and Dubois P. *Polyester-Grafted Cellulose Nanowhiskers: A New Approach for Tuning the Microstructure of Immiscible Polyester Blends.* **ACS Applied Materials & Interfaces**, 2012, 4 (7): 3364-3371.

[109] Morandi G, Heath L, and Thielemans W. *Cellulose Nanocrystals Grafted with Polystyrene Chains through Surface-Initiated Atom Transfer Radical Polymerization (SI-ATRP).* **Langmuir**, 2009, 25 (14): 8280-8286.

[110] Lin N, Huang J, and Dufresne A. *Preparation, properties and applications of polysaccharide nanocrystals in advanced functional nanomaterials: a review.* **Nanoscale**, 2012, 4 (11): 3274-3294.

[111] Wohlhauser S, Delepierre G, Labet M, Morandi G, Thielemans W, Weder C, and Zoppe J O. *Grafting Polymers from Cellulose Nanocrystals: Synthesis, Properties, and Applications.* **Macromolecules**, 2018, 51 (16): 6157-6189.

[112] Zhu J Y, Sabo R, and Luo X. *Integrated production of nano-fibrillated cellulose and cellulosic biofuel (ethanol) by enzymatic fractionation of wood fibers.* **Green Chemistry**, 2011, 13 (5): 1339-1344.

[113] Xia J, Zhang Z, Liu W, Li V C F, Cao Y, Zhang W, and Deng Y. *Highly transparent 100% cellulose nanofibril films with extremely high oxygen barriers in high relative humidity.* **Cellulose**, 2018, 25 (7): 4057-4066.

[114] Sharma S, Zhang X, Nair S S, Ragauskas A, Zhu J, and Deng Y. *Thermally enhanced high performance cellulose nano fibril barrier membranes.* **RSC Advances**, 2014, 4 (85): 45136-45142.

[115] Fang Z, Zhu H, Bao W, Preston C, Liu Z, Dai J, Li Y, and Hu L. *Highly transparent paper with tunable haze for green electronics.* **Energy & Environmental Science**, 2014, 7 (10): 3313-3319.

[116] Yang W, Jiao L, Liu W, Deng Y, and Dai H. *Morphology control for tunable optical properties of cellulose nanofibrils films.* **Cellulose**, 2018, 25 (10): 5909-5918.

[117] Fang Z, Zhu H, Yuan Y, Ha D, Zhu S, Preston C, Chen Q, Li Y, Han X, Lee S, Chen G, Li T, Munday J, Huang J, and Hu L. *Novel Nanostructured Paper with Ultrahigh Transparency and Ultrahigh Haze for Solar Cells.* **Nano Letters**, 2014, 14 (2): 765-773.

[118] Ferrer A, Pal L, and Hubbe M. *Nanocellulose in packaging: Advances in barrier layer technologies.* **Industrial Crops and Products**, 2017, 95 574-582.

[119] de Mesquita J P, Donnici C L, and Pereira F V. *Biobased nanocomposites from layer-by-layer assembly of cellulose nanowhiskers with chitosan.* **Biomacromolecules**, 2010, 11 (2): 473-480.

[120] Li F, Biagioni P, Finazzi M, Tavazzi S, and Piergiovanni L. *Tunable green oxygen barrier through layer-by-layer self-assembly of chitosan and cellulose nanocrystals.* **Carbohydrate polymers**, 2013, 92 (2): 2128-2134.

[121] Marais A, Utsel S, Gustafsson E, and Wågberg L. *Towards a super-strainable paper using the layer-by-layer technique.* **Carbohydrate polymers**, 2014, 100 218-224.

[122] Wågberg L, Decher G, Norgren M, Lindström T, Ankerfors M, and Axnäs K. *The build-up of polyelectrolyte multilayers of microfibrillated cellulose and cationic polyelectrolytes.* **Langmuir**, 2008, 24 (3): 784-795.

[123]   Svagan A J, Hedenqvist M S, and Berglund L. *Reduced water vapour sorption in cellulose nanocomposites with starch matrix.* **Composites Science and Technology**, 2009, 69 (3): 500-506.

[124]   Shanmugam K, Doosthosseini H, Varanasi S, Garnier G, and Batchelor W. *Flexible spray coating process for smooth nanocellulose film production.* **Cellulose**, 2018, 25 (3): 1725-1741.

[125]   Zhang L, Batchelor W, Varanasi S, Tsuzuki T, and Wang X. *Effect of cellulose nanofiber dimensions on sheet forming through filtration.* **Cellulose**, 2012, 19 (2): 561-574.

[126]   Varanasi S and Batchelor W J. *Rapid preparation of cellulose nanofibre sheet.* **Cellulose**, 2013, 20 (1): 211-215.

[127]   Song N, Jiao D, Cui S, Hou X, Ding P, and Shi L. *Highly anisotropic thermal conductivity of layer-by-layer assembled nanofibrillated cellulose/graphene nanosheets hybrid films for thermal management.* **ACS applied materials & interfaces**, 2017, 9 (3): 2924-2932.

[128]   Hubbe M A, Ferrer A, Tyagi P, Yin Y, Salas C, Pal L, and Rojas O J. *Nanocellulose in thin films, coatings, and plies for packaging applications: A review.* **BioResources**, 2017, 12 (1): 2143-2233.

[129]   Abdul Khalil H P S, Davoudpour Y, Saurabh C K, Hossain M S, Adnan A S, Dungani R, Paridah M T, Islam Sarker M Z, Fazita M R N, Syakir M I, and Haafiz M K M. *A review on nanocellulosic fibres as new material for sustainable packaging: Process and applications.* **Renewable and Sustainable Energy Reviews**, 2016, 64 823-836.

[130]   Mondal S. *Review on Nanocellulose Polymer Nanocomposites.* **Polymer-Plastics Technology and Engineering**, 2018, 57 (13): 1377-1391.

[131]   Bhanvase B and Sonawane S. *Ultrasound assisted in situ emulsion polymerization for polymer nanocomposite: A review.* **Chemical Engineering and Processing: Process Intensification**, 2014, 85 86-107.

[132]   Sapkota J, Natterodt J C, Shirole A, Foster E J, and Weder C. *Fabrication and Properties of Polyethylene/Cellulose Nanocrystal Composites.* **Macromolecular Materials and Engineering**, 2017, 302 (1): 1600300.

[133]   Mabrouk A B, Salon M B, Magnin A, Belgacem M, and Boufi S. *Cellulose-based nanocomposites prepared via mini-emulsion polymerization: Understanding the chemistry of the nanocellulose/matrix interface.* **Colloids and Surfaces A: Physicochemical and Engineering Aspects**, 2014, 448 1-8.

[134]   Mabrouk A B, Salon M C B, Magnin A, Belgacem M N, and Boufi S. *Cellulose-based nanocomposites prepared via mini-emulsion polymerization: Understanding the chemistry of the nanocellulose/matrix interface.* **Colloids and Surfaces A: Physicochemical and Engineering Aspects**, 2014, 448 1-8.

[135]   Kian L K, Saba N, Jawaid M, and Sultan M T H. *A review on processing techniques of bast fibers nanocellulose and its polylactic acid (PLA) nanocomposites.* **International Journal of Biological Macromolecules**, 2019, 121 1314-1328.

[136]   Sullivan E M, Moon R J, and Kalaitzidou K. *Processing and characterization of cellulose nanocrystals/polylactic acid nanocomposite films.* **Materials**, 2015, 8 (12): 8106-8116.

[137]   Huang L, Zhang X, Xu M, Chen J, Shi Y, Huang C, Wang S, An S, and Li C. *Preparation and mechanical properties of modified nanocellulose/PLA composites from cassava residue.* **AIP Advances**, 2018, 8 (2): 025116.

[138]   Arjmandi R, Hassan A, Haafiz M, Zakaria Z, and Islam M S. *Effect of hydrolysed cellulose nanowhiskers on properties of montmorillonite/polylactic acid nanocomposites.* **International journal of biological macromolecules**, 2016, 82 998-1010.

[139]   Goffin A-L, Raquez J-M, Duquesne E, Siqueira G, Habibi Y, Dufresne A, and Dubois P. *Poly (ε-caprolactone) based nanocomposites reinforced by surface-grafted cellulose nanowhiskers via extrusion processing: morphology, rheology, and thermo-mechanical properties.* **Polymer**, 2011, 52 (7): 1532-1538.

[140]   Sehaqui H, Salajková M, Zhou Q, and Berglund L A. *Mechanical performance tailoring of tough ultra-high porosity foams prepared from cellulose I nanofiber suspensions.* **Soft Matter**, 2010, 6 (8): 1824-1832.

[141]   De France K J, Hoare T, and Cranston E D. *Review of Hydrogels and Aerogels Containing Nanocellulose.* **Chemistry of Materials**, 2017, 29 (11): 4609-4631.

[142]   Lavoine N and Bergström L. *Nanocellulose-based foams and aerogels: processing, properties, and applications.* **Journal of Materials Chemistry A**, 2017, 5 (31): 16105-16117.

[143]   Deville S. *Freeze-casting of porous biomaterials: structure, properties and opportunities.* **Materials**, 2010, 3 (3): 1913-1927.

[144]   Aulin C, Netrval J, Wågberg L, and Lindström T. *Aerogels from nanofibrillated cellulose with tunable oleophobicity.* **Soft Matter**, 2010, 6 (14): 3298-3305.

[145]   Martoïa F, Cochereau T, Dumont P J J, Orgéas L, Terrien M, and Belgacem M N. *Cellulose nanofibril foams: Links between ice-templating conditions, microstructures and mechanical properties.* **Materials & Design**, 2016, 104 376-391.

[146]   Long L-Y, Weng Y-X, and Wang Y-Z. *Cellulose aerogels: Synthesis, applications, and prospects.* **Polymers**, 2018, 10 (6): 623.

[147]   Zhang X, Yu Y, Jiang Z, and Wang H. *The effect of freezing speed and hydrogel concentration on the microstructure and compressive performance of bamboo-based cellulose aerogel.* **Journal of wood science**, 2015, 61 (6): 595-601.

[148] Jiang F and Hsieh Y-L. *Super water absorbing and shape memory nanocellulose aerogels from TEMPO-oxidized cellulose nanofibrils via cyclic freezing–thawing.* **Journal of Materials Chemistry A**, 2014, 2 (2): 350-359.

[149] Wang X, Zhang Y, Jiang H, Song Y, Zhou Z, and Zhao H. *Tert-butyl alcohol used to fabricate nano-cellulose aerogels via freeze-drying technology.* **Materials research express**, 2017, 4 (6): 065006.

[150] Pons A, Casas L, Estop E, Molins E, Harris K D M, and Xu M. *A new route to aerogels: Monolithic silica cryogels.* **Journal of non-crystalline solids**, 2012, 358 (3): 461-469.

[151] Deville S. *Ice-templating, freeze casting: Beyond materials processing.* **Journal of Materials Research**, 2013, 28 (17): 2202-2219.

[152] Zhai T, Zheng Q, Cai Z, Xia H, and Gong S. *Synthesis of polyvinyl alcohol/cellulose nanofibril hybrid aerogel microspheres and their use as oil/solvent superabsorbents.* **Carbohydrate Polymers**, 2016, 148 300-308.

[153] Zhang F, Ren H, Dou J, Tong G, and Deng Y. *Cellulose Nanofibril Based-Aerogel Microreactors: A High Efficiency and Easy Recoverable W/O/W Membrane Separation System.* **Scientific Reports**, 2017, 7 (1): 40096.

[154] Munier P, Gordeyeva K, Bergström L, and Fall A B. *Directional Freezing of Nanocellulose Dispersions Aligns the Rod-Like Particles and Produces Low-Density and Robust Particle Networks.* **Biomacromolecules**, 2016, 17 (5): 1875-1881.

[155] Tashiro K and Kobayashi M. *Calculation of crystallite modulus of native cellulose.* **Polymer Bulletin**, 1985, 14 (3): 213-218.

[156] Lundahl M J, Cunha A G, Rojo E, Papageorgiou A C, Rautkari L, Arboleda J C, and Rojas O J. *Strength and Water Interactions of Cellulose I Filaments Wet-Spun from Cellulose Nanofibril Hydrogels.* **Scientific Reports**, 2016, 6 30695.

[157] Walther A, Timonen J V I, Díez I, Laukkanen A, and Ikkala O. *Multifunctional High-Performance Biofibers Based on Wet-Extrusion of Renewable Native Cellulose Nanofibrils.* **Advanced Materials**, 2011, 23 (26): 2924-2928.

[158] Hooshmand S, Aitomäki Y, Norberg N, Mathew A P, and Oksman K. *Dry-Spun Single-Filament Fibers Comprising Solely Cellulose Nanofibers from Bioresidue.* **ACS Applied Materials & Interfaces**, 2015, 7 (23): 13022-13028.

[159] Xu Z, Liu Y, Zhao X, Peng L, Sun H, Xu Y, Ren X, Jin C, Xu P, and Wang M. *Ultrastiff and strong graphene fibers via full-scale synergetic defect engineering.* **Advanced Materials**, 2016, 28 (30): 6449-6456.

[160] Fumiko K and Tsunehisa K. *Magnetic alignment and patterning of cellulose fibers.* **Science and Technology of Advanced Materials**, 2008, 9 (2): 024212.

[161]   Kim J, Chen Y, Kang K-S, Park Y-B, and Schwartz M. *Magnetic field effect for cellulose nanofiber alignment.* **Journal of Applied Physics**, 2008, 104 (9): 096104.

[162]   Håkansson K M, Fall A B, Lundell F, Yu S, Krywka C, Roth S V, Santoro G, Kvick M, Wittberg L P, and Wågberg L. *Hydrodynamic alignment and assembly of nanofibrils resulting in strong cellulose filaments.* **Nature communications**, 2014, 5

[163]   Håkansson K M O, Fall A B, Lundell F, Yu S, Krywka C, Roth S V, Santoro G, Kvick M, Prahl Wittberg L, Wågberg L, and Söderberg L D. *Hydrodynamic alignment and assembly of nanofibrils resulting in strong cellulose filaments.* **Nature Communications**, 2014, 5 4018.

[164]   Mittal N, Ansari F, Gowda.V K, Brouzet C, Chen P, Larsson P T, Roth S V, Lundell F, Wågberg L, Kotov N A, and Söderberg L D. *Multiscale Control of Nanocellulose Assembly: Transferring Remarkable Nanoscale Fibril Mechanics to Macroscale Fibers.* **ACS Nano**, 2018, 12 (7): 6378-6388.

[165]   Wang S, Jiang F, Xu X, Kuang Y, Fu K, Hitz E, and Hu L. *Super-Strong, Super-Stiff Macrofibers with Aligned, Long Bacterial Cellulose Nanofibers.* **Advanced Materials**, 2017, 29 (35): 1702498.

[166]   Torres-Rendon J G, Schacher F H, Ifuku S, and Walther A. *Mechanical Performance of Macrofibers of Cellulose and Chitin Nanofibrils Aligned by Wet-Stretching: A Critical Comparison.* **Biomacromolecules**, 2014, 15 (7): 2709-2717.

[167]   Iwamoto S, Isogai A, and Iwata T. *Structure and Mechanical Properties of Wet-Spun Fibers Made from Natural Cellulose Nanofibers.* **Biomacromolecules**, 2011, 12 (3): 831-836.

[168]   Lundahl M J, Klar V, Wang L, Ago M, and Rojas O J. *Spinning of Cellulose Nanofibrils into Filaments: A Review.* **Industrial & Engineering Chemistry Research**, 2017, 56 (1): 8-19.

[169]   Wu Weibing Z L. *Functionalization and Applications of Nanocrystalline Cellulose.* **Progress in Chemistry**, 2014, 26 (0203): 403-414.

[170]   Ye C, Malak S T, Hu K, Wu W, and Tsukruk V V. *Cellulose Nanocrystal Microcapsules as Tunable Cages for Nano- and Microparticles.* **ACS Nano**, 2015, 9 (11): 10887-10895.

[171]   Wu W, Huang F, Pan S, Mu W, Meng X, Yang H, Xu Z, Ragauskas A J, and Deng Y. *Thermo-responsive and fluorescent cellulose nanocrystals grafted with polymer brushes.* **Journal of Materials Chemistry A**, 2015, 3 (5): 1995-2005.

[172]   Qiu X and Hu S. *"Smart" Materials Based on Cellulose: A Review of the Preparations, Properties, and Applications.* **Materials**, 2013, 6 (3):

[173]   Kim J, Yun S, and Ounaies Z. *Discovery of Cellulose as a Smart Material.* **Macromolecules**, 2006, 39 (12): 4202-4206.

[174]   Li S, Huang J, Chen Z, Chen G, and Lai Y. *A review on special wettability textiles: theoretical models, fabrication technologies and multifunctional applications.* **Journal of Materials Chemistry A**, 2017, 5 (1): 31-55.

[175]   Yu S, Guo Z, and Liu W. *Biomimetic transparent and superhydrophobic coatings: from nature and beyond nature.* **Chem Commun (Camb)**, 2015, 51 (10): 1775-94.

[176]   Tuteja A, Choi W, Mabry J M, McKinley G H, and Cohen R E. *Robust omniphobic surfaces.* **Proceedings of the National Academy of Sciences**, 2008, 105 (47): 18200-18205.

[177]   Liu T L and Kim C-J C. *Turning a surface superrepellent even to completely wetting liquids.* **Science**, 2014, 346 (6213): 1096-1100.

[178]   Tuteja A, Choi W, Ma M, Mabry J M, Mazzella S A, Rutledge G C, McKinley G H, and Cohen R E. *Designing Superoleophobic Surfaces.* **Science**, 2007, 318 (5856): 1618-1622.

[179]   Zhang L, Zhong Y, Cha D, and Wang P. *A self-cleaning underwater superoleophobic mesh for oil-water separation.* **Scientific Reports**, 2013, 3 2326.

[180]   Tian D, Zhang X, Tian Y, Wu Y, Wang X, Zhai J, and Jiang L. *Photo-induced water–oil separation based on switchable superhydrophobicity–superhydrophilicity and underwater superoleophobicity of the aligned ZnO nanorod array-coated mesh films.* **Journal of Materials Chemistry**, 2012, 22 (37): 19652.

[181]   Jiang L, Zhao Y, and Zhai J. *A Lotus-Leaf-like Superhydrophobic Surface: A Porous Microsphere/Nanofiber Composite Film Prepared by Electrohydrodynamics.* **Angewandte Chemie**, 2004, 116 (33): 4438-4441.

[182]   Choi H-J, Shin J-H, Choo S, Ryu S-W, Kim Y-D, and Lee H. *Fabrication of superhydrophobic and oleophobic Al surfaces by chemical etching and surface fluorination.* **Thin Solid Films**, 2015, 585 76-80.

[183]   Li L, Li B, Dong J, and Zhang J. *Roles of silanes and silicones in forming superhydrophobic and superoleophobic materials.* **Journal of Materials Chemistry A**, 2016, 4 (36): 13677-13725.

[184]   Hou Y, Wang Z, Guo J, Shen H, Zhang H, Zhao N, Zhao Y, Chen L, Liang S, Jin Y, and Xu J. *Facile fabrication of robust superhydrophobic porous materials and their application in oil/water separation.* **Journal of Materials Chemistry A**, 2015, 3 (46): 23252-23260.

[185]   Wu Y, Jia S, Qing Y, Luo S, and Liu M. *A versatile and efficient method to fabricate durable superhydrophobic surfaces on wood, lignocellulosic fiber, glass, and metal substrates.* **Journal of Materials Chemistry A**, 2016, 4 (37): 14111-14121.

[186]   Zhang H, Li Y, Lu Z, Chen L, Huang L, and Fan M. *A robust superhydrophobic TiO2 NPs coated cellulose sponge for highly efficient oil-water separation.* **Scientific Reports**, 2017, 7 (1): 9428.

[187]   Jiang L, Tang Z, Clinton R M, Breedveld V, and Hess D W. *Two-Step Process To Create "Roll-Off" Superamphiphobic Paper Surfaces.* **ACS Applied Materials & Interfaces**, 2017, 9 (10): 9195-9203.

158

[188] Liu S, Zhou H, Wang H, Zhao Y, Shao H, Xu Z, Feng Z, Liu D, and Lin T. *Argon Plasma Treatment of Fluorine-Free Silane Coatings: A Facile, Environment-Friendly Method to Prepare Durable, Superhydrophobic Fabrics.* **Advanced Materials Interfaces**, 2017, 4 (11): 1700027.

[189] Jiang L, Tang Z, Clinton R M, Hess D W, and Breedveld V. *Fabrication of highly amphiphobic paper using pulp debonder.* **Cellulose**, 2016, 23 (6): 3885-3899.

[190] Xie L, Tang Z, Jiang L, Breedveld V, and Hess D W. *Creation of superhydrophobic wood surfaces by plasma etching and thin-film deposition.* **Surface and Coatings Technology**, 2015, 281 125-132.

[191] Qing Y, Yang C, Hu C, Zheng Y, and Liu C. *A facile method to prepare superhydrophobic fluorinated polysiloxane/ZnO nanocomposite coatings with corrosion resistance.* **Applied Surface Science**, 2015, 326 48-54.

[192] Yang M, Liu W, Jiang C, He S, Xie Y, and Wang Z. *Fabrication of superhydrophobic cotton fabric with fluorinated TiO2 sol by a green and one-step sol-gel process.* **Carbohydrate Polymers**, 2018, 197 75-82.

[193] Khanjani P, King A W T, Partl G J, Johansson L-S, Kostiainen M A, and Ras R H A. *Superhydrophobic Paper from Nanostructured Fluorinated Cellulose Esters.* **ACS Applied Materials & Interfaces**, 2018, 10 (13): 11280-11288.

[194] Zhao H, Park K C, and Law K Y. *Effect of surface texturing on superoleophobicity, contact angle hysteresis, and "robustness".* **Langmuir**, 2012, 28 (42): 14925-34.

[195] Fan M, Dai D, and Huang B. *Fourier transform infrared spectroscopy for natural fibres*. Place: InTech, 2012.

[196] Hundhausen U, Militz H, and Mai C. *Use of alkyl ketene dimer (AKD) for surface modification of particleboard chips.* **European Journal of Wood and Wood Products**, 2009, 67 (1): 37-45.

[197] Yang Q, Saito T, and Isogai A. *Facile fabrication of transparent cellulose films with high water repellency and gas barrier properties.* **Cellulose**, 2012, 19 (6): 1913-1921.

[198] Wang P, Chen M, Han H, Fan X, Liu Q, and Wang J. *Transparent and abrasion-resistant superhydrophobic coating with robust self-cleaning function in either air or oil.* **Journal of Materials Chemistry A**, 2016, 4 (20): 7869-7874.

[199] Zhang Z-h, Wang H-j, Liang Y-h, Li X-j, Ren L-q, Cui Z-q, and Luo C. *One-step fabrication of robust superhydrophobic and superoleophilic surfaces with self-cleaning and oil/water separation function.* **Scientific Reports**, 2018, 8 (1): 3869.

[200] Thomas B, Raj M C, B A K, H R M, Joy J, Moores A, Drisko G L, and Sanchez C. *Nanocellulose, a Versatile Green Platform: From Biosources to Materials and Their Applications.* **Chemical Reviews**, 2018, 118 (24): 11575-11625.

[201] Tayeb P and H. Tayeb A. *Nanocellulose applications in sustainable electrochemical and piezoelectric systems: A review.* **Carbohydrate Polymers**, 2019, 224 115149.

[202] Sabo R, Yermakov A, Law C T, and Elhajjar R. *Nanocellulose-enabled electronics, energy harvesting devices, smart materials and sensors: A review.* **Journal of Renewable Materials**, 2016, 4 (5): 297-312.

[203] Muhd Julkapli N and Bagheri S. *Nanocellulose as a green and sustainable emerging material in energy applications: a review.* **Polymers for Advanced Technologies**, 2017, 28 (12): 1583-1594.

[204] Khalil H A, Bhat A, and Yusra A I. *Green composites from sustainable cellulose nanofibrils: A review.* **Carbohydrate polymers**, 2012, 87 (2): 963-979.

[205] Pakharenko V, Pervaiz M, Pande H, Sain M, and Sain M. *Chemical and Physical Techniques for Surface Modification of Nanocellulose Reinforcements.* **Interface/Interphase in Polymer Nanocomposites**, 2016, 283-310.

[206] Wang J, Liu X, Jin T, He H, and Liu L. *Preparation of nanocellulose and its potential in reinforced composites: A review.* **Journal of Biomaterials Science, Polymer Edition**, 2019, 30 (11): 919-946.

[207] Rol F, Belgacem M N, Gandini A, and Bras J. *Recent advances in surface-modified cellulose nanofibrils.* **Progress in Polymer Science**, 2019, 88 241-264.

[208] Duran N, Paula Lemes A, and B Seabra A. *Review of cellulose nanocrystals patents: preparation, composites and general applications.* **Recent patents on nanotechnology**, 2012, 6 (1): 16-28.

[209] Ravnjak D, Moze A, and Plazl I. *Hydrolysis of micron alkylketene dimert particles under alkaline conditions.* **Chemical and biochemical engineering quarterly**, 2006, 20 (4): 463-469.

[210] Shankar S and Rhim J-W. *Preparation of nanocellulose from micro-crystalline cellulose: The effect on the performance and properties of agar-based composite films.* **Carbohydrate Polymers**, 2016, 135 18-26.

[211] Yang L, Lu S, Li J, Zhang F, and Cha R. *Nanocrystalline cellulose-dispersed AKD emulsion for enhancing the mechanical and multiple barrier properties of surface-sized paper.* **Carbohydrate Polymers**, 2016, 136 1035-1040.

[212] Kumar S, Chauhan V S, and Chakrabarti S K. *Separation and analysis techniques for bound and unbound alkyl ketene dimer (AKD) in paper: A review.* **Arabian Journal of Chemistry**, 2016, 9 S1636-S1642.

[213] Bai L, Huan S, Xiang W, and Rojas O J. *Pickering emulsions by combining cellulose nanofibrils and nanocrystals: phase behavior and depletion stabilization.* **Green Chemistry**, 2018, 20 (7): 1571-1582.

[214] Ojala J, Visanko M, Laitinen O, Österberg M, Sirviö J A, and Liimatainen H. *Emulsion Stabilization with Functionalized Cellulose Nanoparticles Fabricated Using Deep Eutectic Solvents.* **Molecules (Basel, Switzerland)**, 2018, 23 (11): 2765.

[215] Aaen R, Brodin F W, Simon S, Heggset E B, and Syverud K. *Oil-in-Water emulsions stabilized by cellulose nanofibrils—The effects of ionic strength and pH.* **Nanomaterials**, 2019, 9 (2): 259.

[216] Deng Y and Jiang H. *The Effect of Inorganic Salts and Precipitated Calcium Carbonate Filler on the Hydrolysis Kinetic of Alkylketene Dimer.* **Journal of Pulp and Paper Science**, 2000, 26

[217] Karademir A, Chew Y, Hoyland R, and Xiao H. *Influence of fillers on sizing efficiency and hydrolysis of alkyl ketene dimer.* **The Canadian Journal of Chemical Engineering**, 2005, 83 (3): 603-606.

[218] Asakura K, Iwamoto M, and Isogai A. *Effects of Fatty Acid Components Present in AKD Wax on Emulsion Stability and Paper Sizing Performance.* **Journal of Wood Chemistry and Technology**, 2005, 25 (1-2): 13-26.

[219] Lindström T and Larsson Per T. *Alkyl Ketene Dimer (AKD) sizing – a review.* **Nordic Pulp & Paper Research Journal**, 2008, 23 (2): 202.

[220] Kondo T and Sawatari C. *A Fourier transform infra-red spectroscopic analysis of the character of hydrogen bonds in amorphous cellulose.* **Polymer**, 1996, 37 (3): 393-399.

[221] Song X, Chen F, and Liu F. *Preparation and characterization of alkyl ketene dimer (AKD) modified cellulose composite membrane.* **Carbohydrate Polymers**, 2012, 88 (2): 417-421.

[222] Yang Q, Takeuchi M, Saito T, and Isogai A. *Formation of Nanosized Islands of Dialkyl β-Ketoester Bonds for Efficient Hydrophobization of a Cellulose Film Surface.* **Langmuir**, 2014, 30 (27): 8109-8118.

[223] Yoshida Y, Heux L, and Isogai A. *Heterogeneous reaction between cellulose and alkyl ketene dimer under solvent-free conditions.* **Cellulose**, 2012, 19 (5): 1667-1676.

[224] Zhang N and Lu X. *Mechanical, thermal and combustion properties of intumescent flame retardant biodegradable poly (lactic acid) composites.* **Plastics, Rubber and Composites**, 2018, 47 (10): 458-467.

[225] Ye L, Ren J, Cai S-y, Wang Z-g, and Li J-b. *Poly(lactic acid) nanocomposites with improved flame retardancy and impact strength by combining of phosphinates and organoclay.* **Chinese Journal of Polymer Science**, 2016, 34 (6): 785-796.

[226] Favaro S, Ganzerli T, de Carvalho Neto A, Da Silva O, and Radovanovic E. *Chemical, morphological and mechanical analysis of sisal fiber-reinforced recycled high-density polyethylene composites.* **eXPRESS Polymer Letters**, 2010, 4 (8):

[227] Kalb B and Pennings A J. *General crystallization behaviour of poly(l-lactic acid).* **Polymer**, 1980, 21 (6): 607-612.

[228] Zhao H, Kwak J H, Conrad Zhang Z, Brown H M, Arey B W, and Holladay J E. *Studying cellulose fiber structure by SEM, XRD, NMR and acid hydrolysis.* **Carbohydrate Polymers**, 2007, 68 (2): 235-241.

[229] Ciolacu D, Ciolacu F, and Popa V I. *Amorphous cellulose—structure and characterization.* **Cellulose chemistry and technology**, 2011, 45 (1): 13.

[230] Widiastuti I. *Polylactide nanocomposites for packaging materials: A review.* in *AIP Conference Proceedings*. Year

[231] Farah S, Anderson D G, and Langer R. *Physical and mechanical properties of PLA, and their functions in widespread applications—A comprehensive review.* **Advanced drug delivery reviews**, 2016, 107 367-392.

[232] Dubey S P, Thakur V K, Krishnaswamy S, Abhyankar H A, Marchante V, and Brighton J L. *Progress in environmental-friendly polymer nanocomposite material from PLA: Synthesis, processing and applications.* **Vacuum**, 2017, 146 655-663.

[233] Gazzotti S, Rampazzo R, Hakkarainen M, Bussini D, Ortenzi M A, Farina H, Lesma G, and Silvani A. *Cellulose nanofibrils as reinforcing agents for PLA-based nanocomposites: an in situ approach.* **Composites Science and Technology**, 2019, 171 94-102.

[234] Arrieta M, Peltzer M, López J, and Peponi L. *PLA-based nanocomposites reinforced with CNC for food packaging applications: From synthesis to biodegradation.* Place: Springer, 2017.

[235] Frone A N, Berlioz S, Chailan J-F, and Panaitescu D M. *Morphology and thermal properties of PLA–cellulose nanofibers composites.* **Carbohydrate polymers**, 2013, 91 (1): 377-384.

[236] Clarkson C M, El Awad Azrak S M, Chowdhury R, Shuvo S N, Snyder J, Schueneman G, Ortalan V, and Youngblood J P. *Melt spinning of cellulose nanofibril/polylactic acid (CNF/PLA) composite fibers for high stiffness.* **ACS Applied Polymer Materials**, 2018, 1 (2): 160-168.

[237] Ng H-M, Sin L T, Bee S-T, Tee T-T, and Rahmat A R. *Review of Nanocellulose Polymer Composite Characteristics and Challenges.* **Polymer-Plastics Technology and Engineering**, 2017, 56 (7): 687-731.

[238] Gupta A, Simmons W, Schueneman G T, Hylton D, and Mintz E A. *Rheological and thermo-mechanical properties of poly (lactic acid)/lignin-coated cellulose nanocrystal composites.* **ACS Sustainable Chemistry & Engineering**, 2017, 5 (2): 1711-1720.

[239] Goussé C, Chanzy H, Cerrada M L, and Fleury E. *Surface silylation of cellulose microfibrils: preparation and rheological properties.* **Polymer**, 2004, 45 (5): 1569-1575.

[240] Xu S, Gu J, Luo Y, and Jia D. *Effects of partial replacement of silica with surface modified nanocrystalline cellulose on properties of natural rubber nanocomposites.* **Express Polymer Letters**, 2012, 6 (1):

[241] Shojaeiarani J, Bajwa D S, and Hartman K. *Esterified cellulose nanocrystals as reinforcement in poly(lactic acid) nanocomposites.* **Cellulose**, 2019, 26 (4): 2349-2362.

[242] Clarkson C M, El Awad Azrak S M, Chowdhury R, Shuvo S N, Snyder J, Schueneman G, Ortalan V, and Youngblood J P. *Melt Spinning of Cellulose Nanofibril/Polylactic Acid (CNF/PLA) Composite Fibers For High Stiffness.* **ACS Applied Polymer Materials**, 2019, 1 (2): 160-168.

[243] de la Motte H, Hasani M, Brelid H, and Westman G. *Molecular characterization of hydrolyzed cationized nanocrystalline cellulose, cotton cellulose and softwood kraft pulp using high resolution 1D and 2D NMR.* **Carbohydrate polymers**, 2011, 85 (4): 738-746.

[244] Fraschini C, Chauve G, and Bouchard J. *TEMPO-mediated surface oxidation of cellulose nanocrystals (CNCs).* **Cellulose**, 2017, 24 (7): 2775-2790.

[245] Hoeng F, Denneulin A, Neuman C, and Bras J. *Charge density modification of carboxylated cellulose nanocrystals for stable silver nanoparticles suspension preparation.* **Journal of Nanoparticle Research**, 2015, 17 (6): 244.

[246] Sehaqui H, Zimmermann T, and Tingaut P. *Hydrophobic cellulose nanopaper through a mild esterification procedure.* **Cellulose**, 2014, 21 (1): 367-382.

[247] Börjesson M and Westman G. *Crystalline nanocellulose—preparation, modification, and properties.* **Cellulose-fundamental aspects and current trends**, 2015, 159-191.

[248] Dehnad D, Emam-Djomeh Z, Mirzaei H, Jafari S-M, and Dadashi S. *Optimization of physical and mechanical properties for chitosan–nanocellulose biocomposites.* **Carbohydrate Polymers**, 2014, 105 222-228.

[249] Meaurio E, López-Rodríguez N, and Sarasua J R. *Infrared Spectrum of Poly(l-lactide): Application to Crystallinity Studies.* **Macromolecules**, 2006, 39 (26): 9291-9301.

[250] Gitari B, Chang B P, Misra M, Navabi A, and Mohanty A K. *A Comparative Study on the Mechanical, Thermal, and Water Barrier Properties of PLA Nanocomposite Films Prepared with Bacterial Nanocellulose and Cellulose Nanofibrils.* **2019**, 2019, 14 (1): 23.

[251] Arjmandi R, Hassan A, Mohamad Haafiz M K, and Zakaria Z. *Effects of Micro- and Nano-cellulose on Tensile and Morphological Properties of Montmorillonite Nanoclay Reinforced Polylactic Acid Nanocomposites.* Place: Springer Singapore, 2016.

[252] Lu J, Sun C, Yang K, Wang K, Jiang Y, Tusiime R, Yang Y, Fan F, Sun Z, Liu Y, Zhang H, Han K, and Yu M. *Properties of Polylactic Acid Reinforced by Hydroxyapatite Modified Nanocellulose.* **Polymers**, 2019, 11 (6):

[253] Mohammadi P, Toivonen M S, Ikkala O, Wagermaier W, and Linder M B. *Aligning cellulose nanofibril dispersions for tougher fibers.* **Scientific Reports**, 2017, 7 (1): 11860.

[254] Lee W J, Clancy A J, Kontturi E, Bismarck A, and Shaffer M S P. *Strong and Stiff: High-Performance Cellulose Nanocrystal/Poly(vinyl alcohol) Composite Fibers.* **ACS Applied Materials & Interfaces**, 2016, 8 (46): 31500-31504.

[255] Zhu B, Fan T, and Zhang D. *Adsorption of copper ions from aqueous solution by citric acid modified soybean straw.* **Journal of Hazardous Materials**, 2008, 153 (1): 300-308.

[256] Gong R, Jin Y, Chen F, Chen J, and Liu Z. *Enhanced malachite green removal from aqueous solution by citric acid modified rice straw.* **Journal of Hazardous Materials**, 2006, 137 (2): 865-870.

[257] Rouhi M, Razavi S H, and Mousavi S M. *Optimization of crosslinked poly(vinyl alcohol) nanocomposite films for mechanical properties.* **Materials Science and Engineering: C**, 2017, 71 1052-1063.

[258] Obokata T and Isogai A. *The mechanism of wet-strength development of cellulose sheets prepared with polyamideamine-epichlorohydrin (PAE) resin.* **Colloids and Surfaces A: Physicochemical and Engineering Aspects**, 2007, 302 (1-3): 525-531.

[259] Zhang W, Zhang Y, Lu C, and Deng Y. *Aerogels from crosslinked cellulose nano/micro-fibrils and their fast shape recovery property in water.* **Journal of Materials Chemistry**, 2012, 22 (23): 11642-11650.

[260] Sharma S and Deng Y. *Dual mechanism of dry strength improvement of cellulose nanofibril films by polyamide-epichlorohydrin resin cross-linking.* **Industrial & Engineering Chemistry Research**, 2016, 55 (44): 11467-11474.

[261] Geng L, Chen B, Peng X, and Kuang T. *Strength and modulus improvement of wet-spun cellulose I filaments by sequential physical and chemical cross-linking.* **Materials & Design**, 2017, 136 45-53.

[262] Niazi M B K, Jahan Z, Berg S S, and Gregersen Ø W. *Mechanical, thermal and swelling properties of phosphorylated nanocellulose fibrils/PVA nanocomposite membranes.* **Carbohydrate Polymers**, 2017, 177 258-268.

[263] Ibrahim M M, El-Zawawy W K, and Nassar M A. *Synthesis and characterization of polyvinyl alcohol/nanospherical cellulose particle films.* **Carbohydrate Polymers**, 2010, 79 (3): 694-699.

[264] Jeon J G, Kim H C, Palem R R, Kim J, and Kang T J. *Cross-linking of cellulose nanofiber films with glutaraldehyde for improved mechanical properties.* **Materials Letters**, 2019, 250 99-102.

[265] Zhu H, Narakathu B B, Fang Z, Aijazi A T, Joyce M, Atashbar M, and Hu L. *A gravure printed antenna on shape-stable transparent nanopaper.* **Nanoscale**, 2014, 6 (15): 9110-9115.

[266] Tang A, Yan C, Li D, and Chen S. *Acid-catalyzed crosslinking of cellulose nanofibers with glutaraldehyde to improve the water resistance of nanopaper.* **Journal of Bioresources and Bioproducts**, 2018, 3 (2): 59-64.

[267] Wang W, Wang J, Shi X, Yu Z, Song Z, Dong L, Jiang G, and Han S. *Synthesis of mesoporous TiO_2 induced by nano-cellulose and its photocatalytic properties.* **BioResources**, 2016, 11 (2): 3084-3093.

[268] Chen H, Peng Y-P, Chen K-F, Lai C-H, and Lin Y-C. *Rapid synthesis of Ti-MCM-41 by microwave-assisted hydrothermal method towards photocatalytic degradation of oxytetracycline.* **Journal of Environmental Sciences**, 2016, 44 76-87.

[269] Shen D, Dai Y, Han J, Gan L, Liu J, and Long M. *A nanocellulose template strategy for the controllable synthesis of tungsten-containing mesoporous silica for ultra-deep oxidative desulfurization.* **Chemical Engineering Journal**, 2018, 332 563-571.

[270]   Fan M, Dai D, and Huang B. *Fourier transform-materials analysis.* **Fourier transform-materials analysis**, 2012, 45-68.